DEVELOPMENT OF AN ENHANCED WIDE-BAND ERBIUM DOPED FIBER AMPLIFIER USING HIGH CONCENTRATION ACTIVE MEDIUM

By

BELAL AHMED HAMIDA G. ALLAH

A thesis submitted in fulfilment of the requirement for the degree of Doctor of Philosophy

Kulliyyah of Engineering
International Islamic University Malaysia

JUNE 2013

ABSTRACT

In the point-to-point transmission an optical signal suffers mainly from attenuation and dispersion. The ongoing research has been focusing on containing this issue by proposing innovative designs in order to provide for an element compensating these effects. This research work focuses on the development of a new design of wide band high concentration optical amplifier. It suggests compensating for attenuation and dispersion both using the same technique. It consists of two stages of 1.5m and 9m long Erbium-Doped Fiber (EDF) optimized to operate in C-band and L-band, respectively. Further, a Chirped Fiber Bragg grating (CFBG) is used in each section to reflect the amplified signal back to the active area so that the overall gain spectrum can be enhanced over a wider frequency spectrum. Using a semi-analytical model (GainMaster), is suggested to verify the proposed design. A numerical model is carried out to implement the energy rate equations for the erbium ions population inversions. In addition, an extensive work has been carried out to implement this design experimentally. The experimental results show that the proposed amplifier gives a wider (1540nm to 1610m) flat high gain (22dB) with variation of ±3dB and low noise figure less than (6.5dB) at low input signal power (-30dBm) . Though solved by CFBG partially, this work has not carried out a quantified exploration of issues related to dispersion, mainly due to unavailability properly characterized equipment. Also an extensive work has been carried out to evaluate the performance of the proposed amplifier by comparing the performance against other available amplifiers. The performance shows that the band width 5nm higher than the existing amplifier with low noise figure about 7dB and gain flatness about 70nm which is higher than the other two amplifiers by 30dm.

خلاصة البحث

احتدمت سرعة تطوير نظام الارسال البصري من نقطة إلى نقطة بشكل ملحوظ في السنوات القليلة الماضية، وركزت الجهود على زيادة مسافة الارسال للنظام البصري مع تقليل الكلفة الكلية. لكن، وبالرغم من هذا التحسن مايزال هناك الكثير من المحدوديات، و فضاءات واسعة للتحسين. التوهين والانبساط هما الأثران الخطيان اللذان يشوهان الاشارة البصرية. اقترح الكثير من الباحثين انشاء شبكات وسيطة ذات أجهزة تعويض للتغلب على هذه الأثار. مع ذلك، فإن المشكلة لم تحل بشكل كامل، لأن البحث ركز على طول موجي واحد أو نطاق موجي ضيق.

يركز هذا البحث على تطوير مضخم بصري جديد ذو نطاق واسع وتركيز عالي، بحيث يستطيع التصميم الجديد تعويض الآثار الناتجة عن التوهين والانبساط في صندوق واحد. يتركب المضخم من قسمين من Erbium-doped fiber (EDF) بطول 1.5 م و 9م محسن بحيث يعمل على حزمتي C-band و L-band على التوالي. علاوة على ذالك، التصميم يستعمل التقنية المطبقة حديثا لنظام Multi-Wavelength Chirped Fiber Bragg Grating (CFBG) بشكل متوالي لعملية تمرير مزدوجة. يستخدم CFBG في كل مقطع لعكس الاشارة المضخمة إلى المساحة الفعالة لتحسين وتسوية الكسب الكلي للفيض. تم بناء نموذج شبه تحليلي (GainMaster) للتحقق من التصميم المقترح. أنجز أيضا نموذج عددي من معادلات معدل الطاقة لانعكاس كثافة أيونات الايربيوم. بالاضافة إلى هذا، تم انجاز اختباري شامل لبناء هذا التصميم عمليا. تظهر نتائج التجارب أن المضخم المقترح يعطي تضخيم مستوي عالي وشكل ضوضاء صغير. عند ادخال اشارة بقدرة -30 dBm عند جهاز الادخال ، تم الحصول على متوسط كسب مستوي بمقدار **22dB** بتذبذب بمقدار dB 3± على مدى فيض موجي من 1540 نانو متر إلى 1610 نانو متر. وعلى طول نفس المدى الموجي السابق تغير شكل الضوضاء من 4 إلى dB 7. كذلك، الكسب المستوي شوهد في مدى فيضي يمتد من طول موجي 1535 نانو متر إلى 1605 نانو متر وبتذبذب كسب أقل من dB 2 عند إشارة دخل 0 dBm عند جهاز الادخال . ان تقنية CFBG ساهمت في الحصول علي نتائج جيدة نتيجة تقليل من ثاثير Dispersion ولكن وبسبب عدم توفي بعض المعدات التقنية لم يتم قياس قياس نسبة لفاعلية من استخدام CFBG. كذالك،

تم القيام بعمل واسع لتقييم أداء المضخم المقترح بمقارنته مع نظائره من المضخمات المتاحة بحثيا. ختاما، إنه من المرجو أن تحفز نتائج هذا البحث البحاثين على دمج نماذج لمعوضات التشتت مع المضخمات البصرية، حيث أن المضخم المقترح بإمكانه تحسين تطبيقات على نطاق واسع لأنظمة التضمين بالتقسيم الموجي ذات المسافات الطويلة و شبكات الألياف البصرية المحلية.

APPROVAL PAGE

The Thesis of Belal Ahmed Hamida G.Allah has been approved by the following:

_____
Ahmed Wathik Naji
Supervisor

_____
Sheroz Khan
Co-supervisor

_____
Wajdi Al-Kateeb
Co-supervisor

_____
Rafiqul Islam
Internal Examiner

_____
Saad Osman
Internal Examiner

_____
Kaharudin Dimyati
External Examiner

_____
Najibah Mohd Zin
Chairman

DECLARATION

I hereby declare that this thesis is the result of my own investigations, except where otherwise stated. I, also declare that it has not been previously or concurrently submitted as a whole for any other degrees at IIUM or other institutions.

Belal Ahmed Hamida G.Allah

Signature……. Date……....

To my dear parents, wife, colleagues and friends.

INTERNATIONAL ISLAMIC UNIVERSITY MALAYSIA

DECLARATION OF COPYRIGHT AND AFFIRMATION OF FAIR USE OF UNPUBLISHED RESEARCH

DEVELOPMENT OF AN ENHANCED WIDE-BAND ERBIUM DOPED FIBER AMPLIFIER USING HIGH CONCENTRATION ACTIVE MEDIUM

Affirmed by Belal Ahmed Hamida

…….. ……..

Signature Date

ACKNOWLEDGEMENTS

In the Name of Allah, the Most Compassionate, the Most Merciful. All praise and thanks should be to ALLAH (S.W.T.) the Almighty, who has enabled me to accomplish this work. Prayers and peace be upon the messenger of Allah, Prophet Mohammed (P.B.U.H.) for endowing light of guidance in my life.

First, I would like to express my sincere appreciation and gratitude to my supervisors; Dr. Ahmed Wathik Naji, Sheroz Khan, Wajdi Al-Khateeb and Harith Ahmad, for their excellent supervision, guidance, encouragement and support. I am also grateful to them for providing the opportunities to publish this work, both in journals and conferences.

I would like to express heartfelt gratitude to my parents who have never given up praying for my success from the very beginning of my life. Without them, I would not be the person I am today. My deep and sincere gratitude goes to my beloved wife, my sons and my daughters whose continuous motivation, affection, and moral support have enabled me to complete this work. I would like to dedicate this work to my parents, my brothers, my sisters and my family.

I would like to express my sincere thanks to my colleagues and friends for their friendly cooperation and support.

Lastly, I offer my regards and blessings to all of those who supported me in any way during the completion of this work

TABLE OF CONTENTS

LIST OF FIGURES

LIST OF TABLES

LIST OF SYMBOLS

θ_c	Critical Angle
$\Delta\lambda$	spectral width
λ	Wavelength
τ	Time for a pulse to travel a path having length l
L	Path Length
M	material dispersion
n	Refractive Index
n_{eff}	Effective refractive index
λ_g	The Wavelength of The Guided Medium
V_g	guided velocity
C	Free Space Velocity (Speed of Light)
E_1	Atom's Discrete Energy of Ground level
E_2	Atom's Discrete Energy of Upper level
h	Planck's constant, h= 6.626 x 10-34
f	Photon Frequency
ΔE	Difference of Energy, $\Delta E = Ep = E_2 - E_1$
N_1	Atom Density for Energy Level E_1
N_2	Atom Density for Energy Level E_2
K	Boltzmann constant
T	The Absolute Temperature
R_{12}	Pumping Rate
W_{12}	Stimulated Absorption Rate
W_{21}	Stimulated Emission Rate
A_{21}	Spontaneous Decay Rate
ρ	Total Ion Density
G_0	Small-Signal Gain
$\pm_{SE}$	Emission Cross Section of the Signal
$\pm_{SA}$	Absorption Cross Section of the Signal
$\pm_{PE}$	Emission Cross Section of the Pump
$\pm_{PA}$	Absorption Cross Section of the Pump
V_s	Signal Frequency
V_p	Pump Frequency
d_S	Overlap Factor of the Signal
d_P	Overlap Factor of the Pump
A	Effective Cross-Sectional Area of the Distribution of Erbium Ions
P_S^+	Forward Signal Power
P_S^-	Backward Signal Power
P_p	Pump Power
P_a^+	Forward Spontaneous Emission Powers of EDFA
P_a^-	Backward Spontaneous Emission Powers of EDFA

SiO_2	Silicon Dioxide
η_{SP}	Spontaneous Emission Factor
$P^{+}_{A(2nd\ Stage)}$	Forward Spontaneous Emission Power of EDFA in the Second Stage
$P^{-}_{A(2nd\ Stage)}$	Backward Spontaneous Emission Power of EDFA in the Second Stage

LIST OF ABBREVIATIONS

WDM	Wavelength Division Multiplexing
SOA	Semiconductor Amplifier
DRA	Distribute Raman Amplifier
EDFA	Erbium Doped Fiber Amplifier
OFCS	Optical Fiber Communication System
ASE	Amplified Spontaneous Emission
DCF	Dispersion Compensating Fiber
CFBG	Chirped Fiber Bragg Grating
SP	Single Pass
DP	Double Pass
EDF	Erbium Doped Fiber
DWDM	Dense Wavelength-Division-Multiplexed
TLS	Tunable Laser Source
OSA	Optical Spectrum Analyzer
Zr-EDF	Zirconia based Erbium-doped fiber
Si-EDF	Silicon based Erbium-doped fiber
Bi-EDF	Bismuth based Erbium-doped fiber
MCVD	Modified Chemical Vapor Deposition
SNR	Signal-Noise Ratios
FBG	Fiber Bragg Grating
SMF	Single-Mode Fibers
VOA	Variable Optical Attenuator
MCVD	Modified Chemical Vapor Deposition

CHAPTER 1

INTRODUCTION

1.1 INTRODUCTION

Optical communication is regarded one of the most reliable communication means for transfer of data and information. The changes this technology has been undergoing so rapidly over the last decade are mostly in the form of its capability of increased capacity rate and reduction in feature sizes as well as dimensions (Peter, 1989). The tremendous increase in the number of internet users, the data transfer as a result when combined together, are leading to high volume of data traffic flow we handle every day (Jerrard, 1980). All this has created an enormous demand for broad-band Dense Wavelength-Division-Multiplexed (DWDM) optical communication systems (Arumugam, 2001). Since the beginning of this century, fiber optic communication has revolutionized the world terminating into making the use of mobile communication cheaper, affordable and be with features of multimedia serving millions of its users at finger tips (Ji, 2005).

Thousands of years back, human had used the light for communication of alarms and indication and in recent times when the satellite are employed for communications, ships are still carrying lamps for signaling at sea routes, while signaling mirrors are standard means for survival packs consisting of tools and supplies needed to be used as an aid to survival emergency situations. The belief of light travelling not in straight lines is also established since very long, and that was the first step in using light for communication technology. Later on, light started being used for audio communication and speech data. The medium used was a tube using

two mirrors at the ending and receiving ends, although not clear speech over a distance close to two hundred meters, but it could be understood at least, and hence this was a pioneer task in making light used for communication of speech.

In 1870s Irish physicist, John Tyndall, conducted new experiment to disprove the belief that light travels in straight lines and gave birth to a revolution in communications technology demonstrating the propagation of light down through a stream of falling water via total internal reflection. This demonstration made the scientific foundation for today's modern fiber optic technology. Later on making use of the same principle of light propagation, (Alexander, 1880) used the light for the transmission of speech in the effort of extending his telephone services. This speech transmission system consisted of using a tube with flexible mirror at its ends, and named this device as photo-phone. Nevertheless, the sound transmitted was not so clear and the distance was only close to two hundred meter but the message could at least be understood.

By 1960s, ruby laser emerged as the new invention to become a successful contender for making use of light directly for transmission of data in communication systems. However, the data need a clear path between the transmitter and receiver. Fiber started becoming known as medium of optic communication with some good results of 1000dB/km in glass existing of that time as against the 5-10 dB/km losses experienced by communication through in coaxial cable (Keiser, 2000).

The company called Corning Glass works successfully developed optical fiber in 1970 with an attenuation of 20dB/km which was reasonably low when looked at from communication services and users of that time. Then commissioned in 1975 was the first commercial fiber system that operated at a wavelength around 0.8µm and which used Gallium Arsenide (GaAs) semiconductor lasers as the light source. This

first-generation system operated at the bit rate of 45Mbps with repeaters spacing of 10km apart. General Telephone and Electronics sent the first live telephone traffic through fiber optics at a 6Mbps in 1977. The second generation of fiber optic communication was developed in the 1980s mainly for commercial purposes, which operated at 1.3µm using Gallium Arsenide Phosphide (GaAsP) semiconductor lasers as the light source (Armitage, 1988).

Today, optical fiber communication has been established as one of the most promising technologies for medium and long distance data transmissions. Moreover, optical fiber communication plays a vital role in the development of high-speed and high quality telecommunication systems. Furthermore, it is used in providing telecommunication links and in establishing the local area networks (LAN) as well as the use of internet for use in voice and high signaling rates. This is due mainly to the first man-made Fiber-optic Link around the Globe (FLAG) which was completed in 1997. The FLAG is made of 27, 300km length structure of fiber cable that starts from Porthcurno in Cornwall (UK). It runs buried under sea through Atlantic, Mediterranean, Red Sea, Indian and the Pacific Oceans to finally end in Miura (Japan). The FALG route track from UK to Japan was finally decided after having made an extensive survey of the geological and oceanic conditions while taking into considerations recommendations by universities and geological institutions. It has been made sure that FLAG remains hazards-resilient and capable to face natural disasters. At selected points decided in the light of recommendation made for its prospective use, FLAG sends out pair to cities on lands including Penang in Malaysia during all this run, FLAG crosses land at two locations—one point is one where it crosses from Mediterranean to Red Sea in Egypt, avoiding the Suez Canal ship traffic;

and second point is where it crosses from Indian Ocean to Pacific Ocean in Thailand, avoiding the sea traffic at the Straits of Malacca (Bjarklev, 1989).

The fiber type could be made either a) Step-index multimode or b) Step-index single mode, or c) graded index. The single-mode fiber was released in 1981, improving the system performance greatly; however the practical connectors capable of working with single mode fiber proved difficult to be developed. In 1980s, these systems were operating at bit rates of up to 1.7Gb/s having a repeater spacing close to 50km. Using conventional in GaAsP semiconductor lasers, third-generation fiber-optic system started operation at 1.55µm with specified losses of 0.2dB/km. In the third generation the system suffered from having to face the issues and challenges of dealing with pulse-spreading at that wave-length. The third-generation systems furnished 2.5Gbit/s data rate with repeater spacing larger than 100km. The problem of limiting the laser spectrum to a single longitudinal mode as well as using dispersion-shifted fibers was overcome with having a minimal dispersion at 1.55µm (Urquhart, 1988).

By the end of 1990s and through 2000s, research and industry promoters companies (such as KMI Research, and RHK Technology) predicted massive increase in demand for fiber optic communication bandwidth. This was mainly due to increasing use of the internet, and commercialization of various bandwidth-intensive consumer services, including video on demand. As a result the internet data traffic started increasing exponentially at a rate faster than what was forecasted for circuit complexity integration years ago Nowadays, many companies have joined forces to work together on reducing the cost of the fiber-optic communications(Djafar, 2001).

1.2 SIGNIFICANCE OF OPTICAL FIBER COMMUNICATION

An optical fiber communication system has numerous advantages over its electrical radio-frequency counterpart. The most important among such advantages is the ability of fiber communication through its multiplexing technique, called Wave-length Division Multiplexing (WDM) (Buet, 2001). According to WDM bit streams from various receivers are multiplexed together at the sending station while a de-multiplexer at the receiver station separates these streams into their individual receivers, leading to 30Tb/s using both C and L-bands simultaneously mainly. Another main advantage of optical fiber communication is its less signal transmission loss through the utilization of low attenuation fiber capable of covering longer transmission distances than electrical communication systems under similar operating conditions, making it the most preferred choice in long-haul communication links. An optical fiber communication system has some unique advantages including the following:

1.2.1 Enormous bandwidth

The information carrying capacity of a transmission system is directly proportional to the carrier frequency of the transmitted signals. The optical carrier frequency is in the range of 10^{13} to 10^{15} Hz while the radio wave frequency is about 106 Hz and the microwave frequency is about 10^{10} Hz (Senior, 1992). Thus the optical fiber yields greater transmission bandwidth than the conventional transmission systems, and the data rate of voice, data, image and video signals are increased to a greater extent in the optical fiber transmission system.

1.2.2 Small size and weight make it Robust

An optical fiber is often no wider than the diameter of a human hair. The fiber cables can be bent or twisted without damage. Thus even after applying protective layers, they are smaller and much lighter than corresponding copper cables. Furthermore, the optical fiber cables are superior to the copper cables in terms of storage, handling, installation and transportation, maintaining comparable strength and durability.

1.2.3 Dielectric waveguide

Optical fibers are made from silica which is an electrical insulator. Therefore they do not pick up any electromagnetic wave or any high current lightning. Further the optical fibers are not affected by any interference originating from power cables, railway power lines and radio waves. There is no crosstalk between fibers even though there are so many fibers in a cable because of the absence of optical interference between the fibers (Palais, 1998).

1.2.4 Security Concerns

Optical fibers are very hard to be affected by undesirable intruding spikes and flickers similar to the way in copper-wired installations. Accordingly fiber-optic based communication is a preferable choice by security sensitive premises of banks and other such sensitive government institutions minimizing the issues stemming from Wiki leaks

1.3 PRINCIPLES OF OPTICAL FIBER TRANSMISSION SYSTEM

Optical fiber transmission systems are operating on the basic principle according to which light is made to get loaded with information data for being transmitted over

longer distances in a medium made of glass. Basically it consists of transmitter, fiber trunk and receivers (Jeunhomme, 1990)

Optical fiber communication is growing extensively, and optical fibers to the extent of over 600 million kilometers have been laid down amounted to cash in billions dollars. Typically, a link of optical fibers transmission system can be hundreds of kilometers and some could be extended up to several thousands of kilometers with additional amplifiers and repeaters (Ma, 1998). Similarly, the data rate of each optical fiber transmission channel could reach up to 40Gb/s (Miyakawa, 2002), which is dominantly limited by the problems of attenuation and dispersion, (Agrawal, 2005; Gordon, 1991). The attenuation causes the signal to become weaker while the dispersion causes the pulses to spread out, eventually leading the pulse to get overlapped, losing thus information as a result (Hansen, 1995).

Intercity systems have now been widely implemented with the application of Single-Mode Fibers (SMF), repeater spacing of up-to 40km or more is achieved (Keiser, 2000). Basically an optical transmission system consists of a link of fiber optic as a transmission medium between transmitters and receivers. Information is converted from electrical to optical domain, modulated and multiplexed before being injected into the fiber optic. Optical fiber carries the information by guiding the laser beam in its core making use of the total internal reflection law. At the receiver end, the signal is converted back into an electrical domain by a photo detector, amplified and demodulated to get back the original information that was sent.

1.4 OPTICAL AMPLIFIER

During transmission over long distances (>100 km), the light signals suffer from attenuation losses, and hence it becomes necessary to compensate for such from

sources installed for this purpose on the fiber run, this compensation is done through device termed as optical amplifiers. In the long distance optical fiber communication systems, the amplifiers are installed at some distance span (100km) for amplifying the light pulses back to their normal strength for their onward journey down the cable.

Initially this was accomplished by optical to electrical and electrical to optical conversions, using an optoelectronic module consisting of an optical receiver, regeneration and equalization system, and an optical transmitter meant to send the data back. However, such methods proved to be costly besides leading to add onto the complexity of system at the end while reducing the operational bandwidth of the system. The Erbium Doped optical Fiber Amplifier is the alternant solution which eliminates the convention stage between electrical and optical domains. This is done by inserting a length of 10m long fiber for every 100km length of the main fiber, simplifying the whole mechanism and improving the SNR considerably.

An optical amplifier is a device (shown in Figure 1.1) that amplifies the signal strength of an optical signal without the need for conversion and rec-conversion procedures

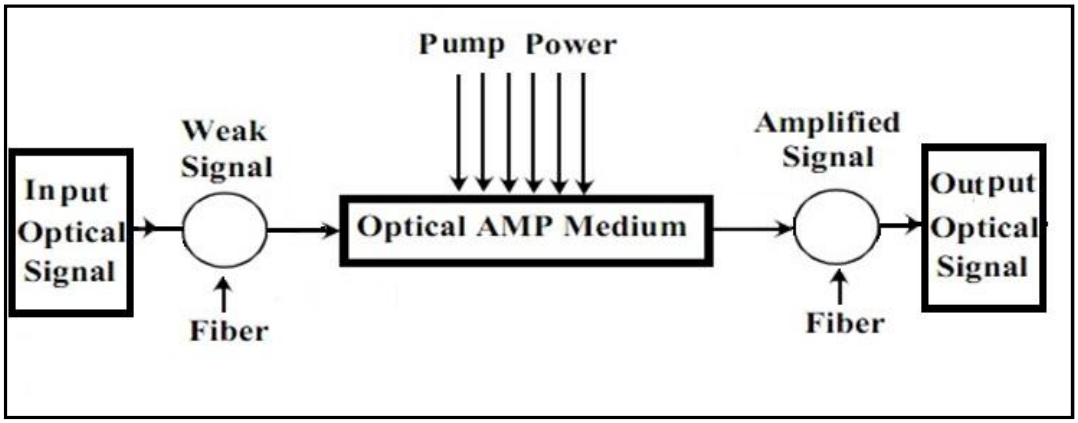

Figure 1.1: Simple diagram of an optical amplifier

The advantages of using Optical amplifier include flexibility, low cost, reliability, non-sensitivity to light polarization and enhanced suitability for wavelength division multiplexing (WDM). The two main types of optical amplifiers are Fiber Amplifier and Semiconductor Amplifier.

1.4.1 Semiconductor Optical Amplifiers

Semiconductor optical amplifier (SOA) amplifies a given light signal by pumping it through electrical means by making use semiconductor electronics. The dominant advantages of SOA include their small size, operation on a low power laser and the amplification source providing light is through electrical means. The nonlinear operations of cross phase modulation, cross gain modulation, four waves mixing and wavelength conversion can be equally carried in a typical SOA (Bijan, 2011). However, the issues of higher noise, lower gain, and high cross-talk levels due to nonlinear phenomenon such as four wave mixing, moderate polarization dependence and high nonlinearity with fast transient time affect the performance of SOA. Thus, the gain reacts rapidly to changes of signal power or the light strength of the pumping source, leading to phase changes distorting the signals and eventually leading to loss of information.

1.4.2 Fiber amplifier

Fiber amplifier of optical amplifier can be divided into two types namely: i) Raman Amplifier and ii) Rare Earth Doped fiber Amplifiers.

1.4.2.1 Distribute Raman Amplifier

Distribute Raman Amplifier (DRA) amplifies the signal by using the nonlinear interaction between the signal and a laser source by injecting laser into an undoped relatively long fiber (10km) or doped short fiber (10m). This indicates that it relies on an intrinsic non-linearity in silica fiber. The advantages of the DRA include compatibility with installed single mode fiber; variable broadband operation may be possible, application of a lower average power over a span and good for lower crosstalk. While the main disadvantages in DRA includes required high pump power of about 1W, with high noise figure issue, the cost is expensive due to using high power and sophisticated way of gaining high gain.

1.4.2.2 Rare Earth-Doped Fiber Amplifiers

Rare earth metals or rare earth elements or rare earth material are a set of seventeen chemical elements in the Periodic Table, including Scandium and Yttrium. Scandium and yttrium which are considered rare earth elements since they tend to occur in the same ore deposits as the lanthanides and exhibit similar chemical properties (Connelly, 2005). The optical fiber can be used as a gain medium for telecommunication and computer networking, where the gain medium is the core of an optical fiber doped with rare earth materials such as Praseodymium, Ytterbium, Erbium or Thulium. The chemical properties of rare earth elements made them indispensable and non-replaceable in many electronic, optical, magnetic and catalytic applications. Moreover, they are fast depleting due to their daily contribution to our lives in products like hybrid cars, catalytic converters, wind power generators, many household appliances, industrial motors, MRI machines, iPods and computer hard drives. Fiber optic cables remained no exception, and soon their advantages of

flexibility made these appeared being used in manufacturing fiber cables. The rare-earth doped fibers were fabricated in a wide variety of methods to suit different design of amplifiers. Bundled together, optical fibers allow long distances, needing fewer repeaters and hence reducing cost extra-considerably.

The importance and popularity of fiber amplifiers doped by rare earth elements is increasing in optical communications; however, the most commonly used doping technique is that of is Erbium-Doped Fiber Amplifiers (EDFAs) capable to amplify signals with low light signal loss and with as low wavelength range as 1550nm. As a result, EDFAs have been proving to be the best choice for optical amplification in most of the present and future light wave communication systems.

The basic principle of EDFA depends on the power of light (one wavelength) pumped in in order to excite the input signal (another wavelength) into population inversion using (WDM). The assorted light is guided into fiber with erbium ions doped into the fiber core (Papannareddy, 1997; Nadir, 2007 a). The optical signal propagating along the fiber gets amplified from the stimulated emission of the excited ions. Furthermore, the active medium of doped fiber amplifier is created by light doping of silica fiber core with rare earth elements such as Ytterbium (Yb) or Erbium (Er). When the photons belonging to the signal at a different wavelength from the pumped light meet at the excited erbium atoms, they give up some of their energy to the signal and return to their lower-energy state subsequently.

This is a significant point as the erbium gives up its energy in the form of additional photons which are exactly in the same phase and direction as the signal being amplified (Hagimoto, 1989). Thus, the signal is amplified along its direction of travel only, and as such an EDFA becomes a very attractive device in single mode finer communication system. Due to the potential advantages of its high pump to

signal power which transfer efficiency stands at more than 50%. Furthermore, the EDFA has other advantages such as wide spectral band amplification with relative gain more than 20dB, efficient pumping, large dynamic range, low noise figure, polarization independent, low insertion loss, high output power (not gain but raw amount of possible output power) and finally Low distortion and minimal crosstalk (Becker, 2002; Nagaraju, 2009; Naji, 2011).

1.5 PROBLEM STATEMENT

A particular attraction of using EDFAs in WDM systems is their high gain and A3 adequate amplification bandwidth to amplify data channels with the highest data rates without introducing any effects of gain narrowing. Despite the past development in the EDFA design, there are limitations and rooms for enhancement. One of the open issues is the EDFA amplification band, where it is considered as challenge and key factor for any EDFA configuration designed for WDM network. The researcher focuses on increasing the EDFA amplification band practically to increase the amplification of more channels. Moreover, the difficulty in implementing any WDM system including EDFA's is that the EDFA bandwidth gain is wavelength dependent, the EDFA does not amplify the wavelength of the channels equally, while EDFA in a WDM system are often required to have equal gain spectra in order to achieve uniform output powers and similar signal-noise ratios (SNR) (Sun, 1998). Particularly in C and L-band, the amplification of any particular channel is dependent on the signal wavelength, the number of signals present in the system, the input signal powers and its absorption and emission cross-sections (Yoshida, 1995). These current limitations are open and hot areas for researcher to boost the performance of EDFA to be more suitable for WDM networks. Hence controlling the doped fiber length and the pump

power are considered as good technique in designing a flat spectral gain EDFA (Park, 1996; Surinder, 2006). The Fiber manufacturers focus on providing a new generation of active materials which can be used for EDFA. Finally, these matters deserve more researches and attention by proposing an enhanced configuration which makes use of the new active medium to address the current mentioned limitations.

1.6 RESEARCH OBJECTIVES

This research work focuses on the development of an enhanced wide-band high concentration optical amplifier. The research objectives are as follows:

i. Investigation of the theoretical background of EDFA, where the fundamentals of EDFA are explained in details. The principles of EDFA design are also presented from the number of stages point of view

ii. Critical review of the past and current related research works, where an overview of the previous works related to this project is presented, this overview focus on the gain, noise figure, and length of the fiber, bandwidth, strength and weakness of the works.

iii. Investigation of the impact of increasing the doping concentration of the EDF, where the absorption and emission characteristics of low and highly concentrated EDF are discussed. This step focuses on the impact of high doping concentration on the flat gain filters (GFF) for both C and L band, where a simulation works are carried out to evaluate the performance of single pass configuration EDFA using two types of EDF fibers of I-6 and I-25.

iv. Proposal of an enhanced configuration for EDFA using I-25 active medium, where a wide-band EDFA using a double-pass with Chirped Fiber Bragg Grating in parallel configuration is presented. The CFBG was used in both C-

band and L-band stages to allow double-pass propagation and increase the attainable gain.

v. Construction of the proposed configuration using semi analytical model, where wideband and flat-gain optical amplifier is demonstrated using a new serial configuration. A broadband FBG is used in both the C-band and L-band stages to allow a double pass operation and increase the attainable gain.

vi. Development of Mathematical modeling for the new proposed configuration, where the development of an enhanced Wide-band high concentration optical amplifier through Mathematical modeling is presented.

vii. Implementation the proposed amplifier practically using experimental setup

viii. Analysis the performance of the proposed EDFA in term of gain, noise figure and bandwidth.

ix. Evaluate the performance of the proposed EDFA by benchmark it with the other EDFA in the current market.

1.7 RESEARCH METHODOLOGY

A development of an enhanced wide-band high concentration EDFA is carried out in this research work. The steps of the research methodology are as follow:

a) Investigation of the theoretical background of EDFA, where the fundamentals of EDFA are explained in details. The principles of EDFA design are also presented from the number of stages point of view.

b) Critical review of the past and current related research works, where an overview of the previous works related to this project is presented, this

overview focus on the gain, noise figure, and length of the fiber, bandwidth, strength and weakness of the works.

c) Investigation of the impact of increasing the doping concentration of the EDF, where the absorption and emission characteristics of low and highly concentrated EDF are discussed. This step focuses on the impact of high doping concentration on the flat gain filters (GFF) for both C and L band, where a simulation works are carried out to evaluate the performance of single pass configuration EDFA using two types of EDF fibers of I-6 and I-25.

d) Proposal of an enhanced configuration for EDFA using I-25 active medium, where a wide-band EDFA using a double-pass with Chirped Fiber Bragg Grating in parallel configuration is presented. The CFBG was used in both C-band and L-band stages to allow double-pass propagation and increase the attainable gain.

e) Construction of the proposed configuration using semi analytical model, where wideband and flat-gain optical amplifier is demonstrated using a new serial configuration. A broadband FBG is used in both the C-band and L-band stages to allow a double pass operation and increase the attainable gain.

f) Development of Mathematical modeling for the new proposed configuration, where the development of an enhanced Wide-band high concentration optical amplifier through Mathematical modeling is presented.

g) Implementation of the proposal design practically using experiment setup

h) Analysis the performance of the proposed EDFA in term of gain, noise figure and bandwidth.

i) Evaluate the performance of the proposed EDFA by benchmark it with the other EDFA in the current market.

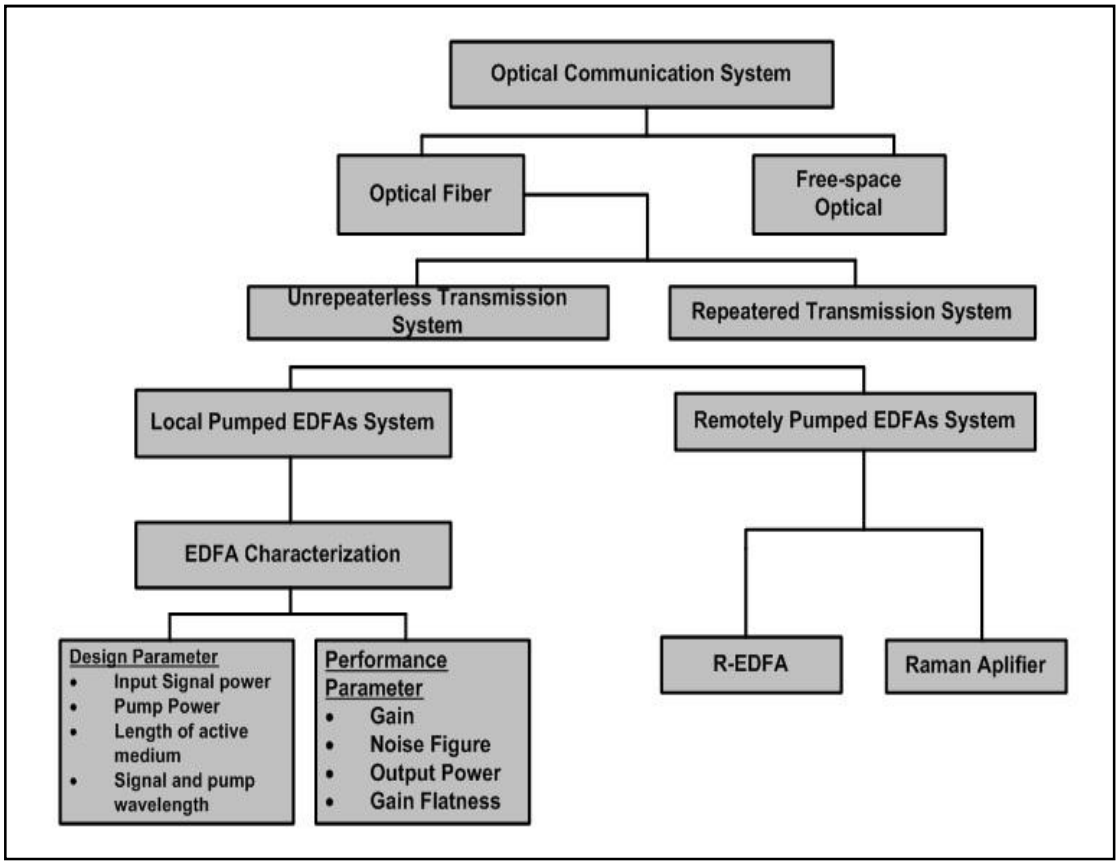

Figure 1.2: Scope of research work

1.8 ORGANIZATION OF THE DISSERTATION

This dissertation is divided into six main chapters beginning with first Chapter 1, where an overview of optical transmission systems is introduced while discussing some of the unrivalled advantages of optical fiber transmission system. Chapter 2 presents the theory and literature review of optical transmission system relevant to the study. Chapter 3 focuses on the effect of the concentration of EDFA, and on the study

of single-pass of the C- and L-band for low (I-6) and high (I-25) concentration. Chapter 4 discusses the wideband of EDFA with different active medium combination in parallel configuration while Chapter 5 presents a new serial configuration design , discusses the experimental setup and analysis the results. Chapter 6 concludes all findings of this research work with suggestions and recommendations for future work.

CHAPTER 2

LITERATURE REVIEW

2.1 INTRODUCTION

Optical fiber communication system (OFCS), as a one of the most reliable communication technologies, has been embracing consumers' needs on the scale that proves it to remain a preferable communication system for the future. This chapter reviews the optical fiber communication system and focuses on the fundamentals of the optical amplification, where the all principles elements, functions, population inversion, energy level atomic system of the EDFA have been discussed in details. Finally, a review on the developments that have been taken place in the form of scientific publications is made to make a platform for undertaking the work in this thesis.

2.2 OPTICAL FIBER COMMUNICATIONS SYSTEM

Optical fiber communication system is established as one of the most promising communication technologies within the area of medium and long distance data transmissions (Ji, 2005). Optical fiber transmission systems can fulfill the bandwidth needs for a practical long-haul transmission distance unheard of from before. It is handling reliably large amount of data streams for transmission through hundreds of kilometers with an acceptable bit error rate (Harun, 2004 a). Optical fiber transmission systems are based on the principle that light can carry more information over longer distances in a glass medium than electrical signals can carry using copper or coaxial cable (Jouinia, 2002). Here, the information data is being transmitted as stream of

light pulses or electromagnetic waves travelling through an optical fiber as a wave-guide. In order to compensate the loss of the wave-guide an optical amplifier is needed. In fact, purely optical amplifiers are usually preferred as on solution for signal regeneration. This is due their ability to convert electrical signal into optical before its transmission followed by its subsequent re-conversion into an electrical after its reception (Abd El–Naser, 2010).

The core characteristic of a telecommunication system is undoubtedly its information-carrying capacity (Chesnoy, 2002), as this is what most of the consumers would like a telecommunication company to have been featured with. The communication of an OFCS channel relies on a carrier of light the frequency of which lies between 100 and 1000 THz (Djafar, 2001). The explosive Internet traffic growth is due to a number of measures undertaken including deregulation of the utility, and such growth has forced the telecommunications companies to invest in increasing the capacity of their networks. Optical networks can deliver the required capacity as the bandwidth on demand. Beside the large capacity of optical communications bandwidth, there are still a number of extremely attractive features of optical systems such as weight/size of the fibers, signal security, low transmission loss, flexibility and reliability. System reliability generally enhanced in comparison with conventional electrical conductor systems. Furthermore, the reliability of the optical components is no longer a problem with predicted lifetimes of 20 to 30 years (Senior, 1992). All these factors also tend to reduce the maintenance time and operational costs.

Worldwide researchers continuously update the technology to improve on the performance of the current system. Optical fiber communication is hindered by factors such as attenuation, dispersion and nonlinear effects. The first two terms are the most common issues that can be redressed with the availability of optical devices

(Lewis,1999 and Naji, 2004), where, the transmission distance of any Optical Fiber Communication System is limited by the attenuation the fiber cause and the dispersion the light suffers while data is passing as stream of light pulses through the fiber (Kazovsky, 1996). Signal attenuation is a major factor in the design of any communication system, and so is it here in FOCS. The attenuation is major limiting factor the total length of the path as all the receivers require that their input power be above some minimum level, while dispersion is a signal wavelength dependent factor that causes information signal distortion. The fiber dispersion has a negative effect on the quality of information bearing signals, which reduces the OFCS performance leading to more data loss in the form of larger error rate.

2.2.1 Attenuation

There are several reasons for losses to occur in an optical communication system at several points along the run of a give fiber optical link. These losses are at the channel input coupler, splices, and connectors and within the fiber itself as a function of the length of the fiber. Fiber losses under consideration are in a range of wavelength from about 500nm to 1600nm in which fiber communications is practically taking place. Reasons for this include the ability to construct low-loss fibers, and the efficiency of light sources and designing appropriate detectors in this region when compared against the difficulty of doing so outside this region.

Optical fibers are made of plastics or glass. The material must be capable of slight variations so that two required refractive indices namely-- one due to core and the second due to cladding, can be obtained. Glass fibers generally have lower absorption than plastic fibers, so they are preferred for long-distance communications due to minimum dispersion normally light signals suffer form. The glass in most of

the applications examples is that formed by fusing molecules of silica (silicon dioxide, SiO_2). The resulting glass is not a compound but a mixture of SiO_2 molecules that have variations in molecular locations throughout the material. This is quite unlike the structure of a crystal, in which the locations of the component atoms form fixed and repetitive patterns.

To obtain different refractive indices, other material elements are to be added to the mixture of SiO_2 molecules. This doping is done with titanium, thallium, germanium, boron, and other such materials. As germanium increases the refractive index of silica, it is often used to dope the core and subsequently raises its index relative to the cladding as required to allow total internal reflection. The result is a high-silica-content glass, which form into a low-loss fiber thus achieving high chemical purity. Fiber loss can be classified into absorption, scattering losses and geometric effects. Figure 2.1 shows the total loss of attenuation that occurs in a silica fiber line.

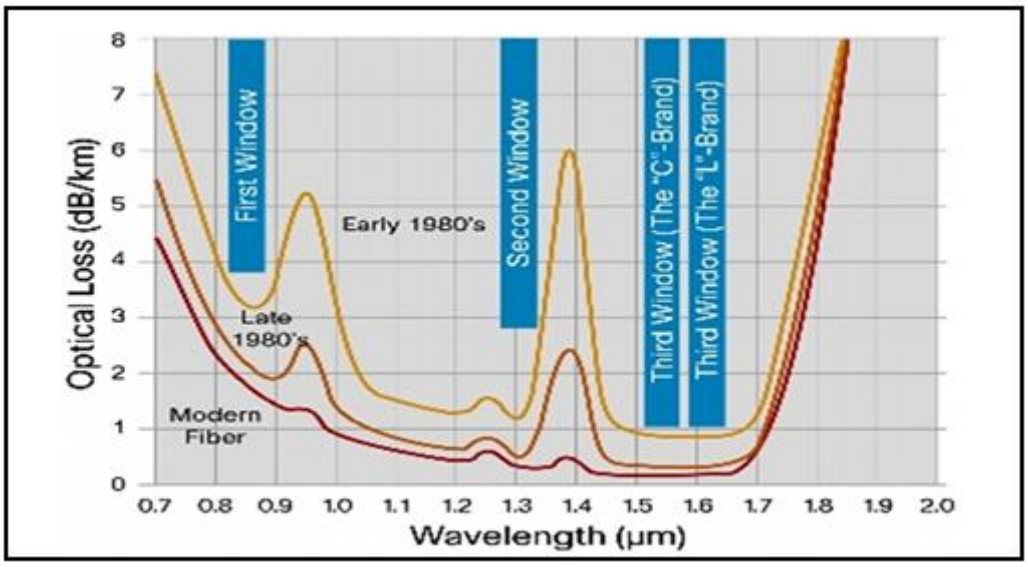

Figure 2.1: The main windows in optical fiber (Jeff Hecht, 1999)

2.2.1.1 Absorption

Material absorption is a loss mechanism related to the material composition and the fabrication process the fiber is made with, which results in the dissipation of some of the transmitted optical power as heat in the waveguide (Chaudhry, 1994). The material absorption can be divided into three categories (Agrawal, 1992):

a) Intrinsic absorption by the basic constituent atoms of the fibre material

b) Extrinsic absorption by impurity atoms in the glass material

c) Absorption by atomic defects in the glass composition.

2.2.1.2 Scattering Losses

Mainly Rayleigh scattering and non-homogeneities cause scattering losses. Rayleigh scattering is a fundamental loss mechanism arising from local microscopic fluctuations in density (Agrawal, 1992). Silica molecules move randomly through the glass in molten state during fiber fabrication as the heat applied provides the energy for the motion. As the liquid cools, the motion ceases, and upon reaching the solid state, the random molecular locations get frozen within the glass (Palais, 1998). This results in localized variations in density leading to random fluctuations of the refractive index on a scale smaller than the optical wavelength. Light scattering in such a medium is known as Rayleigh scattering as shown in Figure 2.2.

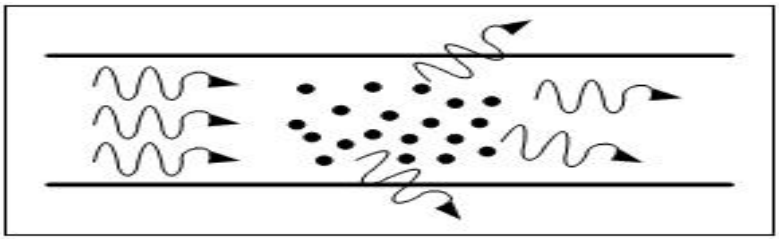

Figure 2.2: Rayleigh scatted, showing attenuation of an incident stream of photons owing to localized variations in refractive index.

Rayleigh scattering applies whenever a wave travels through a medium having scattering objects smaller than a wavelength. Because Rayleigh scattering is proportional (Palais, 1998), it becomes increasingly important as the wavelength diminishes. The Rayleigh scattering loss can be approximated by the expression:

$$L = 1.7(0.85/\lambda)^4 \quad (2.1)$$

Where λ is in micrometers and the loss L is in dB/km.

Material non-homogeneities unintentionally introduced into the glass during manufacturing also cause scattering losses. Imperfect mixing and dissolution of chemicals can cause non-homogeneities within the core and can produce a rough core-cladding interface. The scattering objects in these instances are larger than the optic wavelength. Unlike Rayleigh scattering, the losses introduced by large objects are independent of wavelength, and these losses can be controlled by proper manufacturing techniques.

2.2.1.3 Geometric Effects

Bends in a fiber cable constitute another source of attenuation. There are two types of bending: the macro-bending and the micro-bending (Chang, 1989; Wilczewski, 1996; Faustini, 1997). Macro-bending loss occurs when the fiber cable is subjected to a significant amount of bending a critical value of curvature. The phenomenon bending loss as shown in Figure 2.3 can be explained in several ways. Here, a trapped ray proceeds through a step-index fiber, striking the core-cladding interface at an angle $\theta_1 < \theta c$ (critical angle), so that total reflection occurs (Palais, 1998). The same ray enters the bend and strikes the surface at an angle θ_2, which is clearly less than θ1 which in turn less than the critical angle. The angle θ_2 diminishes as the bend radius

decreases. At some bend radius, $\theta_2$becomes smaller than the critical angle, total reflection does not occur, and a portion of the wave gets radiated to become loss.

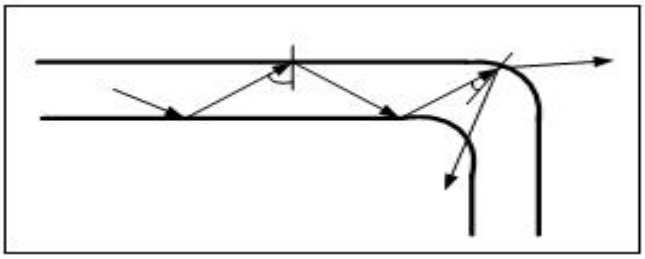

Figure 2.3: Macrobending

Micro-bending loss (Figure 2.4) often occurs when a fiber is sheathed within a protective cable (Palais, 1998). It results from small lateral forces exerted on the fiber during the cabling process and causes losses due to radiation in both single-mode and multimode fibers (Senior, 1992). Micro-bending effects in SMF may also arise after immersion in water due to unbalanced stresses. Asymmetric stresses between different layers of coating and glass can add more micro-bending transmission loss. Micro-bending can be generated at any stage during the manufacturing process or during the cable installation process or during service operation. These losses can be minimized by decreasing the presence of water extractable & water absorption and increasing the threshold strength of coating materials.

It introduces slight surface imperfections, which can cause mode coupling between adjacent modes. The radiatively produced in return is dependent on the amount of applied fiber deformation, the length of fiber, and the exact distribution of power among the different modes. Because of the coupling effect, a fiber having certain attenuation when unsheathed often has an increased loss after the cabling process.

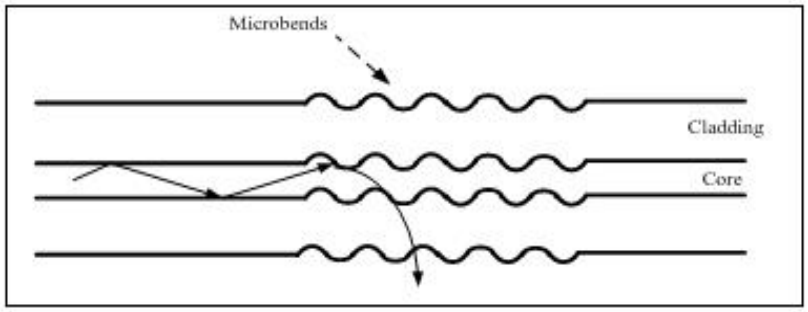

Figure 2.4: Microbending

2.2.2 Optical Signal Dispersion

Dispersion is a phenomenon when the velocity of propagation of an electromagnetic wave is wavelength dependent. There are three types of dispersion phenomena occurring in single mode fiber (SMF): material dispersion, waveguide dispersion and polarization mode dispersion (Palais, 1998).

2.2.2.1 Material Dispersion

When a real source emits a pulse of light into a dispersive glass fiber, this pulse consists of a sum of pulses that are identical and travel at different velocities. Theses pulses reach the end of the fiber at slightly different times, and when summed up at the receiver, these pulses yield an output that is spread out in relation to the input signal. The further the pulse travels, the greater the pulse spreading takes place. Let 'τ' be the time for a pulse to travel a path having length, L. Let the shortest and longest wavelengths be 'λ_1' and 'λ_2' respectively, and source spectral width be $\Delta\lambda = \lambda_2 - \lambda 1$. Then pulse spread per unit length, as per (Palais, 1998), can be written as under:

$$\Delta (\tau / L) = M \Delta\lambda \qquad (2.2)$$

Where, M, is material dispersion with unit of ps / (nm × km).

2.2.2.2 Waveguide Dispersion

Refractive index is the velocity of light in free space divided by the velocity in an unbounded medium. In case of a guided medium, refractive index is considered to be the effective refractive index, n_{eff}, and it is defined as the free space velocity divided by the guided velocity. That is $n_{eff} = c/Vg$. Thus the wavelength in the guided medium is $\lambda g = \lambda_0 / n_{eff}$. The variation of effective refractive index (n_{eff}) for any particular mode will cause pulse spreading, known as waveguide dispersion (Palais, 1998). For waveguide dispersion, and resulting pulse speared is given by:

$$\Delta (\tau / L) = Mg \, \Delta\lambda \qquad (2.3)$$

2.2.2.3 Polarization Mode Dispersion (PMD)

The stresses during cabling installation as well as the imperfections resulting from the manufacturing process cause asymmetric distortions to the fiber. These asymmetric distortions lead ultimately to result into pulse spreading known as polarization mode dispersion. The refractive index variation between two orthogonal polarization modes of single-mode optical fiber is known as birefringence. Birefringence causes one polarization mode to travel faster than the other, resulting in a difference in the propagation time for a given span of fiber length, which is called the Differential Group Delay (DGD).

2.3 OPTICAL FIBER AMPLIFICATION

Optical amplifiers provide solutions to the attenuation problem. Optical amplifiers are designed in such a way that the weakened signal is boosted to a specified power level for the onward transmission of light pulses. As its name implies, optical amplifiers operate in optical domain and maintains the signal's state along the fiber within

transmission distance. They eliminate the need for signal inter-conversion of photons to electrons and vice versa. Moreover, optical amplifiers offer a simple setup of a single in line components' arrangement meant to be used practically for any kind of modulations and transparent to any transmission speeds (Senior, 2000). Optical fiber amplifiers are classified as Doped Fiber Amplifier (DFAs) and Raman amplifier.

2.3.1 Raman amplifier

The availability of high optical pump power sources makes Raman gain in the transmission fiber a realistic possibility for amplifying optical signals (Grubb, 1995). Raman amplification has several attractive features: it is obtainable in any conventional transmission fiber; there is no excess loss if the pump power is absent and the gain spectrum is very broad allowing amplification in any WDM transmission system. Raman gain was first used in optical soliton experiments (Mollenauer, 1990). Later, many Optical Transmission system experiments have included Raman amplification to increase the total distance (Aris, 2005).

Raman amplification occurs due to the transition between vibrational modes in the transmission fiber medium. A fraction of the incident pump light generates light that is downshifted in frequency known as Stokes light at the same time as molecules are excited to a higher energy vibration state. Basically, light is composed of an electric field and a magnetic field oriented perpendicular to each other. When light propagate through a material, the electric or magnetic field may interact with the constituent atoms of that material. Typically, reactions occur between light and an atom's electron cloud because the electron cloud occupies much more space and is more easily deformable than the atomic nucleus. In particular, light may actually shift the electron cloud so it is no longer concentric with the nucleus; consequently, the

center of the positive nuclear charge is no longer in the same position as the center of negative charge from the atom's electron cloud.

In an attempt to retain proper charge balance, a chain vibration reaction process continues throughout the material. This is a type of atomic vibration known as an optical phonon. Whereas entire atoms vibrate with acoustical phonons, only the electron clouds of the atoms actually shift their positions with optical phonons. Therefore, optical phonons may propagate through a material at the speed of light. This phenomenon is known as atomic polarization (Hansen, 1998), and it is key to understanding the origin of Raman amplification.

As stated previously, the initial ionic polarization is the result of an interaction between light and the electron cloud of an ion. Hence, the outcome of such polarization is the formation of an optical phonon and the incident photon must be scattered from the ion with a lower energy than when it started. Specifically, the conservation of energy dictates that the scattered photon must have an energy equal to the energy of the incident photon minus the energy of the resulting optical phonon, or

$$\boldsymbol{E}_{\text{scattered photon}} = \boldsymbol{E}_{\text{incident photon}} - \boldsymbol{E}_{\text{optical phonon}} \tag{2.4}$$

In terms of frequency,

$$\boldsymbol{V}_{\text{scattered photon}} = \boldsymbol{V}_{\text{incident photon}} - \boldsymbol{V}_{\text{optical phonon}} \tag{2.5}$$

This type of scattering of light is known as Raman scattering (Kunihiro, 2003). A energy level diagram of Raman amplification is provided in Figure 2.5. Based on this figure, the incident pumping light changed the balance of the atom's electron cloud and caused changing in the energy levels of the electron. Therefore, the reaction

of the rebalancing process to retain the electron back to ground level caused the releasing of stimulated scattered phonon.

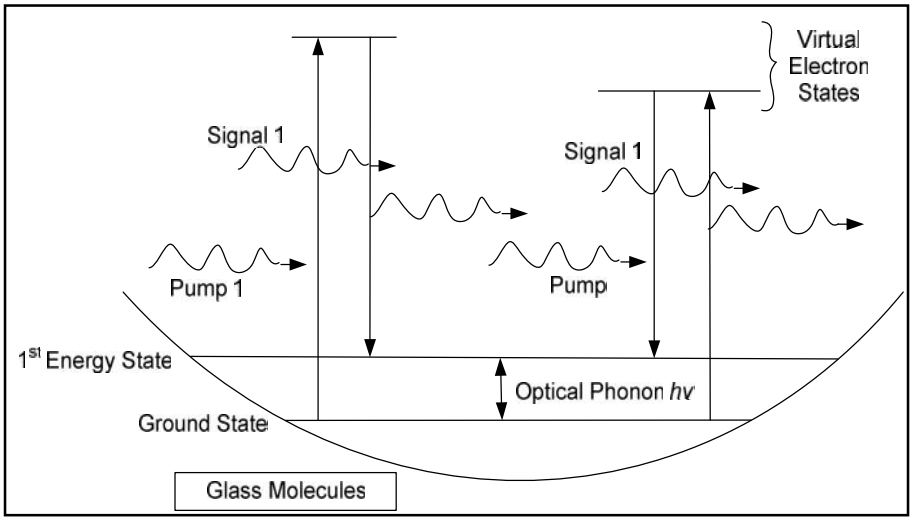

Figure 2.5: Raman amplification energy level diagram.

Raman scattering occurs when an incident photon and an optical phonon are simultaneously annihilated to form a scattered photon with a higher energy. In the first case, when an optical phonon is generated rather than annihilated, the scattered photon is downshifted in frequency from the incident photon, and the new photon frequency is called the Stokes frequency. Similarly, in the second case, when an optical phonon is annihilated, the scattered photon is up shifted in frequency from the incident photon, and this new frequency is known as the anti-Stokes frequency. The magnitude of the frequency shift (Stokes shift) depends on the frequencies of the optical phonon modes supported by the host material. Silica glass fibers support a wide range of optical phonon frequencies due to the amorphous nature of the material. This feature of silica glass is an extremely important property for Raman amplification because it

allows for a very wide Raman gain bandwidth. The Raman gain process is modeled by two coupled differential equations (2.6) and (2.7) (Agrawal, 2005).

$$\frac{dP_S}{dz} = g_R * P_P * P_S - \sim_S * P_S \tag{2.6}$$

$$\frac{dP_P}{dz} = -\frac{\mu_P}{\mu_S} * g_R * P_P * P_S - \sim_P * P_P \tag{2.7}$$

Where subscripts *S* and *P* denote quantities related to the signal and pump light, respectively. *P* is the propagating power and g_R (W^{-1} m^{-1}) is the Raman gain efficiency of the fiber normalized with respect to the effective area A_{eff}, α, is the background loss and, ω, the angular frequency of the light.

The first term on the right-hand side in the pump equation (Equation 2.7) represents pump power depletion. This must be included when the signal power approaches the same level as the pump power. In a preamplifier configuration, pump power depletion may be neglected since the signal power is low, leading to a simpler set of equations. Also, the signal and pump powers are counter-propagating in a preamplifier configuration. Consequently, the equations have to be:

$$\frac{dP_P}{dz} = -\sim_P * P_P \tag{2.8}$$

The distribution of all possible Stokes frequencies that may be produced via Raman scattering is known as the Raman gain spectrum. The Raman gain spectrum depends on both the frequency of the incident light and the nature of the host material. In

general, the peak gain occurs at a frequency of about 13 THz downshifted from the incident radiation (Agrawal, 2005). Raman scattering may be used to amplify an optical signal if the signal propagates simultaneously with a high-power pump beam and the signal falls within the Raman gain spectrum for that pump frequency. In terms of our earlier discussion of Raman scattering, the pump beam is the incident radiation that is scattered to produce photons at the Stokes frequency, which is the same as the frequency of the input signal that need to be amplified.

Since the signal and pump beams co-propagate through the fiber, the signal acts to stimulate emission of Stokes photons at the same modulation and frequency as itself. Spontaneous, or non-stimulated, Raman scattering may also occur and produce noise in the system, but the stimulated Raman scattering used to amplify a signal occurs at a significantly higher rate; hence, Raman amplifiers generally have very low noise figures, even in comparison with the state-of-the-art EDFAs in use today (Namiki, 2001). The key to successful Raman amplification is to ensure that the pump power exceeds the Raman threshold power, where stimulated Raman scattering converts a majority of the pump wave intensity to a Stokes frequency in order to amplify the propagated signal (Agrawal, 2005).

2.4 DOPED FIBER AMPLIFIER

Doped Fiber Amplifier (DFA) is an optical amplifier, which uses rare-earth doping material (such as Erbium and Praseodymium) inside the fiber. Essentially, it is a spliced active fiber connected to a pump laser within a transmission line (Becker, 1990). It works on the principle of stimulated emission. The pump laser is used to provide energy enough to excite ions in a special fiber doped over a given length (active medium) to an upper energy level. Then, the ions stimulated by photons of the

information signal and fall down to lower levels of energy; subsequently, they emit photon energy exactly on the same wavelength of the signal. The first rare earth doped material of Nd^{3+} is used into a single-mode fiber was demonstrated in 1960 by (James, 1991). Since then, rare-earth doped fibers are fabricated in a wide variety of methods to suit different design of amplifiers. The DFAs for the 1300nm windows achieved though doping fluoride based fibers (rather than silica fibers) with elements such as Praseodymium (Pr) (Kunihiko, 1998).

In OFCS, the active medium of DFA, which is operating in the 1550nm window, is created by doping a silica fiber core with the Erbium (Er^{3+}). To date, research works are focusing more on the Erbium-doping, particularly in silica-based fibers. This is due to the emission of Er^{3+} ions within a set of wavelength around 1550nm where the silica fiber exhibits the minimum attenuation of information signal (Yang, 2005). Erbium doped fiber amplifiers (EDFA) provide gains as high as 40dB associated with low noise, as successfully demonstrated with a pump power range of 50 to 100mW (Mears and Payne, 1987; Desurvire, 1989). The amplified output signal can be transmitted through 60-100km before further amplification is required.

The important features of EDFAs include the ability to pump the devices at several different wavelengths, low coupling loss to the compatible fiber transmission medium, and very low dependence of gain on light polarization (Urquhart, 1988). In addition, EDFAs are highly transparent to signal format and bit rate, since they exhibit slow gain dynamics, with carrier lifetimes of 0.1-10ms (Becker, 2002). The result is that the gain responses of EDFAs are constant for signal modulations greater than a few kHz. Consequently, they are immune to interference effects (such as crosstalk and inter modulation distortion) between different optical channels within a broad

spectrum of wavelengths (a 30nm spectral of the C-band ranging from 1530 to 1560 nm) that are injected simultaneously into the amplifier.

2.5 FUNDAMENTALS OF EDFA

Effects of light amplification was first described theoretically by A. L Schawlow and C. H. Townes (Schawlow, 1958), but an analysis of rare earth doped fiber characteristics was studied and demonstrated in 1962 (Becker, 2002), followed by an experimental investigation into Erbium Doped Fiber (Mears, 1987). Later on, many scientists (Desurvire, 1987; Armitage, 1988; Bjarklev, 1989) extensively explored the function and working of EFDA. Finally, the first EDFA was commercialized in 1992. Each free ion of erbium exhibits discrete energy levels.

An energy level refers to an amount of particular energy contained by the ion either corresponding to absorb or emit the energy. Amplification in erbium doped fiber closely related to the changes in energy level of erbium ions. Absorbing energy will increase its energy level to make the ion more excited and vice versa happens on when energy is released. In amplification terms, emitting light is associated with emitting photons. Figure 2.6 shows the possible energy levels for erbium ions as well as possible pumping bands. Absorption of pump photons excites Erbium ions to higher energy states.

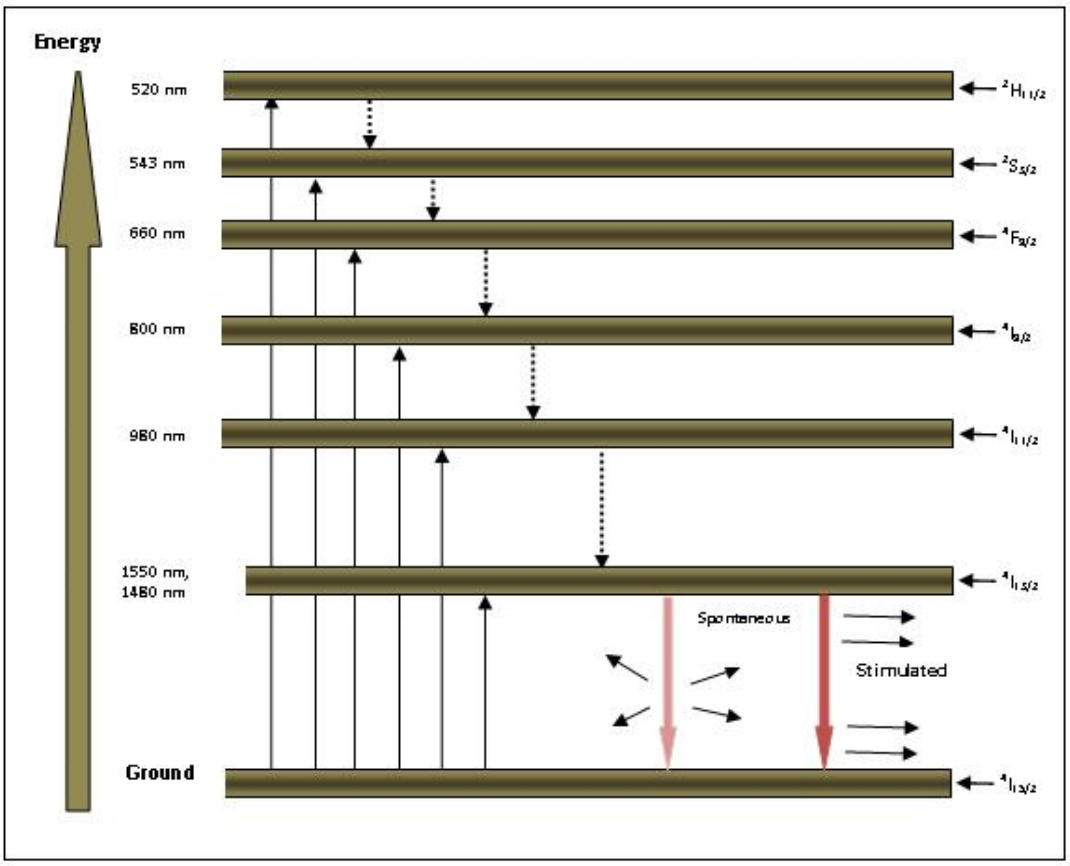

Figure 2.6: Energy levels of Erbium ions with the possible pump bands.

At higher energy levels, the ions may dissipate energy radiation by releasing photons or converting the energy into heat. According to ion energy structure, numbers of stark levels present at a particular energy level. Each ion experiences a different field strength and orientation due to randomness in the glass molecular structure, resulting in different Stark-splitting. The splitting causes a large gain bandwidth of rare-earth doped fiber amplifier. The number of Stark split lines for each level are 7 and 8 for $^4I_{13/2}$ and $^4I_{15/2}$ ions respectively resulting in 56 possible transitions between those lines spreading across 1550nm band at low temperature (Desurvire, 1994).

At 300K temperature, the bands sufficiently overlap giving smooth and continuous transition. The increases of energy gap between levels will also increase the tendency of photon radiation when jumping to lower energy levels. Thus the

transition between $^4I_{13/2}$ and $^4I_{15/2}$ is predominantly radiating resulting in 1550 nm wavelength region. Spectroscopy studies on Erbium glass showing pump wavelengths at 520nm (Desurvire, 1987), 620nm (Mears, 1987), 800nm (Mears, 1980), 980nm (Liaw, 1997; Haugen, 1992) and 1480 nm (Gabla, 1992) have been successfully demonstrated. Availability and maturity of pump laser diodes for 980nm and 1480nm leads these pump wavelengths to be widely deployed (Franz, 2000). The 980nm pump provides low noise of amplifier output but it requires for wavelength accuracy due to the narrow absorption band while 1480 nm pump gives better power conversion efficiency compared to 980 nm band (Desurvire, 1994).

According to Figure 2.5, discrete energy values are separated by energy gaps, following the laws of quantum physics. Ground level E_1 ($^4I_{15}/_2$) indicates the lowest level and E_2 ($^4I_{13/2}$) indicates the first level. Any ion can jump to another level discretely thus changing its energy level. The difference of energy, when an atom moves from upper to lower level releases photon as a quantum of energy. The photon carries energy of which is defined as (Desurvire, 1994):

$$Ep = E2 - E1 = hf \tag{2.9}$$

E_2 and E_1 refer to the atom's discrete energy packets release during transition between levels, where h = 6.626 x 10-34 J.s is a Planck's constant and photon frequency is denoted by f. Changes of an atom energy level from a lower to a higher level require absorbing energy from an external energy source. The atom absorbs this energy and jumps to the higher level. As by nature, the atom tries to get itself to be at its lowest possible energy level. The drop in energy level to lower level radiates photons. The process of providing atoms with external energy from external source is known as pumping which is depicted in Figure 2.6.

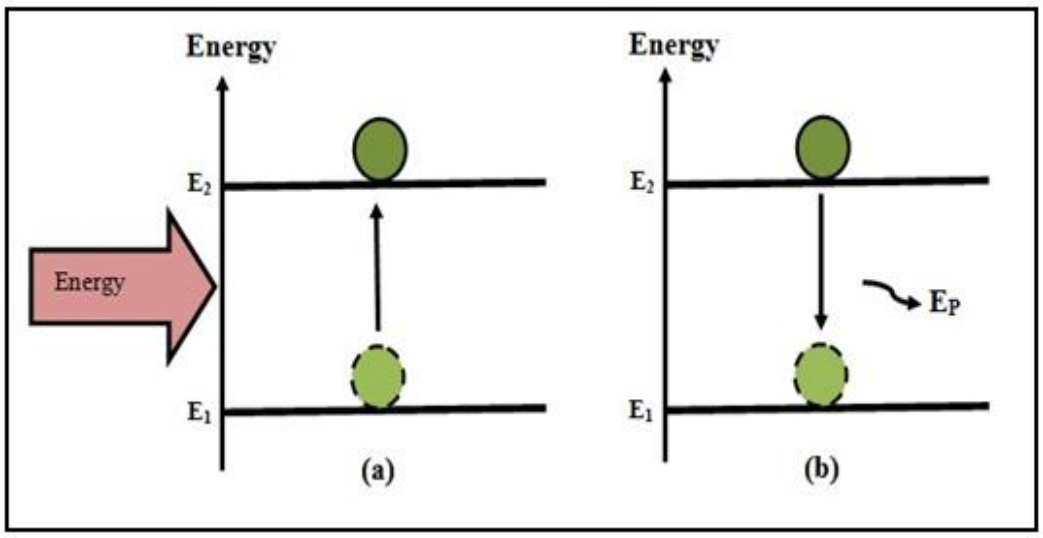

Figure 2.7: Atom with respective energy level (a) light absorption and (b) light emission.

Initially the atom relaxes at E_1 the lowest energy level. Applied external energy is absorbed by the atom and causing it to jump to an upper level, E_2. This condition is known as light absorption. Light emission occurs when the atom from E_2 goes down to the lower energy level shown In Figure 2.7:

i. According to quantum mechanics theory, spontaneous emission always involves transition from a higher energy state to a lower energy state. The spontaneous emission produced would become the noise generated by the amplifier and is referred to as amplified spontaneous emission (ASE).

ii. Stimulated emission where a photon (energy carrying atom) having energy equal to the energy difference between E_2 and E_1 interacts with the atoms in E_2, causing them to return to E_1 along with the creation of more photons. This is also referred to as avalanche multiplication.

Photons produced by stimulated emission are generally of an identical energy to the ones causing it and hence, the light associated with them is of the same frequency, phase and polarization. Furthermore, when an atom is stimulated to emit light energy

by an incident wave, the liberated energy could add to the wave in a constructive manner, providing further amplification.

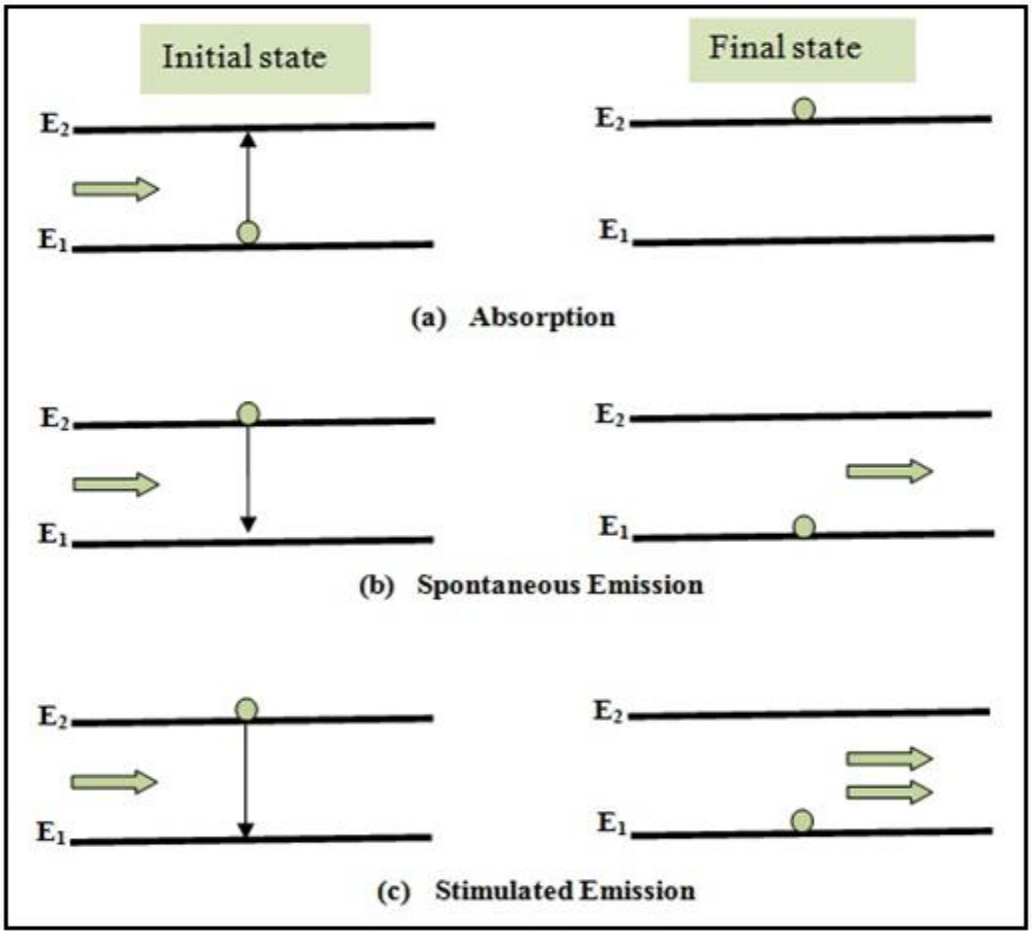

Figure 2.8: Schematic representations of absorption and emission between energy level 1 and 2: (a) absorption (b) spontaneous emission (c) stimulated emission. The black dot indicates the state of the atom before and after transition takes place and the block arrow in: (a) represents bump light (b) represents ASE and (c) represents single light

2.6 POPULATION INVERSION

In atomic systems with thermal equilibrium, the atom density in each energy level obeys the Boltzmann distribution given by (Senior, 1992):

$$N_2 / N_1 = e - [(E_2 - E_1) / KT] = e - hf / KT \quad (2.10)$$

N_1 and N_2 are atom densities for energy levels E_1 and E_2 respectively, K is the Boltzmann constant, T is the absolute temperature and h is Planck's constant. According to the above equation, N_2 is much smaller than N_1 in a normal atomic system at thermal equilibrium. Therefore, stimulated absorption is dominant compared to stimulated emission. In conditions where the thermal equilibrium is achieved, the lower level energy contains more atoms than at the upper level at room temperature. A non-equilibrium distribution of atoms where a population of atoms at upper energy level is greater than the lower is necessary to have optical amplification. This condition is commonly known as population inversion, with $N_2 > N_1$ where both N_2 and N_1 represent the density of atoms in energy levels E_2 and E_1.

Through population inversion, N_2 will become much larger than N_1, resulting in a system with dominant stimulated emission. Population inversion is achieved by injecting power into the system through an external energy source, which is known as pumping. Pumping will excite atoms into the upper energy level E_2 and hence obtain a non-equilibrium distribution. Figure 2.9 shows the atom density curve for both normal and inverted system.

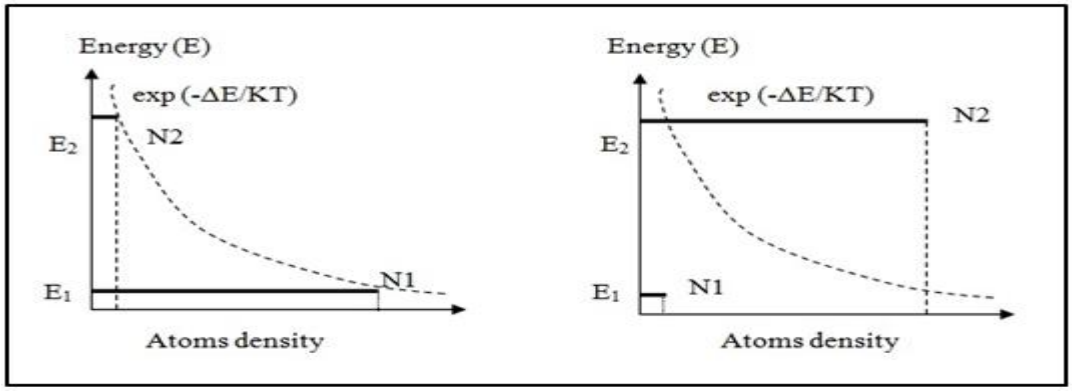

Figure 2.9: Population in a two energy levels system: (a) Boltzman distribution for a system in thermal equilibrium (b) a non-equilibrium (inverted) distribution showing population inversion.

2.7 TWO-LEVEL ATOMIC SYSTEM OF EDFA

This research work deals with the 1480 nm EDFA. For this reason, the following section mainly discusses the theoretical concept for the two energy levels of EDFA. The well-separated spectral lines in Erbium called multiples, which is composed of a certain number of broadened individual energy levels. In a two-level system, the population of ions and the rate equations involve Levels 1 and 2 of Erbium energy level system. The Level 2 involvements are only via the 1480 nm pump wavelength absorption cross section from Level 1 to Level 2 as depicted in Figure 2.10 (Becker, 2002).

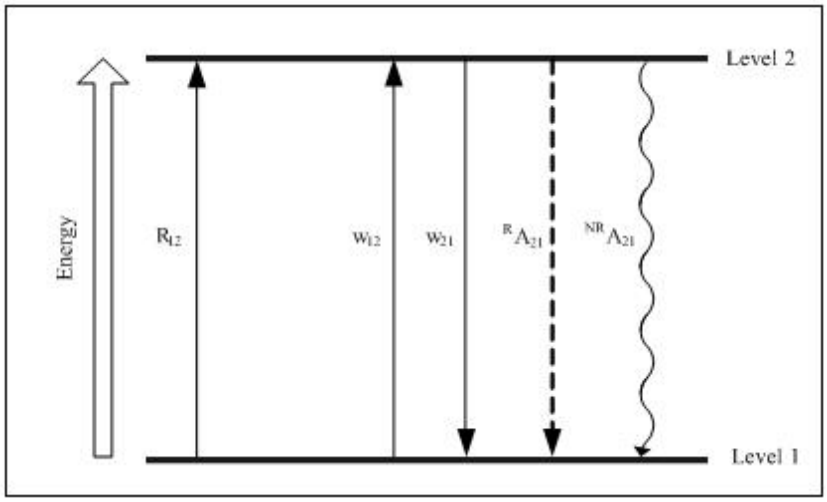

Figure 2.10: Energy level of two-level system

Consider the two energy levels system shown in Figure 2.10. Ground level is denoted by Level 1 and metastable level by Level 2. The metastable level is defined as a level where the lifetime of the system which is long compared to 100μs and it is a usual lifetime of a state which could be emptied by an allowed optical transition (Armitage, 1991). According to Figure 2.10, R_{12} is denoted as pumping rate between Level 1 to level 2.The spontaneous decay rate from Level 2 and 1 is $A_2 = RA_{21} + NRA_{21}$. It is

assumed that spontaneous decay is dominated by the radiative decay rate, i.e. $RA_{21}>>NRA_{21}$. Thus, the spontaneous decay rate between Level 2 to level 1 could be simplified to A_{21}. Generally, the transition rate of an Erbium doped fiber can be defined as thefollowing:

$$Transition\ rate = \pm \frac{I}{h\nu} \tag{2.11}$$

Where σ is the cross-section of the fiber, hv represents the band-gap energy with h being the Planck's constant and v being the frequency. I is the intensity and can be further defined as:

$$I = \frac{P}{A_{eff}} \tag{2.12}$$

Where P is the power and A_{eff} is the effective area of fiber.

The stimulated absorption and emission rates between Level 1 and 2 are denoted by W_{12} and W_{21} respectively. From (2.11) and (2.12), transition rates such as pumping rate (R_{12}), stimulated absorption rate (W_{12}), and stimulated emission rate (W_{21}) are defined below:

$$R_{12} = \frac{\pm_{ap}\Gamma_p}{h\nu_p A_{eff}} P_p \tag{2.13}$$

$$W_{12} = \frac{\pm_{as}\Gamma_s}{h\nu_s A_{eff}} \left[P_s + P_{ase}\right] \tag{2.14}$$

$$W_{21} = \frac{\pm_{es}\Gamma_s}{h\nu_s A_{eff}} \left[P_s + P_{ase}\right] \tag{2.15}$$

However, spontaneous decay rate (A_{21}) depends on the fluorescence lifetime (τ) of the excited energy level, hence, it is defined as:

$$A_{21} = \frac{1}{2} \tag{2.16}$$

The total ion density (ρ) is equal to $N_1 + N_2$. N_1 and N_2 are introduced as fractional densities of ions in the energy levels 1 and 2 respectively. In the initial condition where there is no pump, $N_2 = 0$ and $\rho = N_1$. During excitation through optical pumping, ions from Level 1 will be excited to Level 2 depending on the R_{12}. The following equations show the atomic rate transition for these ion populations (Desurvire, 1994):

$$\frac{dN_1}{dt} = -W_{12}N_1 + W_{21}N_2 + A_{21}N_2 - R_{12}N_1 \tag{2.17}$$

$$\frac{dN_2}{dt} = W_{12}N_1 - W_{21}N_2 - A_{21}N_2 + R_{12}N_1 \tag{2.18}$$

At steady state,

$$\frac{dNi}{dt} = 0 \tag{2.19}$$

Substituting (2.19) into (2.17) for N1 yields,

$$-W_{12}N_1 + W_{12}N_2 + A_{21}N_2 - R_{12}N_1 = 0 \tag{2.20}$$

Further rearranging (2.20) produces the following equation,

$$N_1(W_{12} + R_{12}) = N_2(W_{21} + A_{21}) \tag{2.21}$$

Since $\rho = N_1 + N_2$, where ρ is the total atom density, (2.16) reduces to (2.22),

$$N_1 = \frac{\circ\left(1+\frac{W_{21}}{A_{21}}\right)}{1+\frac{W_{12}}{A_{21}}+\frac{R_{12}}{A_{21}}+\frac{W_{21}}{A_{21}}} \tag{2.22}$$

Substituting (2.12) into (2.22) yields,

$$N_1 = \frac{\circ\left(1+W_{21}{}^2\right)}{1+W_{12}{}^2+W_{21}{}^2+R_{12}{}^2} \tag{2.23}$$

Substituting (2.18) into (2.17) yields,

$$W_{12}N_1 - W_{21}N_2 - A_{21}N_2 + R_{12}N_1 = 0 \tag{2.24}$$

Further rearranging (2.21) and substituting $\rho = N_1 + N_2$. Produces the following equation,

$$N_2 = \frac{\circ\left(\frac{W_{12}}{A_{21}}+\frac{R_{12}}{A_{21}}\right)}{1+\frac{W_{21}}{A_{21}}+\frac{W_{12}}{A_{21}}+\frac{R_{12}}{A_{21}}} \tag{2.25}$$

Substituting (2.12) into (2.25) yields,

$$N_2 = \frac{\circ\left(W_{12}{}^2+R_{12}{}^2\right)}{1+W_{21}{}^2+W_{12}{}^2+R_{12}{}^2} \tag{2.26}$$

2.8 TYPES OF EDFA

EDFA can be categorized to Single and Dual Function EDFA based on the number of Function that the EDFA provide. Single Function EDFA can carry out signal amplification only where the Dual Function EDFA has the ability of amplify the attenuation and compensate the dispersion in a single black box.

2.9 SINGLE FUNCTION EDFA

There are varieties of single function EDFA, which are dependent on the kind of application. Generally, past studies of EDFA are divided the single function EDFA, according to configuration, into stages and passes as follows:

2.10 ONE- STAGE EDFA

One-stage EDFA configuration means using only one EDF structure as an active area. Such a one-stage can be a single-pass or double-pass configuration as shown in Figure 2.11

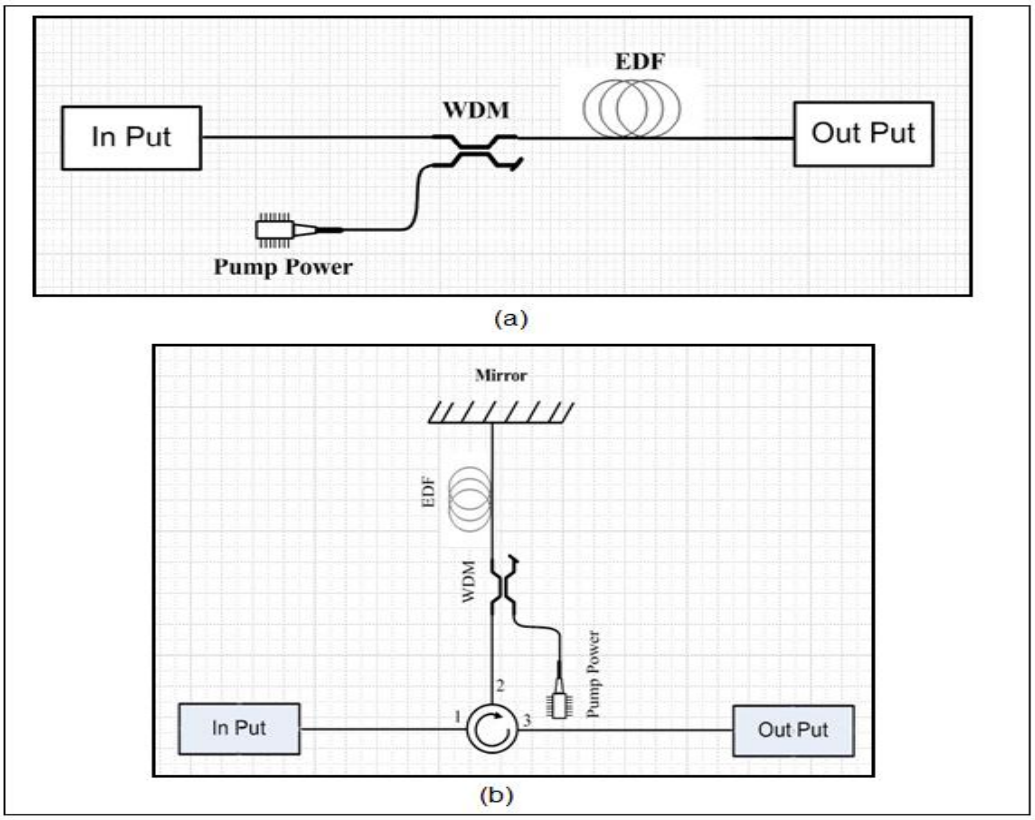

Figure 2.11: Two configurations (a) One-Stage Single Pass (b) One- Stage Double Pass

2.11 SINGLE- PASS

The basic single pass EDFA module or configuration comprises one or two pump laser diode (LD) modules with fiber output. Also one or two Wavelength Division Multiplexing (WDM) is used to collect the light from pump power while employing input and output isolators, and the active medium (EDF). All the optical components have single mode fiber (SMF) pigtails and are spliced together to form an EDFA

module as shown in Figure 2.11(a). In (Chun, 2003) Chun-Liu Zha proposed configuration for automatic gain control of optical EDFA that uses novel dual control lasers optical. The output power change of the surviving signal reduces to 5.7% when 1546nm signal are added and dropped at 1kHz. Meanwhile, the configuration is flexible and the clamped-gains can be tuned in to the range of 13.5–31.5dB. This method has some advantages such as, the grating resonance wavelengths tuned by bending the fiber section that contains the grating. In (Mrinmay, 2007) authors investigate the optical gain and NF for multichannel amplification in EDF under optimized pump condition. They experimentally studied the optical gain and NF for simultaneous multi-channel amplifications in EDFA under optimized pump condition for different input signal levels utilizing optimized fiber lengths. It observed that the gain and NF values primarily depend on the pumping configurations and produced optimum result at bi-directional pumping, whereas the gain-spectra and noise characteristics depend mainly on the population inversion level along the fiber cable length.

Moreover, EDFA is the population inversion along the fiber length controlled by varying the injected pump power. However, bi-directional pumping results in the best combination of gain and NF of EDFA. While co-propagation of pump and signal produces the best results in terms of low noise performance. Moreover, at the higher input signal power, the signal significantly depletes the inversion beyond the pump's ability to replenish it and the NFs increase rapidly with signal power. (Nadir, 2007a) looked at it from another perspective which integrated (SP-EDFA) with a chirped fiber Bragg grating (CFBG) to compensate both the attenuation and dispersion. As well as, considering the high gain and low NF by very low remote pump power .Therefore, the numerical results play an important role in designing an optimized

remotely pumped SP EDFA for the repeater- less long haul OFCS from the point of view of economic usage of pump power.

2.12 DOUBLE PASS

The basic double pass (DP-EDFA) is a state in which signal will pass two times through active medium, the erbium doped fiber (EDF) as shown in Figure 2.11(b). Theoretically it is proven that the double pass method enhances the gain twice compared to single pass procedure (Desurvire,1994). J. B. Rosolem and A. A. Juriollo investigates simple double pass configuration by using a single commercial EDFA for S-band application as well amplifier spontaneous emission (ASE). The design shows excellent gain performance when compared to the previous similar works. However, it is recognized that the gain is not flat which may require a gain-flattening device for gain equalization enhancement (Rosolem, 2008).Author (Hao, 2005) improved the NF of an EDFA with double-pass configuration. However, the amplification gain of proposed double-pass EDFA is at an average value of 1.3dB lower than that of the conventional one. Moreover, the ASE wavelengths will get amplified simultaneously with the signal ones, leading to higher NF, because the HiBi fiber loop mirror does not modulate output spectrum. (Naji, 2006a) proposed an amplifier which is able to maintain gain of higher than 20dB for small signals less than -23dBm with pump power 10mW. Double pass with chirped fiber Bragg grating to compensate the fiber dispersion as well as to amplify the only one weak signal, (Naji, 2006b). In (Nadir, 2007c) the main design objectives of the remotely pumped DP-EDFA are higher gain and low NF. However, the higher remote pump power conflicts with the main design objective of remotely pump power, where increased pump power will increase the NF. While the result in (Naji, 2004) shows that the double-pass EDFA gives a better performance for small signal powers of less than -25dBm and the single-pass EDFA

performs better for higher signal powers of greater than -25dBm. BER is used as the benchmark to indicate the performance of the repeater less transmission systems (Naji, 2007b).

2.13 TWO STAGES OF EDFA

The two-stage EDFA configuration can be double–pass, Triple-pass, or quadruple-pass as shown in Figure 2.12.

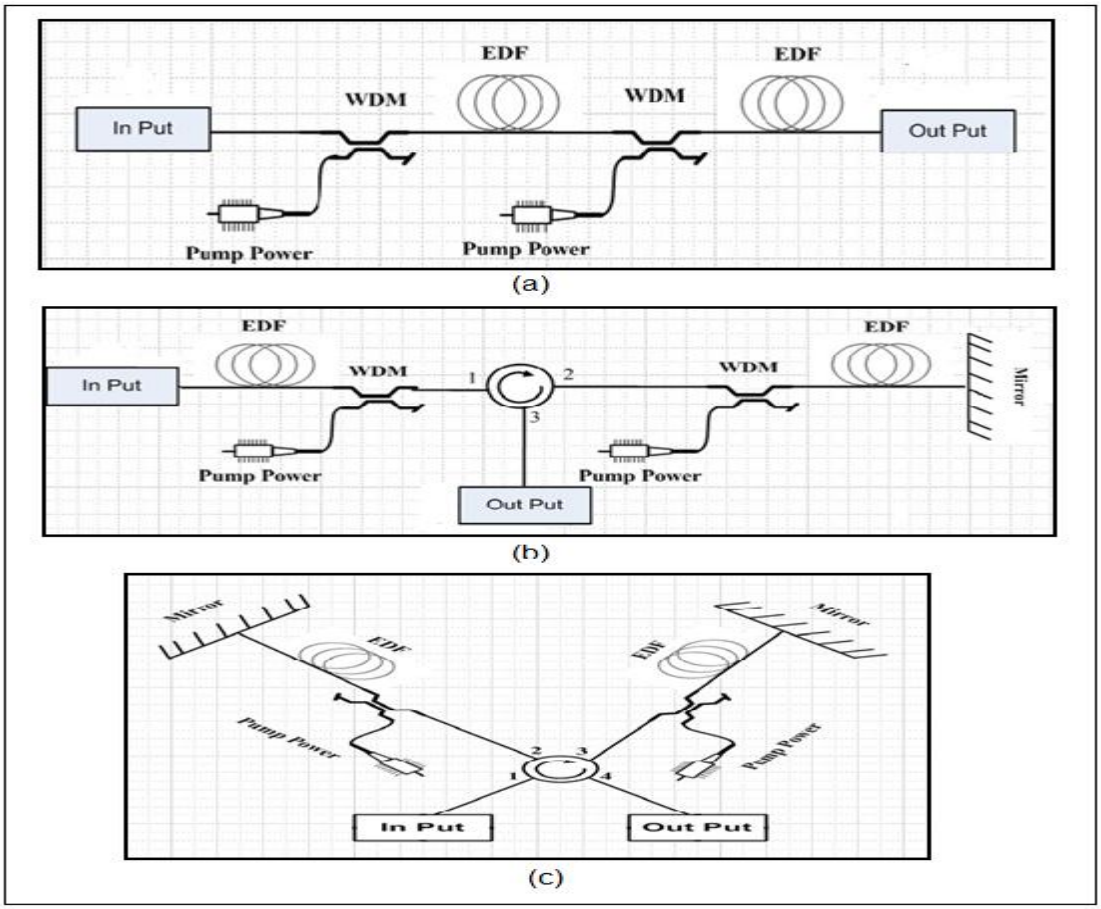

Figure 2.12: two–stage double pass (b) two- stage triple pass (c) two-stage quadruple pass EDFA Configuration

2.14 DOUBLE-PASS AMPLIFIER

A novel highly efficient EDFA structure for long bandwidth from 1570–1610 nm band signal amplification was proposed (Juhan, 1999). Four types of L-band silica-based EDFA were experimented as (a) Type I: Conventional forward pump. (b) Type II: Conventional backward pump. (c) Type III: Unpumped EDF section before forward pump. (d) Type IV: Unpumped EDF section after backward pump. The result shows that the type III has the higher gain and the lower NF 22dB and 5dB respectively compared to the other types. It is to be compared with the rest according to the gain and NF which are dramatic increase in power conversion efficiency (maximum from 11.7% to 25.7%) and small-signal gain (4dB maximum) that had been shown when compared to other EDFA structures with the same pump power and EDF length. However, the configuration is relatively suffering from a small penalty on NFs.

2.15 TRIPLE PASS AMPLIFIER

In another work, (Khairi, 2004 a) proposed a new high gain Erbium-doped fiber amplifier configured in dual-stage triple-pass amplification where the first stage amplifier provides high gains, while the second stage amplifier provides single-pass amplification. The gain value achieved is higher than 37dB at NF 6.5dB when signal power the signal power is set at -40dBm. In addition the design can be cost-effective to increase the receiver sensitivity in optical fiber communication systems. However, the NF value 6.5dB is quite high from the acceptable value of 980nm. According to (Khairi, 2004 b), and (Naji, 2006 b) a maximum is gain 51.72dB with NF of 6.1dB in their experiment at achieved 30% pump ratio. Although, 6.1dB is high compared to the acceptable NF value from 3-5dB. In this work (Belloui, 2003) provided a gain as

high as 37.5 dB with a noise figure of less than 6dB.The proposed design supports the input level as low as -43dBm all achievement with the EDF length of 7m and pump power of 90mW.

On the other hand (Chien, 2004) proposed new S- plus C-band EDFA module where 30 and 36.2dB peak gains are observed at 1506 and 1532nm, respectively when input signal power is -25dBm. Moreover, it provides a broadband ASE light source from 1480 to 1578nm while the optical output level is above -40dBm. However, the results from the experiments showed higher gain for the S and C- band, but the NF quite high at 8.2 and 7.2dBm respectively. In addition, bandwidth is still low whereas the demand today is for high capacity long haul telecommunication systems (Rolland, 1992). Therefore, broad-band EDFA with double-pass configuration is proposed by (Seongtaek, 2001) where the first stage of the EDFA combines C and L-band amplification, and the second-stage only amplifies L -band signals. The signal gain and NF obtained are more than 24dB and less than 6dB. As achieved in (Harun, 2004 b) and (Harun, 2006), the gain of about 22dB with low noise figure over the gain clamped region is maintained below 5dB and 6dB respectively. This is done by reflecting a portion of backward ASE back into the system with gain variation of less than 0.5 dB and input signal power increment up to -12dBm and -8dBm respectively.

In the study conducted by (Tsair, 2008) five different configurations of L-band erbium-doped fiber amplifier EDFAs of low NF and high clamped-gain were examined and compared. Among these configurations minimum gain variation of 2.9 dB and moderate low NF of 4.8 dB can be achieved by using fiber Bragg grating (FBG) and double-pass. This work provides the optimum gain-clamped EDFA configuration for multi-wavelength WDM L-band light wave systems.

2.16 QUADRUPLE PASS AMPLIFIER

Harun (2004c), proposed another type of amplifier, which achieve flat-gain output at 33.5dB. The gain is 13.5 dB higher than that of the single pass system with only 84 mW 980nm pumping power and the NF at flat gain region varies from 6.9 to 11.5dB. Although, the new configuration demonstrated L-band EDFA with high flat-gain, the NF is higher with respect to the pump power 980 nm. While in the work of Chang, (2006), performance three dual pumped double-pass EDFA systems were considered and compared the performances in terms of NF, gain and pump conversion efficiency. Double-pass amplifier with narrow-band reflectors is definitely better than its counterpart, because not much ASE is reflected back when using only a few narrow-band reflectors. Moreover, this new double-pass configuration provides a lower NF 4.4dB and a higher gain 34.4dB. The reason for the performance improvement by using FBGs as reflectors is that a great deal of ASE noise is filtered out and does not re-enter the EDFA to deplete the population inversion (Chang, 2006).

However, when the number of coexisting channels increases, it leads to lower gains as well as higher NF as compared to the situation in which only fewer channels coexist. On the other hand, higher gain of 61dB and NF 7dB is achieved for -50dBm signal power at 1550nm by using a fiber loop–back incorporated with tunable band pass filter (Ali, 2009).

2.16.1 Three stages of EDFA

Three-stage EDFA configuration means three EDFs that working as active areas. The three-stage is represented as follows; Triple–pass with signal passes three times on EDFs configuration as shown in Figure 2:13

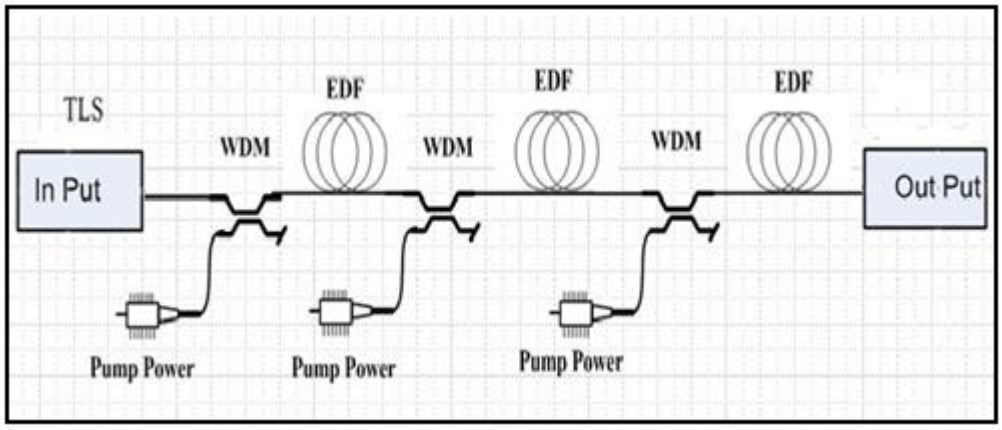

Figure 2.13: Three-stage with three-pass

(Zhi, 2003) conducted theoretical investigation where optimization of a two-pump, three-stage L-band EDFA with high-loss inter-stage element was based on a reliable numerical model. By optimizing the EDF length of each stage properly, both high-output gain and uniform NF profile can be derived even with high-loss inter-stage devices which are about 20.7 dB and 5.5 dB respectively. In addition, WDM channels add/drop scenario the former pump power and population inversion should be kept high to avoid NF degradation. (Qiang, 2004) proposed novel three-stage L-band EDFA structure with ASE pumping. The three configurations with three designs which are the first is conventional signal-stage EDFA, the second one is structure introduced, and the third is the new proposed. The numerical results under pump power 980 nm for various structures showed that gain and NF are 11dB, 19dB, 28.9dB and 5.3dB, 9dB, 3.6dB respectively. As a result, the new proposal performed excellent with respect to other structures where 28.9dB gains with only about 1dB gain ripple and less than 3.6 dB NF (from 1570nm to 1605nm) is provided when the input signal is fixed at –30dBm.

(Chin, 2007) suggested the use of using residual pump power for implementation of low-noise and high-gain L-band EDFAs by using a single 1480 nm

pump laser and -30dBm signal power for all experiments. In addition, reviews of two conventional L-bands EDFA systems have been reported to be able to enhance pump conversion efficiency (Juhan, 1999). The result at 1570nm and 1590nm showed that the first conventional L-band EDFA system got a gain of about 29dB and NF of about 6-7dB. The second conventional L-band EDFA system got a gain about 27dB and NF about 6-7dB. The new configuration comes from modifying the second conventional L-band EDFA system to get higher gain with acceptable NF where a new EDF is added between the two EDFAs in second conventional would definitely deteriorate NF. The gain and the NF for the proposed three-stage EDFA are 36dB and 4.3-4.8dB respectively which clearly shows the difference compared to the first and second conventional L-band EDFA system.

However, adding new EDF that help to reduce the NF produce little positive gain for signals which increased the cost. From the previous work, it was clearly found that pump power play very important role with significant effect on gain and noise figure. Therefore optimizing the pump power is important in order to get higher gain and low noise figure.

2.17 DUAL FUNCTION EDFA

Dual Function EDFA has the ability to provide two functions, attenuation and dispersion compensating in a single device. In additional the single function EDFA, dual function deals with the problem of dispersion, the dispersion problem has been addressed by using techniques of Dispersion Compensating Fiber (DCF), higher order mode compensator, CFBG, and bulk optical phased system. However, the technique mostly in use to compensate dispersion problem is CFBG (Naji, 2007 a). There are

many researchers tried to use CFBG as single band EDFA (SP EDFA) (Naji, 2007 b) and as double pass EDFA (DP EDFA) (Naji, 2006 a; Nadir, 2007 b).

During recent years, broadband has experienced dramatic development at a very fast-growing rate and with a penetration of full ranges of services. Wideband in optical fiber communications is therefore attracting more attention, from both governments and private institutions all over the world, due to the significant impact of wideband on Internet access speed that directly reflects to a indicator of the economy and society developments. For this reason, there is an increasing interest in designing new configurations to enhance the wideband use of the optical fiber communication.

The use of optical amplifiers has extended the span length to a point where the dispersion of the span may limit the system in other performance parameters. Components that provide the required negative dispersion based upon dispersion compensating fiber (DCF), chirped fiber Bragg gratings (CFBG), higher-order spatial mode compensators and a bulk optic phased array (Senior, 1992).

Dispersion compensating fiber (DCF) appears at present to be the most practical approach, especially when compensation over a broad spectral range is required. Fiber designs yielding the desired negative dispersion require a core refractive index difference near to 2%, higher than conventional transmission fiber designs, as well as a smaller core diameter and longer cutoff wavelength. The standard fiber has dispersion at 1550nm of 17ps / (nm × km) and to compensate the dispersion of such fiber it need to connect a shorter length of compensating fiber in series with the link. The compensating fiber typically has dispersion of -100ps / (nm × km) in 1550nm wavelength band (Harry, 1998). Because the dispersion acts in the opposite

direction to the dispersion of the standards fiber, the compensating fiber will lead to reinstate the signal.

In practice, a 100km length of standard Single Mode optical Fiber for operation at 1550nm compensated by connecting it to 17km of Double Clad Fiber (DCF). Therefore, the added length of the fiber sits at one end of the link. This adds to attenuation and additional amplification needed to compensate for the compensating fiber. DCF has a typical attenuation 0.5 dB/km. In addition, the narrow core of DCF makes it more susceptible to non-linear high power effects besides being sensitive to polarization than standard fiber.

Dispersion compensation fiber accomplished by Chirped Fiber Bragg Grating (CFBG) where the periodicity of the grating increasing continuously along the length of the grating. This provides a spectrally dependent delay, the principle of which is depicted in Figure 2.14. The shorter wavelengths (delay) reflected from the front of the grating to compensate the time delay. The longer wavelengths traveling farther into the grating before reflected because it started early. This provides a wavelength dependent time delay for reflection from the grating. The maximum delay time that the grating can offer is twice the transit time through the grating

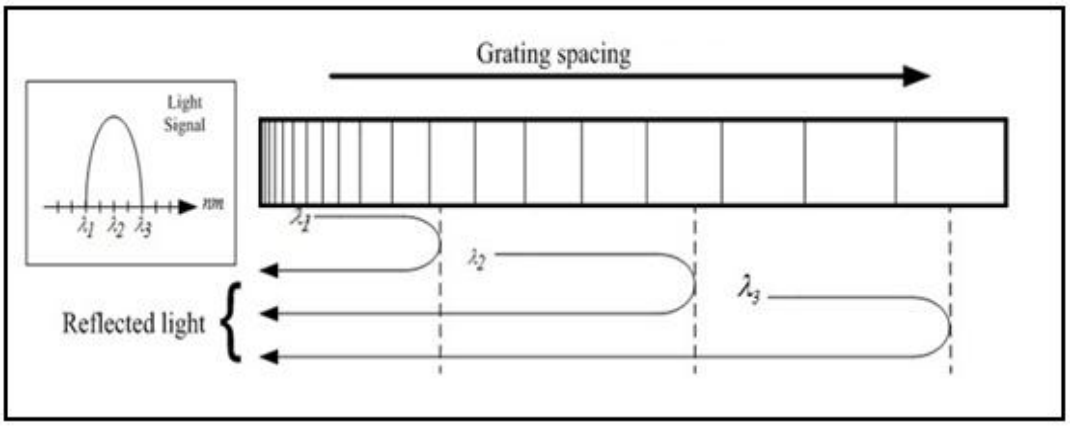

Figure 2.14: Dispersion compensation of a chirped Bragg grating

CFBG is a selective light wavelength reflector, where the wavelength selected is twice the distance between the lines written into the fiber because the light wave has to go through the region between them twice, once into the fiber grating, and once when reflected back out. If D is the grating spacing and n the refractive index of the glass, the reflected wavelength is:

$$a_{grating} = 2nD \tag{2.27}$$

Higher Order Spatial Mode Compensators the large negative waveguide dispersion of the LP_{11} higher-order mode near cutoff in a two-mode fiber may be used as a compensating fiber mechanism. A fiber index difference of greater than 2% is necessary here as well. Theory suggests that a dispersion of 70 times that of conventional fiber (1000ps / (nm × km)) is possible with this technique. Low loss conversion of the LP01 transmission mode to the LP_{11} mode and back is also a requirement for this method (Choi, 2002).

A bulk optic dispersion compensator can provide a chromatic dispersion of –2000 ps / (nm × km) to +2000ps / (nm × km) over a spectral range of 50 nm. Using this device, collimated light from a fiber is sent through a semi cylindrical lens to a 1mm thick angled glass plate. A single-channel, 1800ps/nm compensated, 10GB/s system demonstration has shown the potential of this device. Due to the periodic transmission attenuation characteristics of this device, alignment of channel wavelength spacing with the peak device transmission is required (Smith, 1999).

2.18 RELATED WORK

The purpose of this part is to present an overview of the previous and recent work related to this project, starting from fundamental configuration designs to lead into

most of the currently available amplifiers. The discussion will focus on the gain, noise figure, and length of the fiber, bandwidth, strength and weakness of the work.

(Seongtaek, 2001) proposed broadband parallel EDFA double-pass configuration that obtained more than 24dB and less than 6dB for the gain spectrum and noise figure, respectively. The same signal gain has been achieved with 53% less pump power and 45% shorter erbium-doped fiber length, compared to other such parallel EDFA of conventional type. The result shows that it is possible to reduce the required of the pump power and the EDF length from 22% to 53% that save substantial cost for wide-band WDM transmission systems by using the proposed method. However, the proposal design has two disadvantages, which are the length very long reaches 113m, which means the cost of the amplifier is very high as well as the size.

(Shih Hsu, 2002) has proposed configuration collision between optically C-band plus L-band with bandwidth 70nm from (1530–1600 nm) silica-based wideband gain-clamped (GC) erbium-doped fiber amplifier (EDFA) using a common figure-eight feedback-loop lasing light at 1568 nm, which is just located within the dead-zone between the C- and L-bands. The result shows that compared to the unclamped case, the new proposal is effective in reducing the total gain variation. However, the new design is utilizing four optical circulators, which reflect the total cost of the device. Moreover, the bandwidth of the design can approve by using new technology such as CFBG.

(Sinivasagam, 2004) proposed a wideband silica-based EDFA. The amplifier design is made of dual stage and co-pumped at 980nm with 0dBm input signal power. The result shows that the design operating in both C-band and L-band band region with 3dB bandwidth of 72nm and an average noise figure of 5.6dB with a gain

flatness about 4dB from 1528 nm to 1600 nm. However, the gain spectrum is as low as around 11dB when the input signal power is 0dBm. This is due to the EDFA at high input signal power 0dBm work close to the saturation region. Moreover, the design trying to solve only the problem of attenuation, while the dispersion problem remained.

(Hao, 2005) come out with design of amplifier EDFA that utilizing a high birefringence fiber loop mirror as the amplified spontaneous emission rejecter in order to decrease the noise figure of an erbium-doped fiber amplifier with compared with that EDFA using a conventional 3dB fiber loop mirror. The result shows that the output spectra of the double-pass amplifier based on HiBi fiber loop mirror is highly stable. Furthermore, by adjusting the length of high birefringence fiber, the period of its reflection spectrum can be set to 0.4 or 0.8nm as recommended by the International Telecommunication using division multiplexing or dense wavelength division Union for wavelength usage in wavelength multiplexing systems. However, this work used technique to improve only the noise figures of in L-band while the desired today for the wideband to increase the distance and the speed as well.

Carmelo (2005) reported that the noise performance of gain-clamped EDFAs is dependent on the pump direction, because the pump direction changes the gain dynamics in the doped fiber. The pump counter-propagates with the signal the amplifier noise figure is higher than the co-propagating case, and an all-optical gain-clamped amplifier using circulators to create the feedback loop can present a better noise performance than the configuration using directional couplers in the feedback loop. This happens because the configuration with uses directional couplers needs isolators in the input and output ports, but this is needed by the configuration that uses circulators.

An efficient pumping scheme for EDFA to reach high gain and low noise performance in a double-pass configuration is proposed (Chang, 2006). The main amplifier is composed of two sections of EDFs. A 980nm and a 1480nm pump lasers are used to pump the first section of EDF bi-directionally. The generated backward amplified spontaneous emission noise from this EDF is used to pump a subsequent un-pumped section of EDF. In the double-pass scheme, a narrow-band fiber Bragg grating at each channel wavelength is used to back-reflect the signal to make it amplified twice using the pair of EDFs. Compared to its conventional counterparts, this double-pass configuration provides a lower noise figure and a higher gain. However, the pump conversion efficiency cannot be improved by more than 50% in a 3-channel demonstration by using the proposed configuration (Chang, 2006).

(Bonada, 2007) the characterization of EDFs has special emphasis on the study of the Noise Figure. The signal gain and optical signal-to-noise ratio (OSNR) had been measured for a set of EDF's lengths and pump powers, for future optimization of remotely pumped amplification in PONs. However, they simplified NF expressions that led to unusual values at very low pump powers. Those unusual values can be explained by the analysis of specific viscosity (η_{sp}) versus Gain behavior. More general the NF expressions including shot noise are required to describe adequately the NF of EDFs at low pump powers.

Rosolem (2007) proposes a double-pass EDFA using standard erbium doped fibers for S-band operation. The proposed amplifier configuration employs a single amplification and filtering stage and the EDFA. The results suggest that the basic EDFA configuration can be a promising alternative for S-band operation. However, even the results show some improvement on the gain and noise figure but still the S-band has higher attenuation compared to the C and L-bands.

Tsair (2008) proposed five different configurations of L-band erbium-doped fiber amplifier EDFAs of low NF and high clamped-gain examined and compared. Among these configurations minimum gain variation of 2.9dB and moderate low NF of 4.8dB can be achieved by using fiber Bragg grating (FBG) and double-pass. This work provides the optimum gain-clamped EDFA configuration for multi-wavelength WDM L-band light wave systems. However, the author focused only on single-band during his work while the demand to day for the high bandwidth increases the capacity subsequently, thus leading into increasing the in amount of the information transfer from the transmitter to receiver.

Berkdemir (2009) presents a temperature-dependent analysis of an EDFA to study the effect of cooperative up conversion on the temperature dependent gain (TDG) performance of the C-band at high-concentration. The influence of temperature-dependent rate and light propagation equations, as well that of ASE, as well as the excited state absorption (ESA) is also considered. However, this work focuses to improve only the attenuation on the gain amplification and noise figure while skipping a side the dispersion problem.

(Barıs, 2009) investigates the design parameters for a simulation perspective complex effects occurring during the gain and noise figure improvement operations of EDFA, making use of an optical design simulation tool called OptiSystem. An EDFA with flat gain is simulated getting results as expected. However, this work is is carrying the problem of aliasing at the wavelength from 1560 until 1570 thus affecting the performance of the overall design. An overall comparative summary of contemporary work is tabulated in Table 2.1.

Table 2.1
Related work

Authors/Year	Title	Achievements	Limitations of the work
Tsair Liang , (*Journal Optics Comm*) **2000**	Optimum configuration and design of 1480-nm pumped L-band gain-flattened EDFA using conventional erbium-doped fiber	The investigation result provides the L-band EDFA for multi-wavelength WDM systems. The L-band EDFA is to achieve the highest channel output power while keeping the differential channel output power to be less than 0.7 Db	The band is limited to 32 channels which is operating in L-band , also this work focus on the attenuation only
Seongtaek Hwang,et al. (IEEE Photonics Techno letters) 2001	Broad-Band Erbium-Doped Fiber Amplifier With Double-Pass Configuration	By using this method, the required pump power and EDF length can be reduced by 22–53%, and thus, we can save substantial cost for wide-band WDM transmission systems	The proposal design has two disadvantages, the length very long reaches 113m, which means the cost of the amplifier is very high and the size of the amplifier is big
Chun, et al. (Journal Optics Comm) 2003	Optical automatic gain control of EDFA using two oscillating lasers in a single feedback loop	This simple structure significantly reduces steady state and transient gain deviations, compared with single control laser EDFA. As well as the configuration is flexible and the clamped-gains can be tuned in the range of 31.5–13.5 dB.	The band is limited in one wavelength which is (1546 nm) in C-band, this work is not focus to compensate the dispersion

Naji, et al. (Journal Microw. Op) 2004	Efficient 1480 nm er3+-doped fiber amplifier using narrow-band filtering in double-pass amplification	The EDFA gives higher FOM for small signal powers less than -22dBm for double pass amplification, while single pass gives higher FOM at higher signal powers	The band is limited to one channels 1550.3 nm which is operating in C-band, this work also not focus on dispersion problem.
Qiang Ze-xuan & et al (Journal of Zhejia U S) 2004	A novel 3-stage structure for a low-noise, high-gain and gain-flattened L-band erbium doped fiber amplifier	The present L-band EDFA structure can be optimized to achieve better performance by using e.g. a genetic algorithm (a global optimization method)	Even this work has bandwidth about 35 nm but this only in L-band. Moreover, the work overcome the attenuation only.
Sinivasagam, et al (IEEE Conference) 2004	C-plus L-band EDFA with over 70nm operating range	The amplifier design is made of a dual stage, co-pumped at 980 nm which delivers an average output power of 10.4dBm over the entire 3dB bandwidth of 72 nm at 0 dBm input power representing 100 WDM channels at -20 dBm/ch	This work obtained bandwidth about 72 nm at zero dBm where this input signal power is close to the gain saturation. The small input signal power allow the signal to travel long distance before to reach the saturation
Harun, (ECTI Trans) 2004	Demonstration of Highly Efficient Flat-Gain L-Band EDFA With Two-Stage Double-Pass Configuration	The design came out with suitable gain master for the L-band.	This amplifier has obtained bandwidth about 60nm. However this band is only in L-band.
Hao Zhang, et al (Journal Optics Comm) 2005	Noise figure improvement of a double-pass erbium-doped fiber amplifier by using a HiBi	The experimental observation shows that the output spectra of the double-pass amplifier based on HiBi fiber loop	The proposed design operates with only signal wavelength in L-band 1584.22 nm. the proposal also Ignore to compensate the dispersion

	fiber loop mirror as ASE rejecter	mirror is highly stable which ensures its feasibility for potential use in the future applications	
Naji, M. S. Z. Abidin et al (Jo Mic. Op USA) 2006a	Repeaterless Transmission Incorporating Enhanced Remotely-Pumped EDFA and Distributed Raman Amplifier	The proposed amplifier architecture is able to maintain gain of higher than 20 dB for small signals with 10 mW pump power	The band of this work is limited to one channels 1550.3 nm operating in C-band.
Harun, (Journal of physical) 2006	Gain-clamping techniques in two-stage double-pass L-band EDFA	This scheme achieves a good gain clamping characteristic up to -12 dBm of input signal power with a gain variation of less than ±0.3 dB from a clamped gain of 22 dB	This work focuses only in single wavelength and solves the attenuation problem. Whereas the problem of dispersion still exist
M. Foroni, L. Ruggeri, (Optical fiber conferen) 2006	40 dB gain S-band depressed-cladding EDFA with double-pass configuration	Comparison between SP and DP gain values has demonstrated that the DP configuration allows a gain increase of almost 10 dB.	Even the gain obtained is 40dB; this amplifier is operating for short bandwidth only. As well as, the noise figure is high.
Mrinmay , et al. (Optical And Quantum Electronics) 2007	Study of gain flatness for multi-channel amplification in single stage EDFA for WDM applications	A specific loss spectrum of GFF is obtained by writing a chirped fiber Bragg grating of length 20 mm. Gain variations are studied by changing the total input signal levels from -8.0 dBm to -20.0 dBm and maintained within 20.0 +/- 0.5 dB by	This Proposal is operating in C-band from 1532 to 1558nm only and no focusing on compensating the attenuation only

		using automatic gain control (AGC) circuit	
Nadir, et al (*IEICE Electronics Express*) 2007d	Numerical Analysis and Optimization of Remotely Pumped Double Pass Erbium Doped Fiber Amplifier	numerical results will play an important role in the design of an optimized remotely pumped SP EDFA for the repeater less long haul OFCS	The proposal design has focus on C-band only and overcome the problem of the attenuation of the signal.
Chin-Feng Su , et al. (Journal Optics Comm) **2007**	Gain enhancement of L-band EDFA by using residual pump power in a three-stage configuration	It is noted that a double-pass EDFA can provide a higher gain but, the proposed single-pass system have low cost and NF	This amplifier has obtained bandwidth about 20 nm . However this band is only in L-band
Tsair, Liang et al (Journal Optics Comm) 2008	The L-band EDFA of high clamped gain and low noise figure implemented using fiber Bragg grating and double-pass method	This work provides the optimum gain-clamped EDFA configuration for multi-wavelength WDM L-band light wave systems	This work focus only in single wavelength 1615 nm for L-band and solve the attenuation problem and the problem of dispersion still exist
S. Ali and et al. (Journal appl sce inf) 2009	A new Erbium Doped Fiber Amplifier	The Dual Stage Quadruple Pass (DSQP) has proved to be a high gain EDFA with acceptable NF. It utilizes two pump lasers of 980 nm and TPF filters to suppress noise and amplified spontaneous emission	The proposal design has disadvantages the that improve the gain but the effect of the dispersion remain .

Kaur, Inderpreet Al 2010	Enhancing the Performance of WDM Systems By Using TFF In Hybrid Amplifiers	The gain spectrum of EDFA has been broadened and flattened by cascading EDFA with TDFA along with a dielectric Interference filter (TFF)	This work operation in S and C-band for 65 nm , however, the duration of S-band has high attenuation camper to C-band

2.19 SUMMARY

The basic understanding on Optical Fiber Communication System (OFCS) is given with emphasis on the causes of attenuation and dispersion of light as it travels down the fiber. The phenomenon of light absorption and emission in contrast to energy levels transitions is explained. The principle of light amplification is elaborated, showing how this process avoids the complicated stage of converting light into current signals just for amplification reason. The principle of doping explained shows its potential benefits in enhancing the range and reducing light attenuation and dispersion in OFCS. The concept of how an energy loss due dispersion and attenuation degrades the span and system performance to a level point tempting researchers to explore. The chapter ends in making up a ground for understanding why techniques of dispersion compensating fiber, Fiber Bragg Gratings, higher-order spatial mode compensators are becoming important these days as dispersion compensating components in an optical transmission system.

CHAPTER 3

SIMULATION OF THE HIGHCONCENTRATION ERBIUM-DOPED FIBER

3.1 INTRODUCTION

Since the emergence on the market of its first generation developed in 1988, the Erbium-Doped-Fiber (EDF) has been evolving continuously as an active medium. Every new generation brings in newer design and performance of an amplifier closer to that of the ideal in term of gain and noise figure (Admela, 1998). Recently, Fibercore introduced a new high concentration doping technology opening thus the door for the fifth generation of EDF. The new generation, called IsoGain™ has three developed iterations starting from I-4, I-6, and finally ending up in I-25. The latest active medium fiber (I-25) claims to have addressed the EDFA manufacturers' concerns properly by providing a more suitable solution. This design has been able in producing better flat gain filters (GFF) for facilitating multi-channels sourcing in both C and L band. This chapter reviews the absorption and emission characteristics of the highly concentrated EDF and the simulation of the EDFA using a GainMasterTM software.

3.2 ABSORPTION AND EMISSION CROSS SECTIONS

Two very important parameters in any Erbium-Doped Fiber Amplifier are the absorption and emission cross sections. These parameters are to measure fiber's absorption and emission efficiencies as a function of the wavelength of the laser light travelling through it. The absorption cross-section is the probability of the existence of

an ion absorbing an incident photon in a given cross section area. On the other hand, the emission cross section is the probability of photon emission by an excited ion in a given cross section area. Moreover, the absorption and emission section are the action of the energy levels of the Er^{3+} ions in the active medium when the erbium ions are introduced by external agency into a host medium the energy levels are modified by local electric filed through stark splitting. This phenomena happens when the charge distribution in glass host generates permanent electric field, called legend filed or crystal filed that induces a stark effect which results in the splitting of main levels of the energy levels into sublevels as shown in Figure 3.1. Therefore, in a high concentration active medium, such as that latest introduced by I-25, the increment of the Er^{3+} density in the active medium has a direct effects on the energy of the stark splitting level at $^4I_{15/2}$ and $^4I_{13/2}$. Such phenomena contribute directly to the gain, noise figure and flatness of any EDFA.

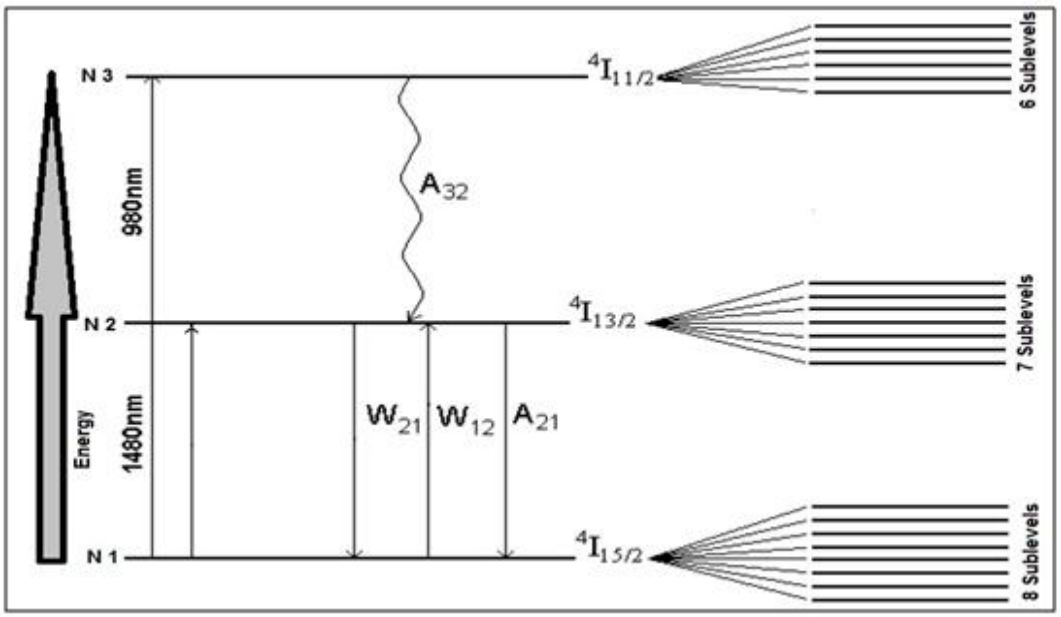

Figure 3.1: Energy level diagram for Erbium corresponding to a stark splitting (Desurvier, 1994)

Unlike other types of EDFA, which uses long distance active medium, the I-25 has a different distribution profile of the pump power over the active medium; this profile has also a direct effect on the gain, noise figure and flatness of the EDFA.

3.2.1 Absorption and Emission of I-4

The lowest-doped variant I-4 will provide the longest optimum gain-length for a given EDFA design but has the advantage that its performance is more tolerant to small changes, either in the accuracy to which this length cut or to small variations in peak absorption as shown in Figure 3.2. This benefit can therefore lower overall costs by lowering EDFA manufacturing tolerances.

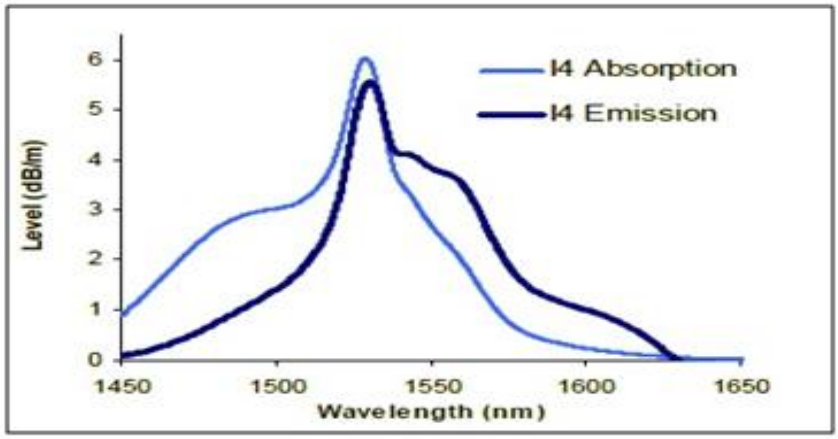

Figure 3.2: The absorption and emission of I-4 EDFA

3.2.2 Absorption and Emission of I-6

I-6 provides a shorter optimum gain length and therefore a reduction in material costs, in return for a slight increase in sensitivity to length and/or variations in absorption as shown in Figure 3.3.

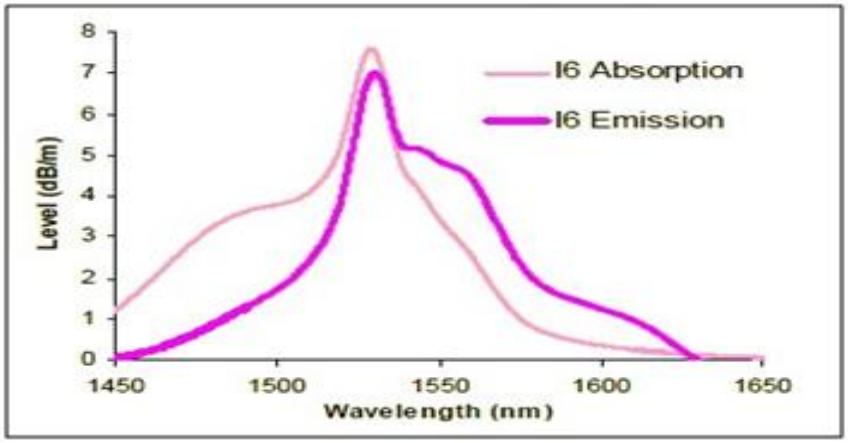

Figure 3.3: The absorption and emission of I-6 EDF.

3.2.3 Absorption and Emission of I-25

The I-25 type fiber is introduced to provide the required gain with only a few meters of EDF in the C-band and reducing the exceptionally long gain lengths required for effective L-band amplification. In addition to enabling the GFF designs and multi-sourcing, the developer of I-25 claims that the new active medium provides the ultimate gain in C-band with only a few meters and it is suitable for reducing the exceptionally long gain lengths required for effective L-band amplification. The absorption and emission profile of I-25 is as shown in Figure 3.4.

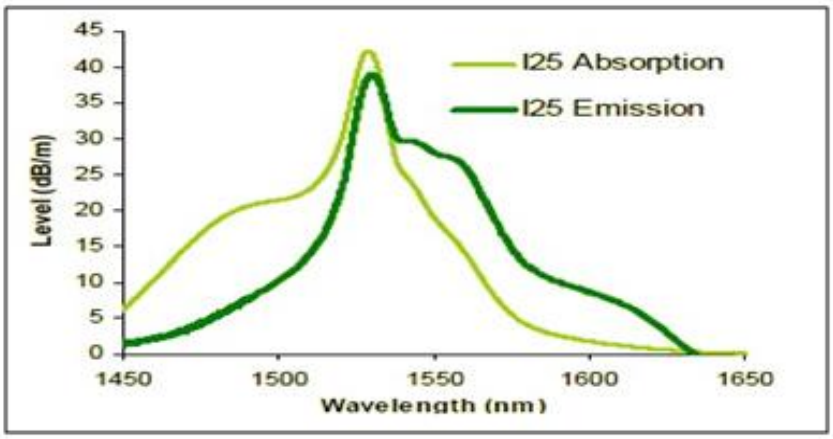

Figure 3.4: The absorption and emission of I-25 EDF.

In conclusion, the I-25 shows a higher absorption and emission profile compared to other fifth generation EDFs (I-4 and I-6). Figure 3.5 illustrates the significant difference in absorption and emission of the I-25 compared to the other two types of EDF.

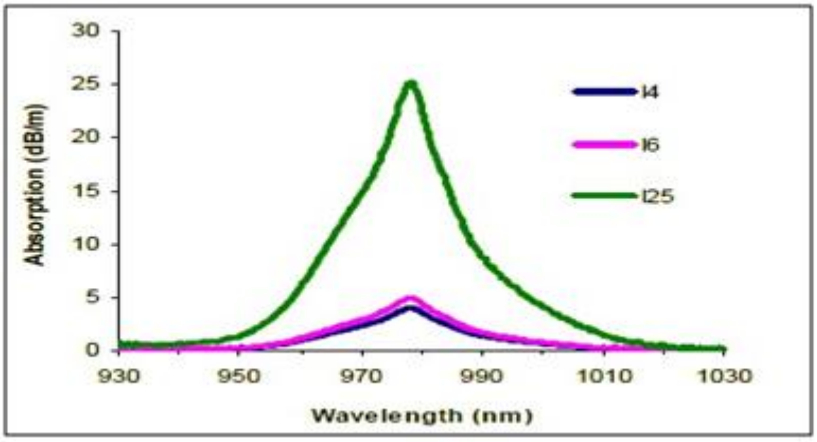

Figure 3.5: The absorption and emission of I-25 EDF.

3.3 ERBIUM-DOPED FIBER AMPLIFIER

The general characteristics of Erbium-doped fiber amplifier (EDFA) are dependent on the amplifier application, specific performance or other similar characteristics required of an EDF amplifier. Generally, the amplifier should be design to achieve optimum performances such as high and flat gain, low noise figure, gain flatness and wide amplification band. An EDFA configuration consists of the main parts as shown in Figure 3.6, where a section (in nm range) of the core of a silica fiber is doped with erbium ions and can be pumped with a laser at power and wavelength sufficient to exhibits gain in the given doped region.

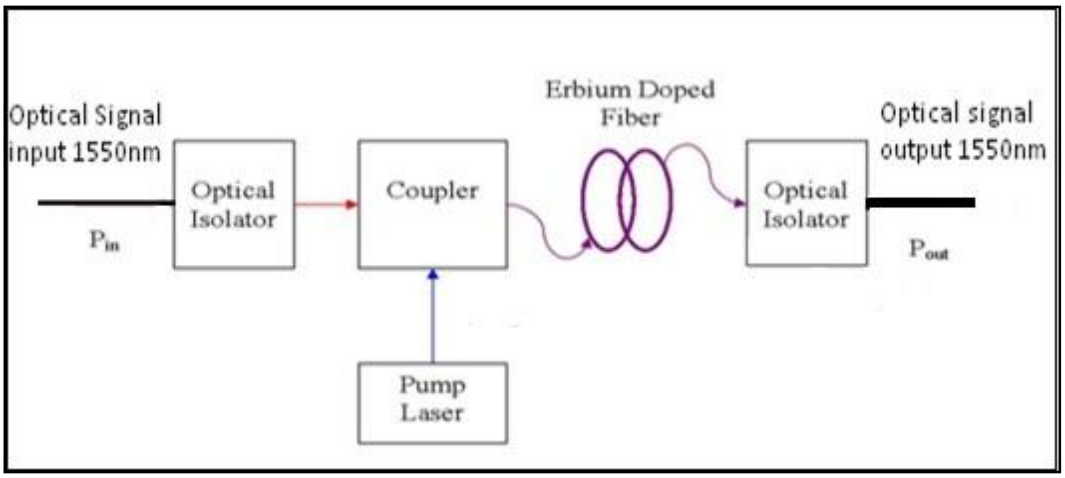

Figure 3.6: Configuration layout of an EDFA

The incoming optical signal combines with light from a pump laser to be transmitted over a length of doped optical fiber. The amplified optical signal is output after having filtered from the pump laser any residual light.

In order to further investigate the differences and the impact of the previous mentioned IsoGain™ active medium on the overall performance of an EDFA, a conventional single pass EDFA (as shown in Figure 3.6) is configured to carry out some simulation and experimental works for both C and L bands.

As shown in Figure 3.7 a tunable laser source (TLS), is utilized to provide the optical input signal for being injected in the EDF through a variable optical attenuator (VOA). This provides the EDFA with features ability to vary the input signal power. The two isolators, before and after the active material region, have isolation of over 55dB. A 1480nm pump laser is used to provide optical energy in a forward pumping direction. A 1480/1550nm wavelength division multiplexer (WDM) is used to multiplex and demultiplex the signal and pump lights. The signal will pass through the EDF and optical spectrum analyzer (OSA) to measure the output optical signal

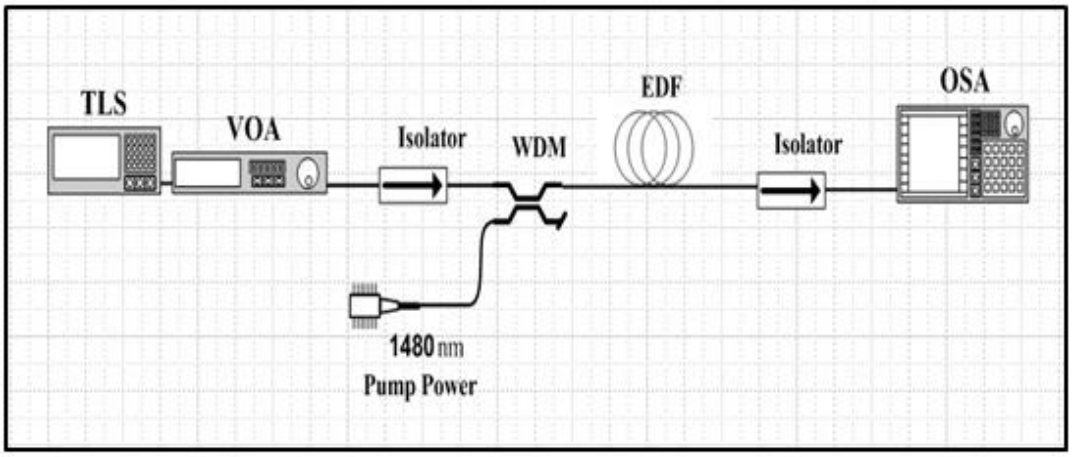

Figure 3.7: Configuration of Single Pass EDFA.

3.4 SIMULATION MODEL OF EDFA

A number of commercial EDFA simulation software is available in the market. Such simulation tools include OptiSystem Amplifier Edition from Optiwave Systems Inc., Bitline EDFA Calculators from Bitline System Pty. Ltd., GainMaster™ from Fibercore Limited and OASIX® from Lucent Technologies. Software simulation tools such as Bitline EDFA Calculators and OptiSystem are very powerful tools to analyze EDF with different structures and designs, where the EDF physical parameters (e.g. Er^{3+} concentration, cross-section data, etc) are configurable. On the other hand, GainMaster™ is capable of analyzing a wide range of configurations and accurately predicting EDFA performance. This software is very much suitable for designing many EDF types according to manufacturers' provisions. GainMaster is used to simulate the above-mentioned EDFA configuration as shown in Figure 3.7.

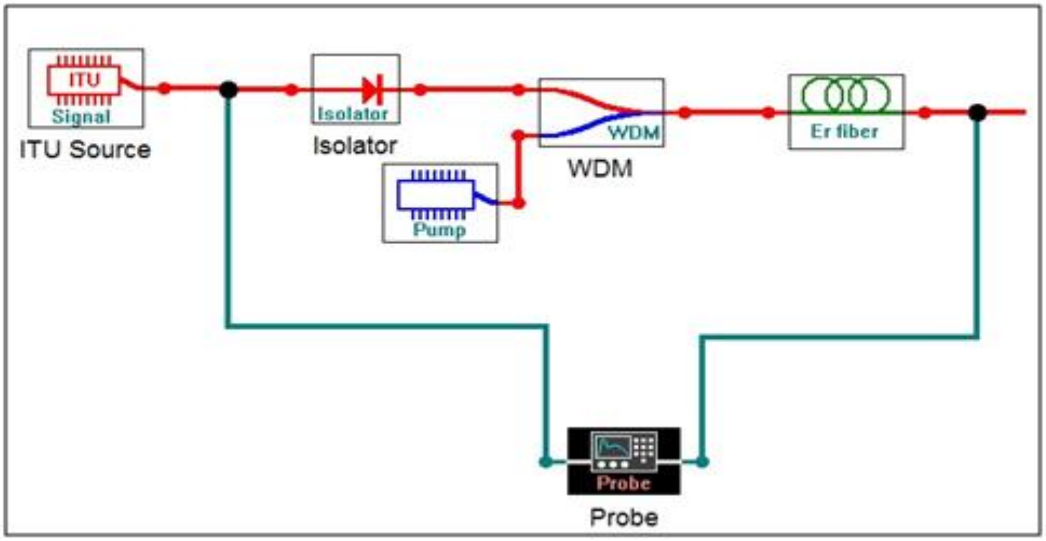

Figure 3.8: Schematic diagram of an EDFA (I-25) with forward pumping configuration obtained from GainMaster™ software tool.

A single signal source operating at power of -30dBm (small input signal power) and wavelength of 1550nm is used as input signal to the EDFA. The EDFA's forward pump comes from the 1480nm, while Wavelength Division Multiplexer (WDM) combines the signal and the pump power. An Isolator is placed after the TLS directly to prevent the reflection of ASE, which may cause problem to the TLS. In this simulation model a probe component is used to take measurements of the amplifier's gain and noise figure. The IsoGain™ I-25 EDF is used as a gain medium in various amplifier configurations. The specifications of the I-25 are as shown in Table 3.1

Table 3.1
Specifications of I-25 EDF

Parameters	Value
Er^{3+} concentration profile	2200 ppm
Peak Absorption (nominally 1530 nm)	41.14 dB/m
Absorption @ 979 nm	24.6 dB/m
Attenuation @ 1200 nm	6.8 dB/km
Coating Diameter	239.5 microns
Core Concentricity	0.09 microns
Cut-off Wavelength	910 nm
Fiber Diameter	125.2 microns
Mode Field Diameter	5.7 microns
Numerical Aperture	0.24
Operating Wavelength	1550 nm

3.5 EDFA DESIGN PARAMETERS

The two main design parameters for any EDFA are pump power and EDF length as discussed in the next sections.

3.5.1 Pump Power

The pump power is the first parameter contributing to the performance of EDFA. Two possible basic pumping configurations used are forward pumping and backward pumping. The forward pumping refers to the pump signal propagating in the same direction as that of the signal, whereas in backward pumping (also called counter-propagating) the pump power signal travels in a direction opposite to the signal. In the small signal regime, both forward and backward pumping yield the same gain and the

pump power is the main affecting factor. This is due to the fact taht Amplified Spontaneous Emission (ASE) noise pattern generated by both pumping configurations are mirror images of each other and hence the average upper state population is the same. However, in terms of noise figure the forward pumping offers a lowest noise figure compared to counter pumping technique. Hence, the signal experiences higher gain per unit length at the beginning than at the end of the fiber in the forward pumping and thus it helps in reducing signal loss that might degrade the noise figure (P. C. Becker, 1999).

Using GainMaster™, the performance of single pass EDFA is investigated using two pump power sources with wavelength 980nm and 1480nm. Whereas the lengths tested vary from being 0.5 to 5m and from 0.5 to 10m for C-band and L-band respectively. The pump power is fixed at the maximum pump power of 150mW for both C-band and L-band. This simulation work is carried out to analyze the impact of laser diode wavelength on the overall performance of EDFA. The simulation results are as shown in Figure 3.9. As illustrated in the figure for both signals (1550nm is representative of C-band and 1590nm representative of L-band), the 1480nm pump power has been found to generate a higher gain than the 980nm. This is due to the higher quantum efficiency of the 1480nm pump over the fiber length. As expected, the 980nm pumped amplifier achieved a small noise figure than that by the 1480nm.

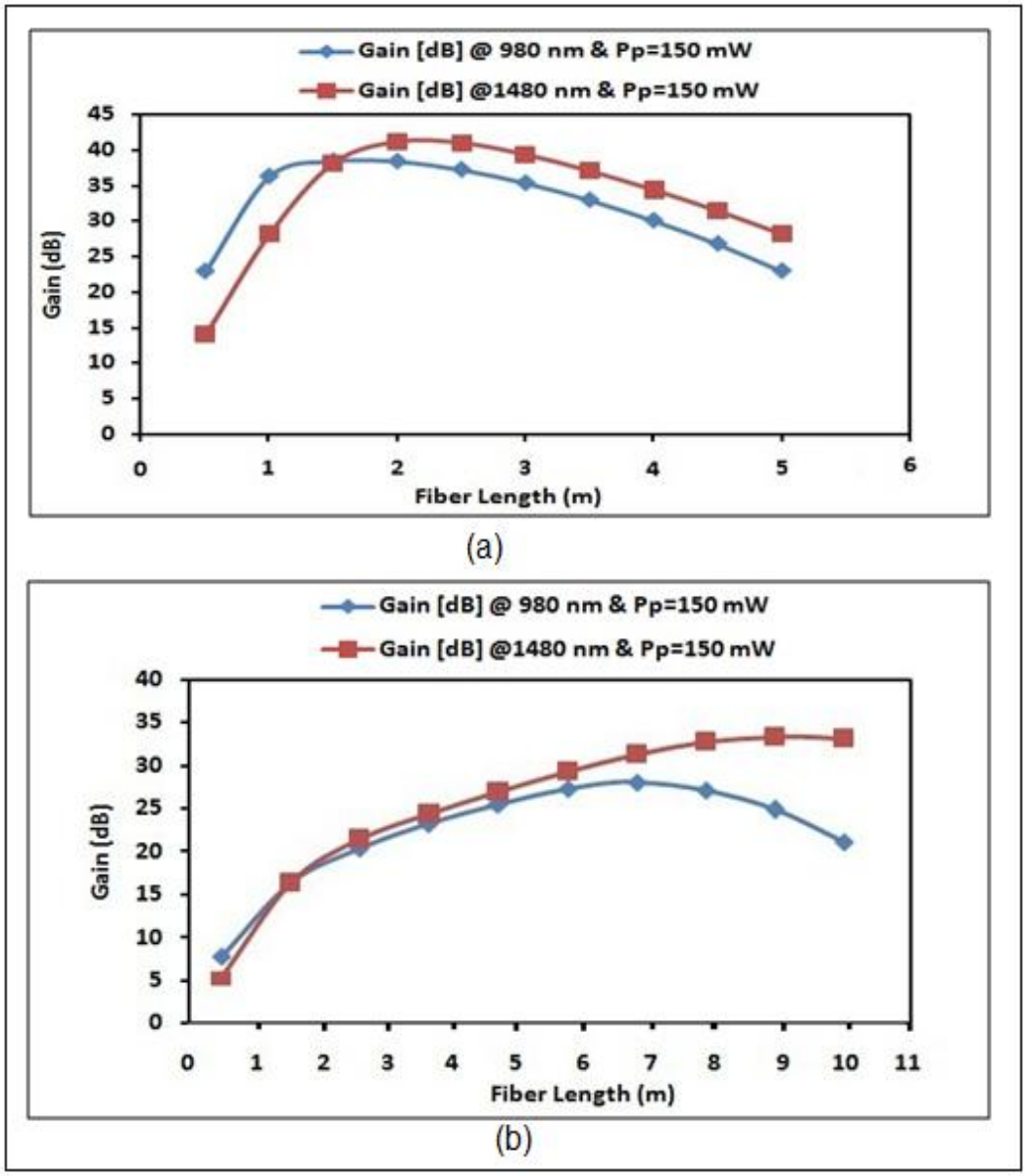

Figure 3.9: Simulation results for forward pumped EDFA with signal at 1550nm and 1590 nm for C-band and L-band respectively with -35dBm: (a) C-band and (b) L-band.

3.5.2 The length of EDF

The EDF parameters of core diameter and cutoff wavelength are designed and specified by the manufacturers for applications depending upon their specific usage requirements. The EDF amplifiers are to designed and optimized differently for best performance. The aim of using specified EDF for an optical amplifier is to have a

maximum signal gain and low noise figure. The optimum length is dependent on the input pump power. In addition, the optimum length also depends on the signal wavelengths, due to the wavelength dependency of the pump absorption and signal gain coefficients (Desurvire, 1994). As the pump absorption and signal, gain coefficients are proportional to the $Er3^{+}$ concentration profile, the optimum fiber length is also a function of the $Er3^{+}$ concentration and doping profiles.

As a conclusion, for any EDFA active medium length, signal wavelengths, pump wavelength and power make up the influencing factors for the EDFA performance. As shown in previous section, the 1480nm pump wavelength generates higher gain than 980nm pump using the same power strength. This is due to the fact that 1480nm wavelength induces higher population inversion than 980nm. On the other hand, the 980nm band has a higher absorption cross-section and hence provides lower more effective noise figure. The 1480nm band has a lower and broader absorption cross-section, yielding higher quantum efficiency and higher output power.

As shown in Figure 3.10 (a), at any particular fiber length in the specified range of 0-5m, the gain of the EDFA increases with the increase of pump power. At higher pump power the population inversion is higher resulting into correspondingly higher gain. On the other hand, at any particular pump power, the gain increases up to a certain fiber length, and then start to decrease after reaching the maximum value at its saturation point. The decrease in gain after reaching the maximum saturation point is due to low or insufficient population inversion at the last section of the fiber, causing signal attenuation instead of signal gain. The optimum fiber length in which the gain achieves maximum value can be determined from its specification graph. At 140mW pump power, the optimum fiber length is approximately 1.5m with maximum gain about 43dB.

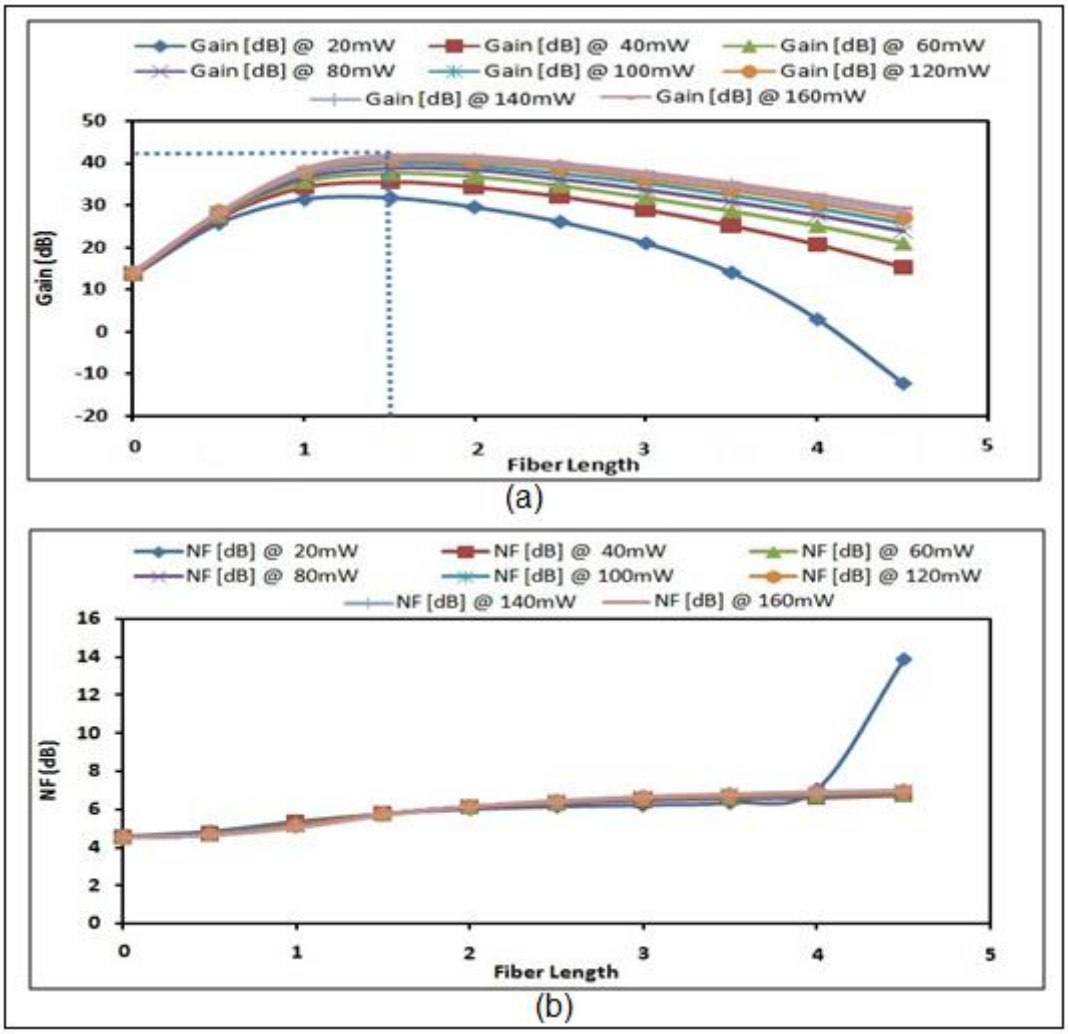

Figure 3.10: Simulation results of forward pumped EDFA with signal at 1550nm and -30dBm for 1480nm pump at different power: (a) gain versus fiber length (b) noise figure versus fiber length.

From the Figure 3.10 (b) it is clear that at any particular fiber length, it is noticed that the noise figure does not vary much with the increase of pump power. Nevertheless, the numerical data from simulation results show a slight decrease (in the order of 0.05dB) in the noise figure when pump power is increased. For the increment of pump power from 20mW to 160mW, the amplifier achieves a relatively high gain that is enough to suppress spontaneous emission, which in turn decreases noise figure. Figure 3.10 (b) also show that for a fixed pump power, the noise figure increases as

the EDF length increases. This is attributed to the decreasing gain after the fiber length has reached its optimum value.

On the other hand, the L-band (1565-1620 nm) is also investigated when the pumped power varies over the range of 20mW to 160mW with longest fiber length 10m.The simulation results for gain and noise figure are shown in Figure 3.11.

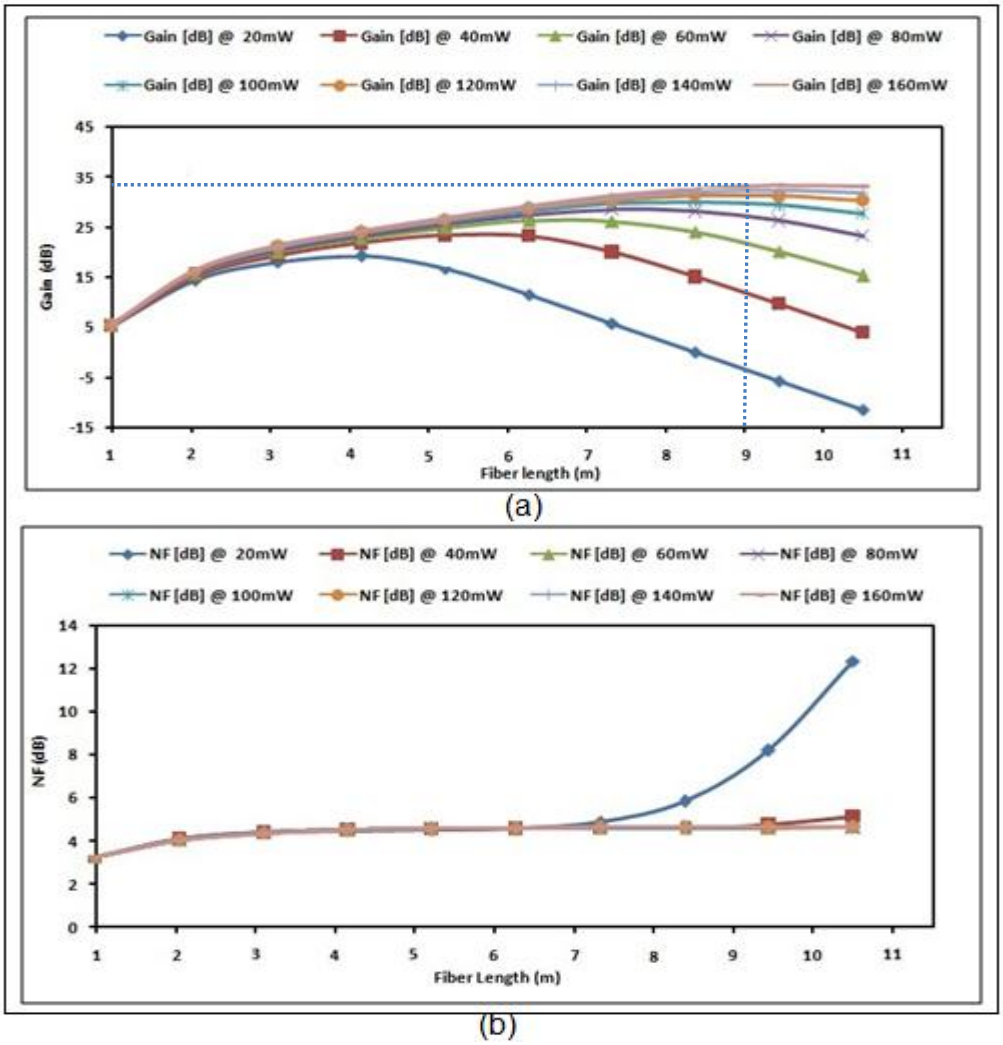

Figure 3.11: Simulation results of forward pumped EDFA with signal at 1550nm and -30dBm for 1480nm pump at different power: (a) gain versus fiber length (b) noise figure versus fiber length.

As shown in Figure 3.11 (a), same as in the case of C-band at any particular pump power, the gain increases up to a certain fiber length, and then starts to decrease after

reaching the maximum saturation point. The decrease in gain after reaching the maximum point is due to low or insufficient population inversion at the last section of the fiber, causing signal attenuation instead of signal gain. The optimum fiber length in which the gain achieves maximum value can be determined from specification graph. At 160mW pump power, the optimum fiber length is approximately 9m with maximum gain about 33.5dB. From Figure 3.11 (b) it is to be observed that the noise figure does not vary much with the increase in pump power.

3.6 EDFA PERFORMANCE PARAMETERS

The previous simulation works show that the optimum fiber length for this EDFA configuration with 1480nm pumped at 140mW and 160mW for C-band and L-band respectively, the optimum fiber length is found to be 1.5m which gives a maximum gain of about 24.76dB. Using this optimum fiber length, more simulations are carried out to investigate the characteristics of I-25. Figure 3.12 shows the gain and noise figure spectra of the EDFA in the C-band region (1520nm to 1565nm).

For the C-band region, Figure 3.12 (a) shows EDFA gain spectrum at two different input signal powers, -30dBm and 0dBm. Theoretically, the gain spectrum is proportional to the difference between emission and absorption cross sections of the EDF, which is a function of wavelength. This behavior is observed in the simulation results. For small signal of -30dBm, the average gain of 22.5dB is obtained over the C-band (1525-1565nm).

For shorter wavelength in the range of 1520-1525nm, the gain is relatively smaller. This is due to bigger difference between the emission and absorption cross sections of EDF. On the other hand, the high input signal power (0dBm) gives low average gain of 6.5dB over the C-band region. In addition, the gain slightly increases

with the increase in wavelength. For instance, the gain starts at as low as 5dB at 1530 nm, then starts up gradually to increase until the end of the fiber where the gain is about 9dB.

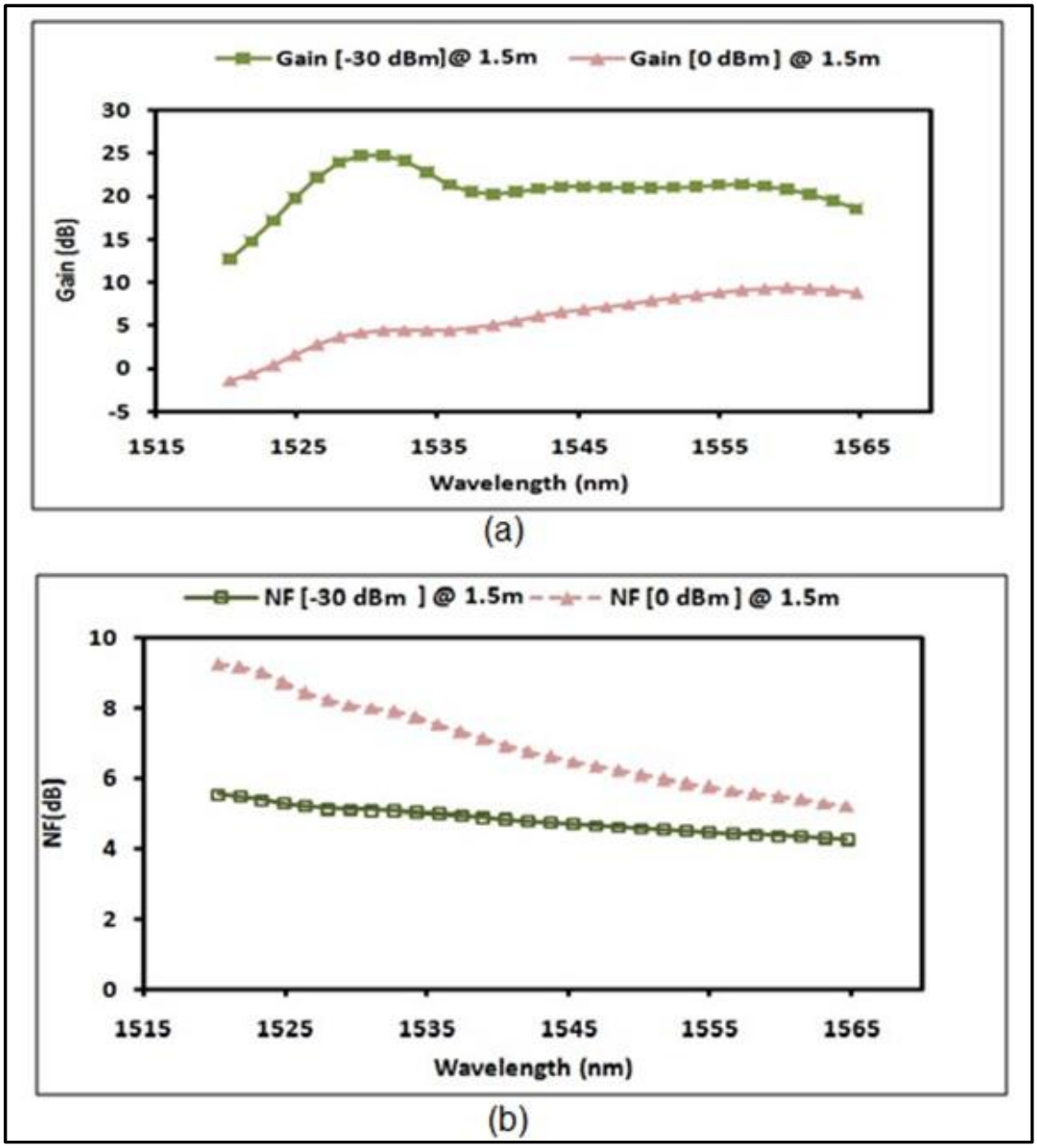

Figure 3.12: Simulation results for EDFA with 1480nm forward pumping at 150mW and fiber length 1.5m: (a) gain spectrum (b) noise figure spectrum.

The noise figure also varies with wavelength as shown in Figure 3.12(b). The noise figure is also a function of the cross section; therefore, longer signal wavelengths will have a lower noise figure. It is observed from the simulation results where noise figure decreases with increase in signal wavelength for both input signal power. It is also observed that the noise figure is lower for large signal because of gain saturation caused by high signal input. Furthermore, the noise figure at the high input signal power is higher by 4dB compared to the low input signal power due to the low input signal power which is close to gain saturation. As a result, the overall average noise figure in C-band region is 4.9dB and 7.3dB for -30dBm and 0dBm respectively.

Figure 3.13(a) shows the EDFA gain spectrum at two different input signal powers of -30dBm and 0dBm for the L-band region (1565nm to 1620nm). As mentioned in the C-band region, the gain spectrum is proportional to the difference between emission and absorption cross sections of the EDF, which is a function of wavelength. From the simulation results at small signal (-30dBm), the average gain of 26.5dB is obtained over the C-band (1530-1565nm). Unlike to the C-band region the L-band at shorter wavelength (1565-1590nm), gain is relatively higher owing to the effect of the population inversion which is larger at smaller input signals, whereas high inputs signal suppress the population inversion and thus reduce the gain.

As for high input signal power of 0dBm, the average gain over the L-band region is very low at about 4.6dB. Besides, the figure shows clearly that the difference of the gain is very big especially at the smaller wavelengths of the L-band. For example, the gain value is 37dB at the wavelength 1565nm at power of -30dB, whereas at the same wavelength the gain is -7dB at power of 0dBm.

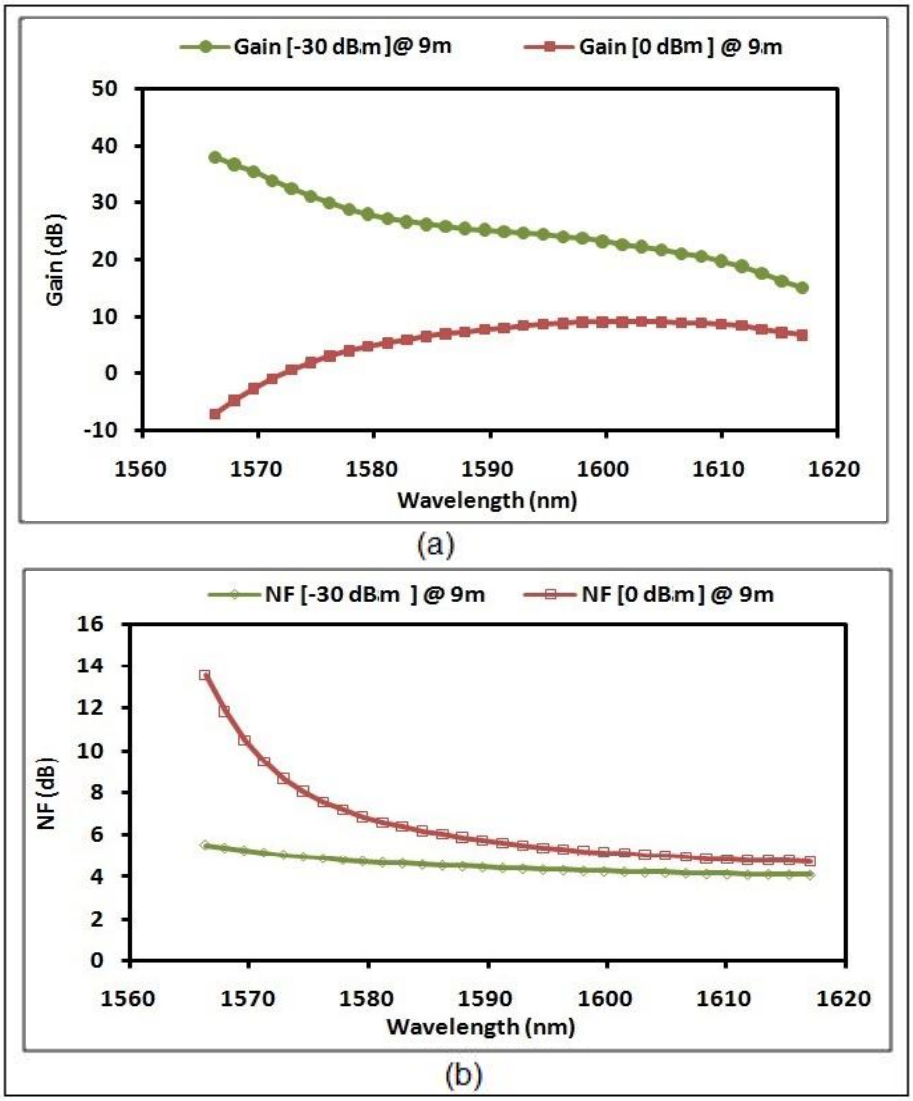

Figure 3.13: Simulation results for EDFA with 1480nm forward pumped at 150mW and fiber length 9m: (a) gain spectrum (b) noise figure spectrum.

Figure 3.13(b) shows the noise figure varies with wavelength. As shown that the simulation results are showing noise figure that decreases with increase in signal wavelength. It is also observed that the noise figure is lower for large signal because of gain saturation caused by high signal input. Furthermore, overall L-band region, the average noise figure is 10dB whereas it is almost fixed for large input signal power with 5.4dB. From the results of simulation both C-band and L-band regions, it is clear

that the low input signal power of -30dBm, the gain is higher than the high input signal power of 0dB.

Figure 3.12(b) shows the noise figure varies with wavelength and the observations from the simulation results show that the noise figure decreases with increase in signal wavelength. Similarly, the noise figure is lower for large signal because of gain saturation caused by high signal input. Furthermore, overall L-band region, the average noise figure is 10dB whereas it is almost constant for large input signal power of 5.4dB. From the simulation results of both the C-band and L-band region, it is so clear that the low input signal power of -30dBm gives a gain higher the high input signal power of 0dB.

3.7 I-25 AND I-6 CONCENTRATION EDFA

The simulation is also carried out using low concentration active material by replacing EDF with different Erbium ions concentrations, namely I-6. The I-25and I-6 EDF has erbium ion concentration of 2200ppm and 440ppm respectively. Therefore, the C-band region is compared between 1.5m of I-25 and 7.5m of I-6 while the L-band region is compared between 9m of I-25 and 45m of I-6, where the total amount of Erbium ions in the fibers is similar. Moreover, for fair comparison both EDFs tested using same single pass configuration. Unlike I-25, I-6 has different specifications from as shown in Table 3.2

Table 3.2
Specifications of I-6 EDF.

Parameters	Value
Er^{3+} concentration profile	440 ppm
Peak Absorption (nominally 1530nm)	8.38 dB/m
Absorption @ 979nm	5.5 dB/m
Attenuation @ 1200nm	7.6 dB/km
Coating Diameter	245.5 microns
Core Concentricity	0.13 microns
Cut-off Wavelength	953nm
Fiber Diameter	124.7 microns
Mode Field Diameter	5.6 microns
Numerical Aperture	0.24
Operating Wavelength	1550nm

The characteristics of the EDFA at low input pump power of -30dBm are shown in Figure 3.14. This is attributed to the difference between the gains of high and low input signal power. From the previous simulation results, both the gain and noise figure at the low input signal power of -30dBm produce better results than the high input signal power of 0dBm.

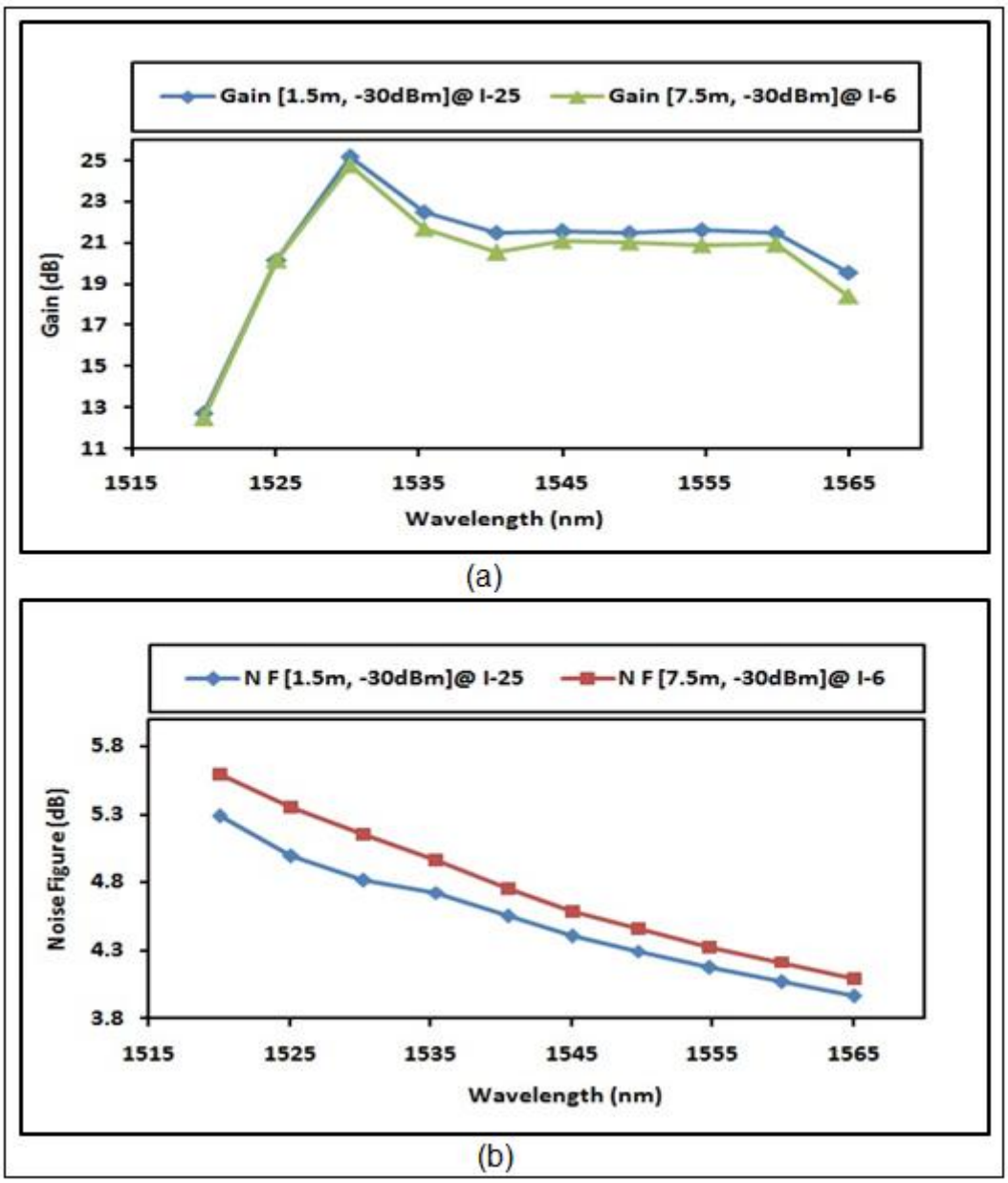

Figure 3.14: Simulation results for C-band EDFA with 1480nm forward pump at 150mW and fiber length 1.5 and 7.5m (a) Gain (b) Noise Figure.

In addition, from the simulation results of the C-band region (1520 nm to 1565 nm), the gain produced from 1.5 m of I-25 is almost the same as the gain of 7.5 m of I-6 as shown on Figure 3.14 (a). For the small input signal power with forward pumping at 1.5m of I-25 gives slightly (average of 0.2dB) higher gain than the 7.5m

of I-6. For this short fiber length, the average inversion is the same for both, and that is how it produces same amount of gain.

The simulation results of L-band region (1565nm to 1620nm) are shown in Figure 3.15. The gain produced from 9m of I-25 is higher by 1.3dB than the gain of 45m of I-6. From the result, gain of wavelengths in the L-band is slightly higher in the case of 9m when compared to 45m, which is owing to the increase in length of fiber, reducing the population inversion consequently. For instance, at the wavelengths of 1580nm until the end the fiber for both the 9m and the 45m the different gain values are all about 1.3dB to 2dB. As for the noise figure is concerned, it is low in both of the cases

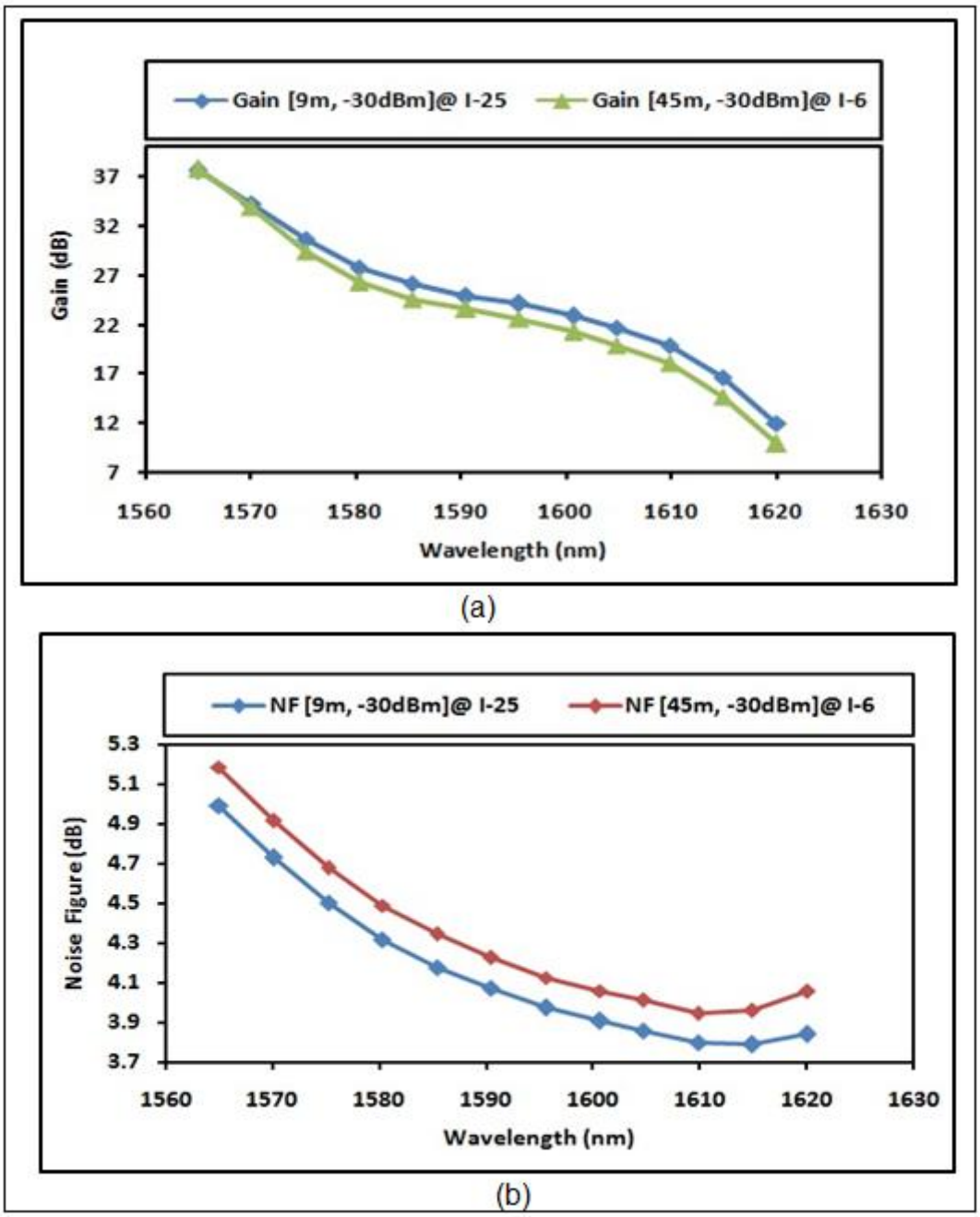

Figure 3.15: Simulation results for L-band EDFA with 1480nm forward pump at 150mW and fiber length 9m and 45m (a) Gain (b) Noise Figure.

Furthermore, the I-25 shows higher Gain Coefficient Efficiency (GCE) as compared to that by the I-6. As shown in Figure 3.16, the GCE of I-25-based EDFA reaches at about 3.2dB/mW while it is only about 2.8dB/mW for I-6 at peak point. It is observed that the GCE for I-25 is accelerated faster than that by the I-6.

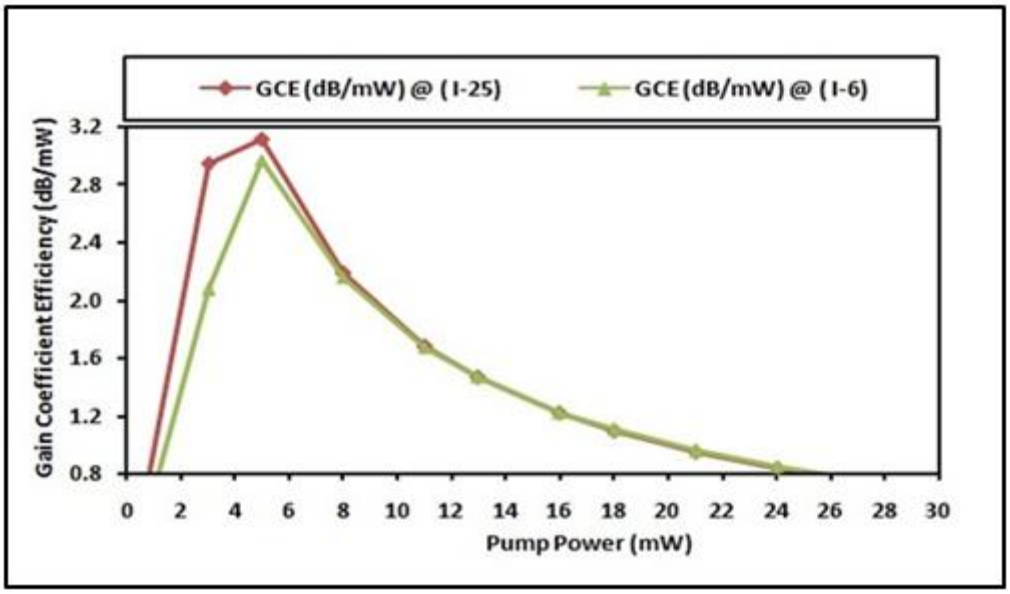

Figure 3.16: Gain coefficient Efficiency for both I-25 and I-6 EDF.

In order to evaluate further in between I-6 and I-25, a new Figure of Merit (FOM) is introduced as follows:

$$FOM = Gain - Noise\ figure \tag{3.1}$$

Figure 3.17 shows FOM for both I-25 and I-6 EDF which clearly shows that the I-25 has a better FOM compared to that by the I-6.

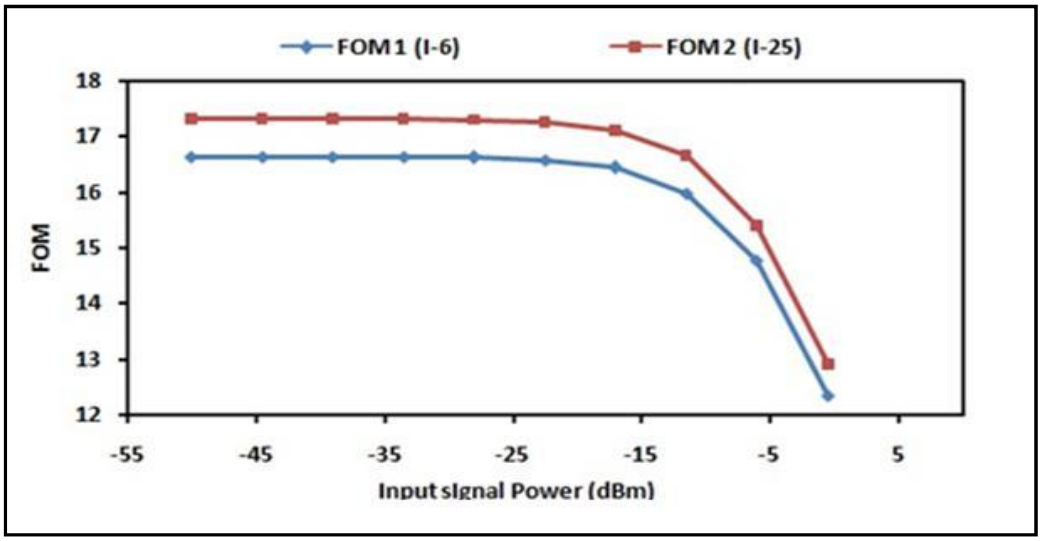

Figure 3.17: Simulation results for EDFA with 1480nm forward pumping at 150mW and fiber length 1.5m: (a) gain spectrum (b) noise figure spectrum

3.7 SUMMARY

The use of simulation tool for EDFA design and performance evaluation is presented. The GainMaster simulation has been carried out to evaluate the performance of single pass configuration EDFA using two types of fibers of I-6 and I-25. Two types of EDF amplifier are evaluated in the C-band and L-band. The new parameters of GCE and FOM are introduced to make further performance analysis of both amplifiers, showing the effect of input signal power, that of the pumped power, and wavelength on gain. Finally, the analysis shows that the newly manufactured I-25 EDF gives a higher performance.

CHAPTER 4

INVESTIGATION ON THE PERFORMANCE OF WIDEBAND EDFAS IN PARALLEL CONFIGURATION

4.1 INTRODUCTION

An optical amplifier is vital in optical communication systems as a device. It amplifies an optical signal directly without the need to first convert it in to electrical signal, amplify it, and then back to optical. There are two major types of optical amplifiers; doped fiber amplifiers and Raman Fiber amplifier (RFA) (Kuntze, 2008).The doped fiber amplifiers are the most popular and they use a doped optical fiber as a gain medium to amplify an optical signal making use the principle of stimulated emission. The most common doped fiber amplifier is the Erbium Doped Fiber Amplifier (EDFA), where the core of a silica fiber is doped with trivalent Erbium ions and can be efficiently pumped with a laser at a wavelength of 980nm or 1480nm,. Such amplifiers exhibit gain either in the conventional band (C-band) or long wavelength band (L-band) regions.

The tremendous growth of the internet and data traffic has created an enormous demand for Dense Wavelength-Division-Multiplexed (DWDM) optical communication systems. Since the silica-based transmission fibers have a wide-band operating window ranging from 1400–1700nm, optical amplifiers with a wider amplification bandwidth are required to cover the full range of the DWDM systems (Harun, 2003; Harun, 2005). In order to extend the wavelength range, several glass hosts such as tellurite, multi-component silicate, and Bismuth oxide-based glass materials have been developed for optical amplifier (Ellison, 1999; Tanabe, 2000;

Wang, 2004). However, in the choice of optical amplifier, silica-based Erbium-Doped Fiber Amplifiers (EDFAs) are preferable due to their proven reliability and compatibility with conventional fiber-optical components. Recently, a highly doped erbium fiber with Erbium ion concentration of 2200ppm has been introduced for an efficient and compact EDFA.

In this chapter, various EDFA configurations are proposed and discussed using a highly doped EDF as the gain medium. Double-pass EDFA is proposed to enhance the gain of the amplifier using a relatively short gain medium. The main objective of this chapter is to realize a wide-band EDFA using a double-pass approach in parallel topology. In this topology, the input port of the forward pumped EDF operating in C-band and L-band is connected to C/L-band WDM coupler for multiplexing and de-multiplexing the channels in the 1530–1560-nm and 1570–1610-nm wavelength regions. CFBG is incorporated in each stage to allow the double-pass operation. The proposed parallel configuration is very simple and applicable to all amplifiers.

4.2 DOUBLE-PASS EDFA

An EDFA can operate either in the C-band or L-band wavelength regions depending on the EDF length used. The L-band operation can be achieved using at least 5-10 times longer length compared to C-band EDFA. The L-band EDFAs are inefficient due to the operating wavelengths that are far from the peak absorption of silica-based erbium-doped fiber (EDF) at 1531nm. In order to improve the gain in this band, a lot of efforts has been proposed by various authors such as (Naji, 2006 a; Nadir, 2007 b). One of the amplifier schemes to achieve a high gain is a double-pass EDFA, which can be used both for C- and L-band operations (Seongtaek, 2001; Paul, 2010).

4.2.1 Experiment

Figure 4.1(a) shows configuration of the proposed double-pass EDFA, which utilizes a silica-based EDF as a gain medium and CFBG as a reflector. The gain medium is a highly doped fiber with Erbium ion concentration of 2200ppm (I-25) and with lengths fixed at 1.5m and 9m for operations in C-band and L-band respectively. A WDM coupler is used to combine the pump light with the signal. The insertion loss of WDM coupler is measured to be approximately 0.9 and 1.8dB in the C-band and L-band spectra, respectively. The EDF is forward pumped by 1480nm laser diode via 1480/1550nm WDM coupler. The double-pass operation is achieved by placing the CFBG at the output end of EDF as shown in Figure 4.1 (a).

The CFBG functions to reflect band the amplified signal into system for re-amplification. The twice-amplified signal is then routed into optical spectrum analyser (OSA) via optical circulator. The experiment is also repeated with a conventional single-pass EDFA, the configuration of which is as shown in Figure 4.1(b). Here, the CFBG is removed from the setup and the OSA is replaced at the output end of the amplifier. In this experiment, the performance of both C- and L-band EDFA are characterized within C-band and L-band regions at 5nm step size using a tuneable laser source (TLS) in conjunction with an optical spectrum analyser (OSA). The performance of the EDFA is investigated for two input signal powers; small input signal of -30dBm and high input signal of 0dBm.

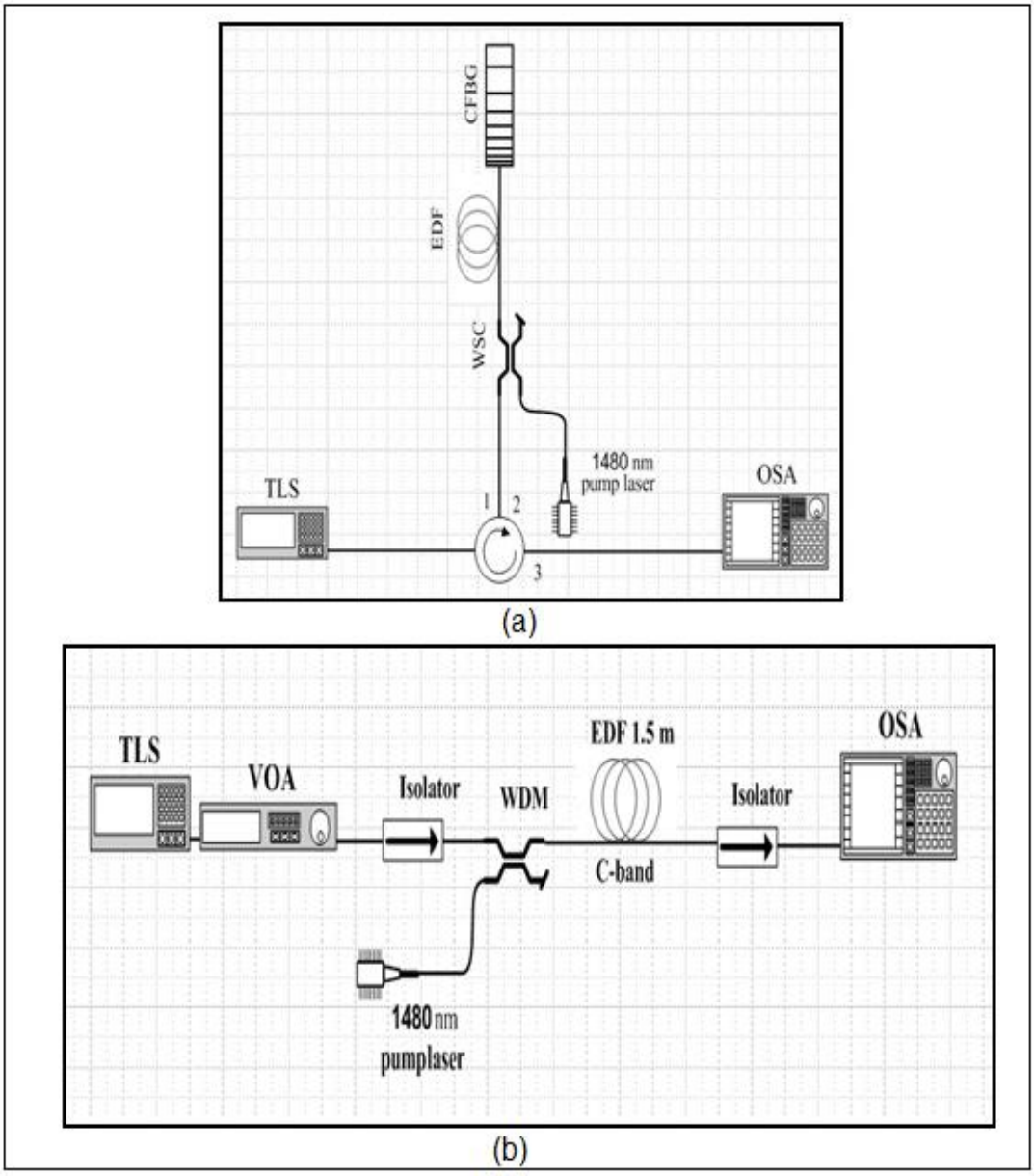

Figure 4.1: Configuration of single EDFAs in (a) double-pass (b) single-pass architectures

In the design of EDFAs, it is necessary to determine optimization of amplifier parameters such as the optimal pumping wavelength, fiber length and pumping power, in order to obtain a maximum gain or bandwidth of the EDFA. The performances of the both single-pass and double-pass amplifiers are also simulated by using named GainMaster^{TM}.

4.2.2 Simulation

Pre-simulation is important to manipulate design parameters such as pump power, pump wavelength, signal power, signal wavelength, fiber length and doping concentration in cost-effective methods. Figure 4.2 shows the schematic diagram of the proposed double-pass EDFA drawing. Those components parameter are set as the experimental EDFA specification. The EDF modelling is based upon the standard models with embedded temperature effects (Giles, 1991; Bolshtyansky, 2000).

The port-3 of circulator shown in Figure 4.2 is connected to a set of reflectors with the ability to simulate only the forward propagation direction from left to right. The set of reflectors is a combination of connectors and tapper device. The return loss of connector and tap percentage of tappers are set as 0dB and 100% respectively. The reflector function is equivalent to converting the backward propagation to forward propagation. Thus, the amplified signal can be measured by probe with results very closely matched to experimental results.

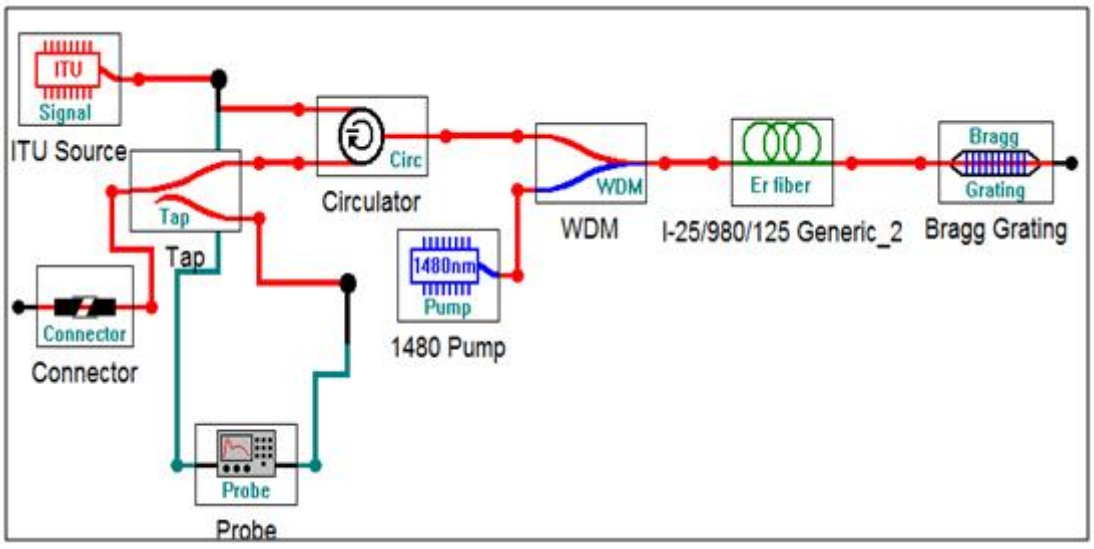

Figure 4.2: Schematic diagram of double-pass EDFA drawn by using Gain Master Software for simulation

4.2.3 Optimizing the pump power for C- and L-band operations

First, the optimum pump power for both C-band and L-band EDFAs is investigated. Figures 4.3 (a) and (b) show the gain and noise figure characteristics of the single-pass and double-pass amplifiers against pump power for the C-band operation at input signal powers of -30dBm and 0dBm, respectively. In the experiment, the TLS is fixed at 1550nm (C-band) and the 1480nm pump power which is made to vary from 20 to 185mW for both single-pass and double-pass amplifiers.

Figure 4.3 (a) shows that the small signal gain is saturated as the 1480nm pump power reaches 60mW for both single-pass and double-pass amplifiers. It is found that the gain is significantly higher in double-pass EDFA compared to that of single-pass EDFA. Gain improvement of more than 10dB is obtained at the saturation region and this is attributed to the double propagation of the test signal in the gain medium, which gain as a result of increase in population inversion. On the other hand, the noise figure is reduced as the pump power increases before it is maintained at a consistent value of lower than 4.2dB at the gain saturation region.

With a high input signal, the gain saturation is obtained at around 170mW for both EDFAs as shown in Figure 4.3(b). The maximum gain of 14.5dB is obtained by the double-pass EDFA, which is 3.4dB higher than the single-pass one. On the other hand, the double-pass EDFA shows a noise figure penalty of 1.4dB compared to the single-pass. This is attributed to the ASE, which is reflected back into the gain medium by the CFBG and thus increases the noise especially at the input part of the amplifier. This contributes to the higher noise figure in the double-pass system. However, the noise figure value for the double-pass EDFA is still lower than 4.4dB at the saturated gain region as shown in Figure 4.3 (b).

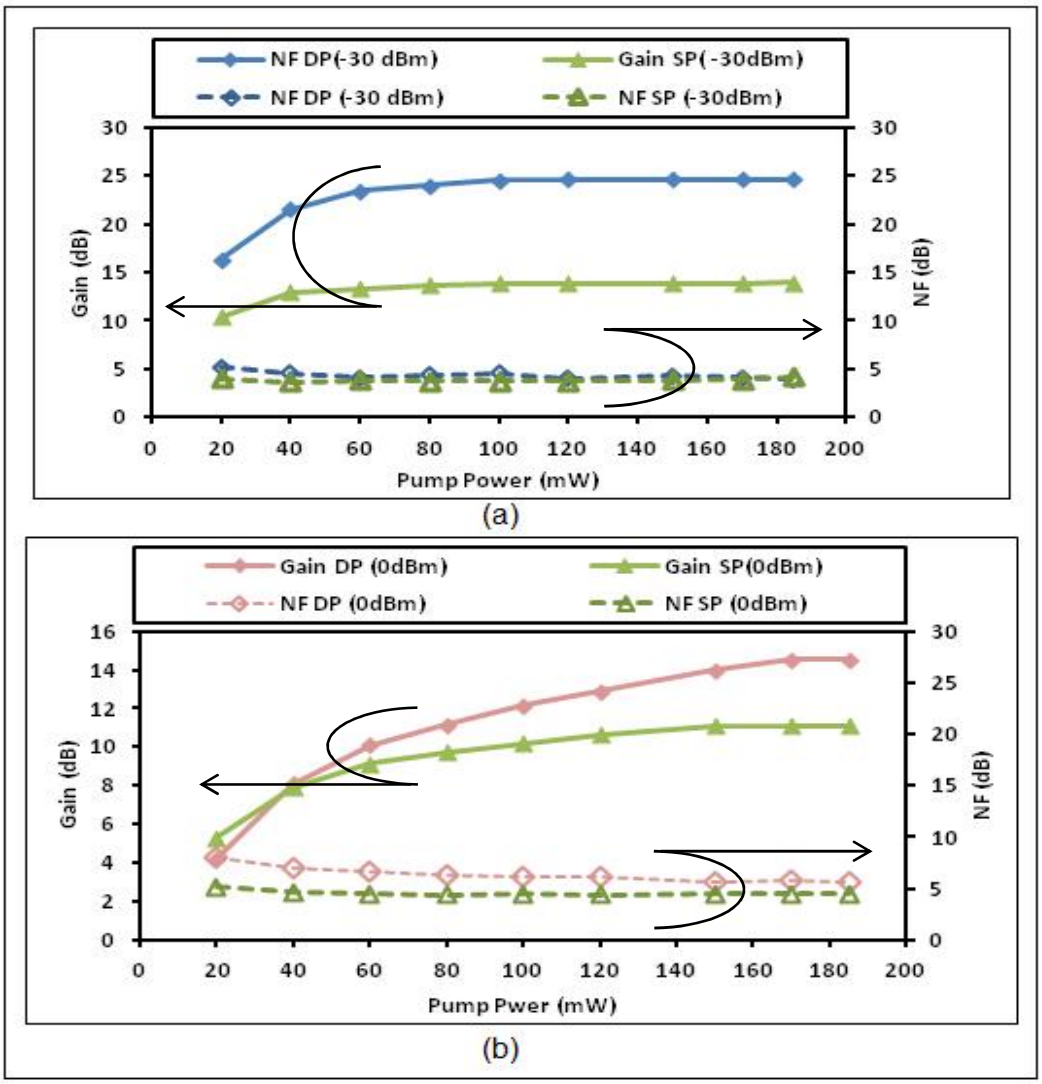

Figure 4.3: Gain and noise figure spectra of the amplifier configured for 1550nm C-band pump power in: (a) single-pass and (b) double-pass configuration.

Figures 4 (a) and (b) show the gain and noise figure characteristics of the single-pass and double-pass amplifiers against pump power for the L-band operation at input signal powers of -30dBm and 0dBm, respectively. In the experiment, the TLS is fixed at 1590nm and the small input gain is observed to saturate at pump power of around 100mW and 80mW for single-pass and double-pass EDFAs, respectively (Figure 4.4a). The gain saturated at a higher pump power at L-band region, which requires a longer EDF length for the amplification through a quasi-two level system. In this system, a C-band signal is absorbed to emit photons in L-band region and thus

requires more pump power for the operation. The maximum gain of 28.5dB is obtained for the double-pass EDFA at small signal, which are 10.8 higher than the single-pass. The gain enhancement is not much different compared to the C-band EDFA, and the corresponding noise figure is around 4.8dB, which is not much different compared to the single-pass EDFA shown in Figure 4.4(a). At high input signal of 0dBm, the double-pass EDFA shows a gain improvement of 3.4dB with 2dB noise figure penalty as compared to the single-pass EDFA shown in Figure 4.4(b).

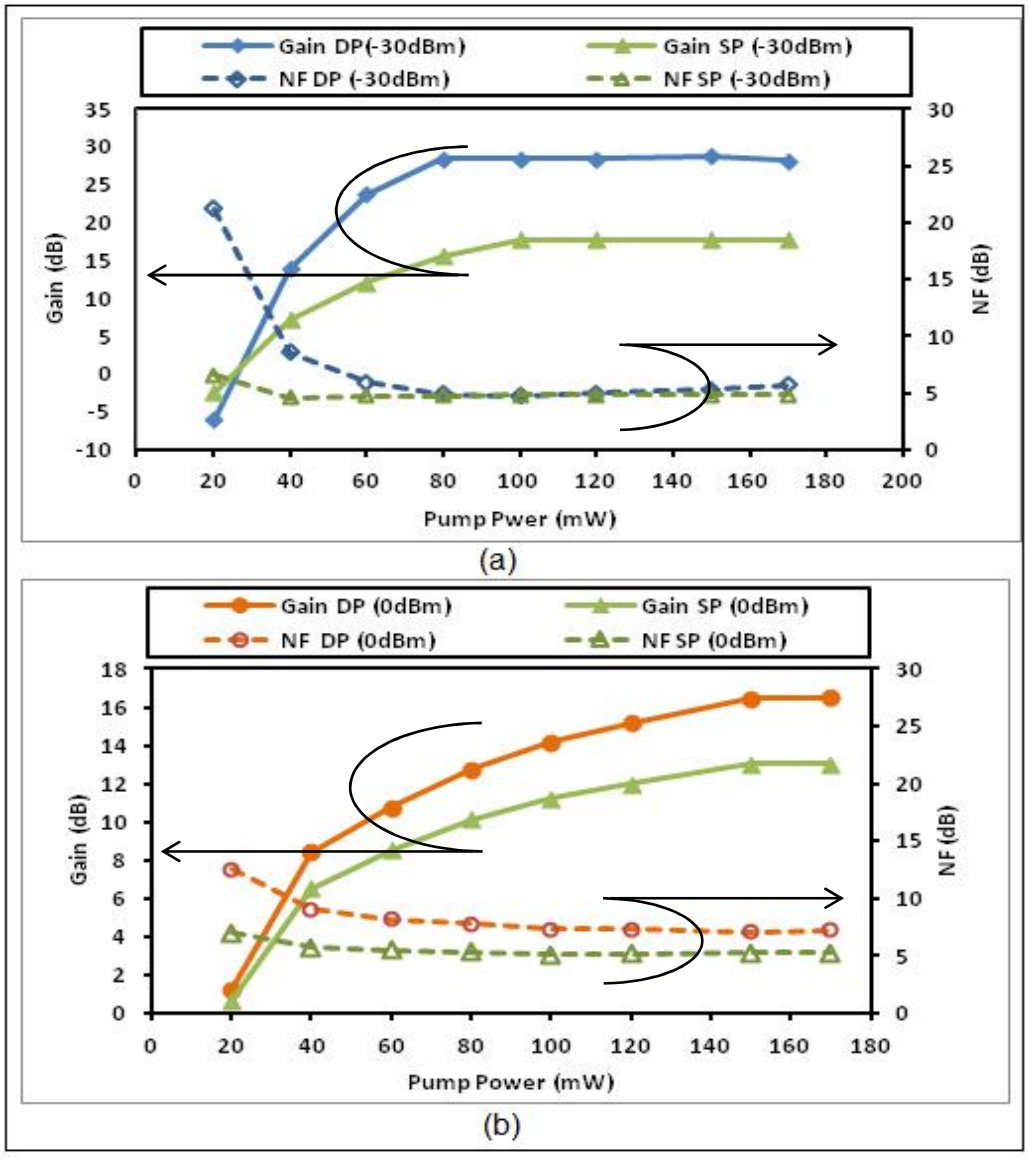

Figure 4.4: Gain and noise figure spectra of the amplifier configured for 1590nm L-band pump power in: (a) single-pass and (b) double-pass configuration

4.2.4 **Test Results of the double-pass C-band EDFA**

Figure 4.5 shows the gain and noise figure spectra of both single-pass and double-pass C-band EDFA at small input signal of -30dBm. The simulation result is also shown for comparison purpose. In the experimental and simulation comparison, the pump power is fixed at saturation region of 60mW. As shown in the figures, both simulation and experimental spectra show a flat gain operation. However, the simulated value is observed to be higher by approximately 4dB for both single-pass and double-pass operations. This is attributed to the experimental setup loss. For instance, the CFBG reflectivity is set as 100% in the simulation, whereas the actual reflectivity is around 95%. It is also found that the gain is so much higher in the double-pass amplifier compared to the single-pass due to the signal passes twice on gain medium. The small input signal power is increased by about 10dB due to the double propagation of the signal in the gain medium.

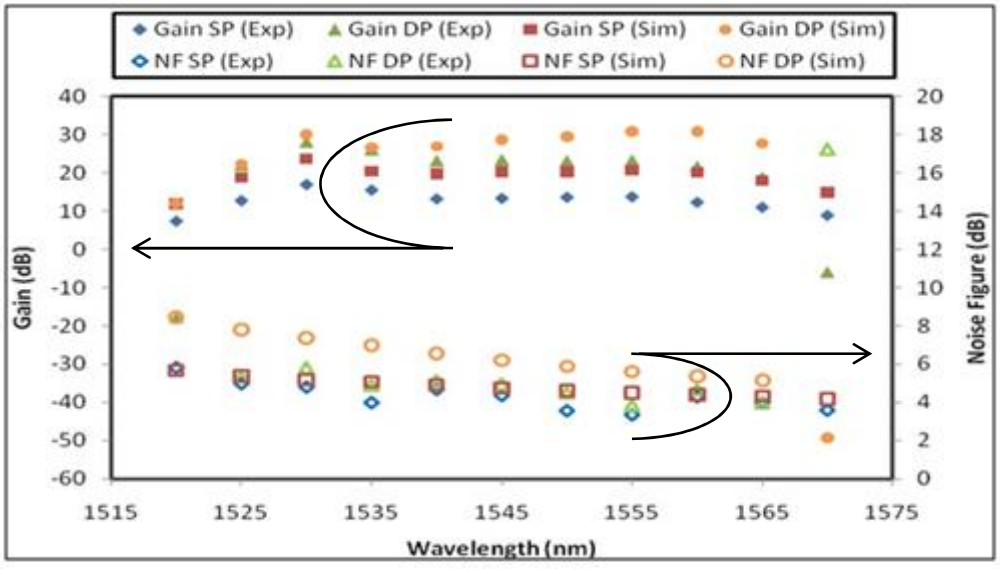

Figure 4.5: Gain (solid symbol) and noise figure (hollow symbol) of the amplifier configured in single-pass and double-pass setup for C-band operation at input signal power of -30dBm

On the other hand, the noise figure is higher in double-pass amplifier compared to single-pass amplifier especially in the region of longer wavelength. For instance, the noise figure increases by 13dB at 1570nm in the double-pass amplifier. This is due to the small ground level absorption at a longer wavelength which causes the population inversion progressively decreased with almost transparent gain. On the other hand, the noise figure is varied from 4 to 8dB especially in the simulated double-pass amplifier. The flat gain of 25dB is obtained over the band of wavelength ranging from 1530nm to 1565nm for double-pass EDFA with a ±3dB gain variation. Similarly, the noise figure is maintained at 5dB with ±0.5dB variation in the C-band region.

Figure 4.6 shows the gain and noise figure spectra of both single-pass and double-pass C-band EDFA at high input signal of 0dBm. As shown, the gain enhancement for double-pass EDFA is not significant at the higher input signal power. The experimental average gain is only enhanced by 1dB due to the effect of population inversion. The effect of the population inversion is larger at smaller input signals whereas high inputs signal suppress the population inversion and thus reduce the gain. As comparison to a simulated gain, the figure shows the gain is so much lower in the simulated gain compared to the experimental gain due to the compatibility of software to execute the simulation perfectly. Thus, the simulated gain is not accurate and realistically practical. On the other hand, the noise figure is higher in double-pass amplifier compared to that of single-pass amplifier due to the same reason as explained earlier. For instance, the highest noise figure penalty of 13dB is observed at 1570nm wavelength region. On the other hand, the simulated noise figure is also not accurate and practical compared to the experimental noise figure. As shown in figure, the average gain spectra of the double-pass amplifier is maintained at 12dB

with a ±2dB gain variation, while the noise figure is varied from 4 to 8dB within the C-band region.

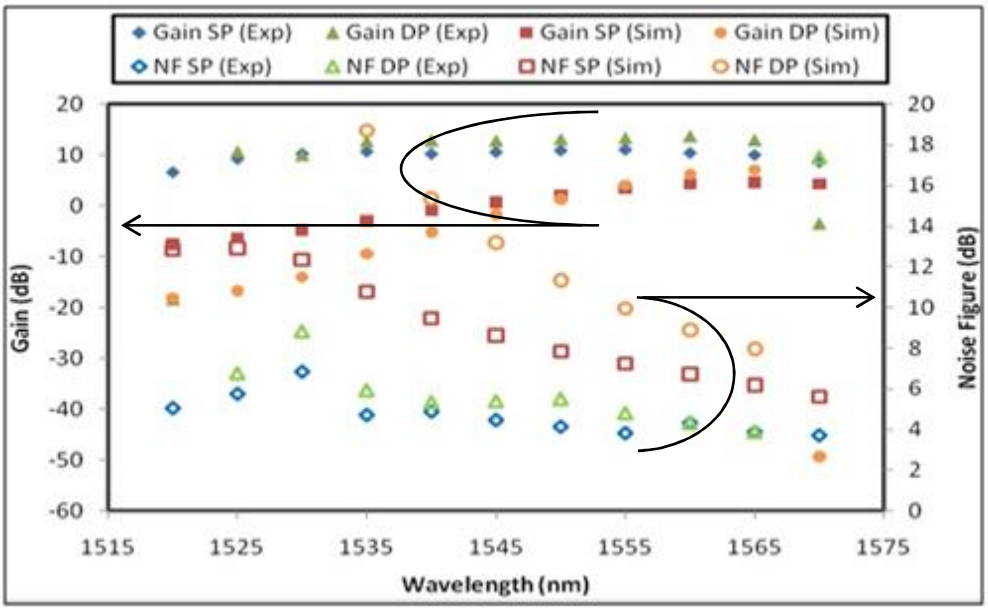

Figure 4.6: Gain (solid symbol) and noise figure (hollow symbol) of the amplifier configured in single-pass and double-pass setup for C-band operation at input signal power of 0dBm.

4.2.5 **Spectrum characteristic of the double-pass L-band EDFA**

Figure 4.7 shows the experimental, simulated gain and noise figure characteristics of both single-pass and double-pass amplifiers at input signal power of -30dBm. In the experiment, the EDF length is fixed at 9m and the 1480nm optimum pump power is fixed at 100mW and 80mW for single-pass and double-pass amplifiers, respectively. In this case, the signal wavelength was varied from 1565 to 1620nm which is within L-band region. As expected, the gain is so much higher in the double-pass amplifier compared to the single-pass amplifier due to the increase in effective length of gain medium. The gain of double-pass amplifier is improved by 16dB at small input signal power due to the double propagation of the signal in the gain medium. It is also

observed that the simulated gain was slightly higher than the experimental gain due to the losses in the experimental setup; such as the splicing, connectors, components and temperature. For instance, the simulated double-pass gain is higher by about 4dB than the experimental gain at 1590nm. On the other hand, it is observed that the noise figure is higher in double-pass amplifier compared to single-pass amplifier especially at 1620nm wavelength region. For instance, the noise figure increased by 13dB at 1620nm in the double-pass amplifier due to the same reason as explained earlier. On the other hand, the noise figure is maintained at 4dB especially in the simulated single-pass amplifier. As shown in figure, the average gain spectra of the double-pass amplifier is maintained at 30dB with a gain variation of ±3dB while the noise figure is maintained at 5dB with a noise figure variation of ±0.5 dB within the L-band region.

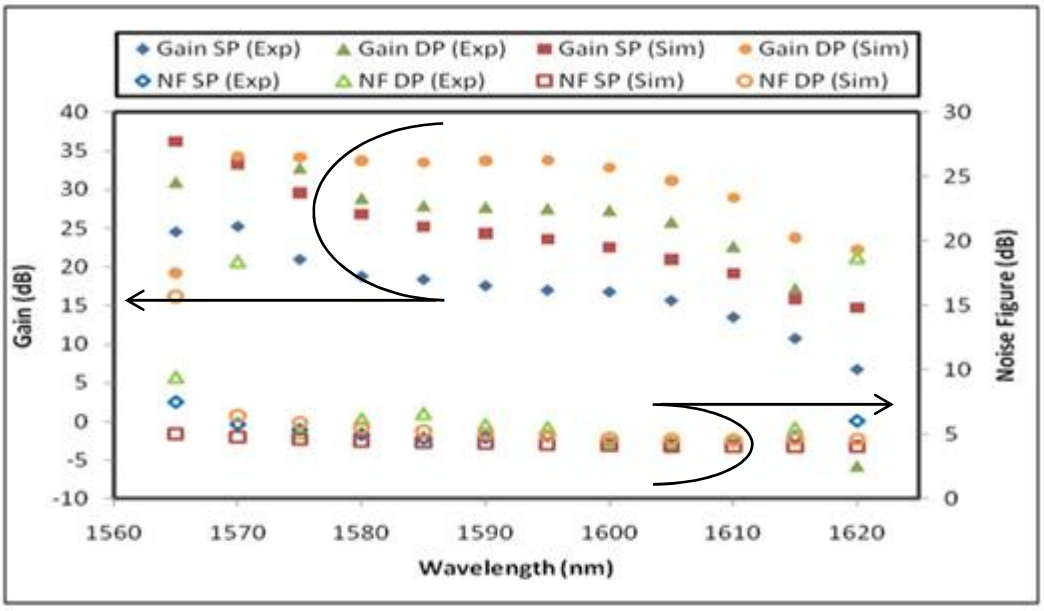

Figure 4.7: Gain and noise figure of the amplifier configured in (SP) and (DP) setup for L-band operation at input signal power of -30dBm.

Figure 4.8 shows the experimental, simulated gain and noise figure characteristics of single-pass and double-pass amplifiers at input signal power of

0dBm. The graph shows that the gain enhancement is not significant at the higher input signal power whereby the experimental average gain is only enhanced by 1dB in

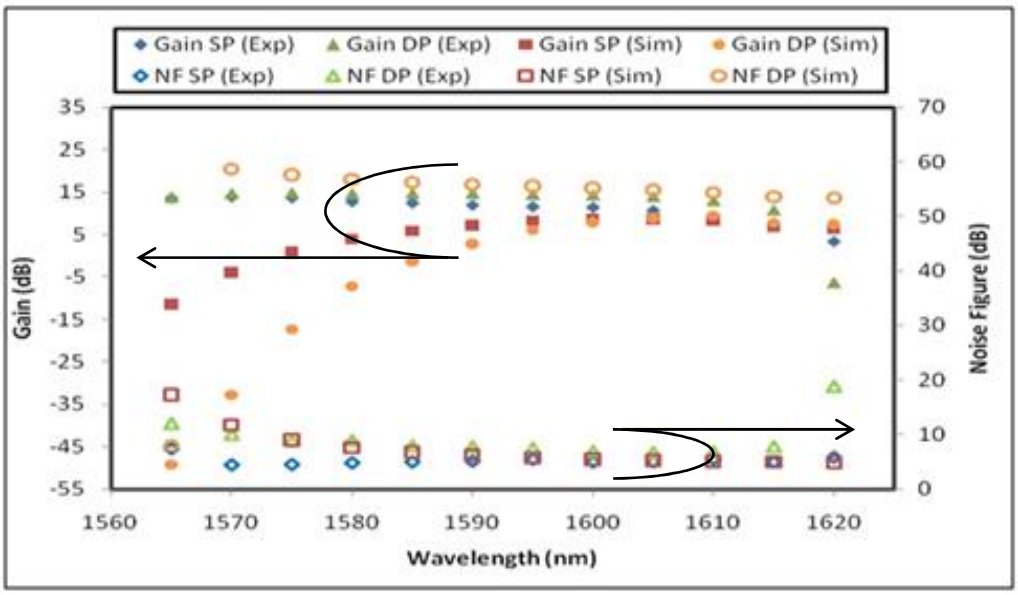

Figure 4.8: Gain and noise figure of the amplifier configured in (SP) and (DP) setup for L-band operation at input signal power of 0dBm.

the double-pass amplifier. This indicates that the effect of the population inversion is larger at smaller input signals whereas high inputs signal suppress the population inversion and thus reduce the gain. As a comparison to the simulated gain, the figure shows that the gain is so much lower in the simulated gain compared to the experimental gain due to the compatibility of software to execute the simulation perfectly. Thus, the simulated gain shown above is not testifying accuracy in the case of L-band only, and such results have got no practical utility seeming the software lacks from limitations in this case. Figure 4.8 also shows the corresponding noise figure spectrum at the higher input signal power. Similarly, the noise figure is higher by 13dB in double-pass amplifier compared to single-pass amplifier especially at 1620nm wavelength region due to the same reason as explained earlier. It was also

observed that the simulated noise figure is not accurate and practical compared to that obtained by the experimental value of noise figure. The average gain of the double-pass amplifier is maintained at 14dB with a gain variation of ±0.5dB while the noise figure is varied from 4 to 8dB within the L-band region. The experimental setup results lack from features exhibiting resemblance with simulations results.

4.3 WIDEBAND EDFA BASED ON PARALLEL CONFIGURATION

In this section, an earlier reported double-pass EDFAs operating in C-band and L-band region are combined in parallel configuration to demonstrate a wide-band optical amplifier. Both EDFAs use silica-based EDF with an Erbium ion concentration of around 2200ppm inside the core. Generally, silica-based EDFs are preferred optical amplifiers due to their proven reliability and compatibility with conventional fiber-optic components. The proposed wideband EDFA with two pieces of silica-based EDF in double-pass parallel configuration is shown in Figure 4.9. At the input of the optical amplifier, a C/L-band WDM coupler is used to separate the WDM signals to C- and L-bands. The C-band and L-band signals were amplified by a piece of 1.5m and 9m long EDF, respectively. Both 1.5m and 9m long EDFs are forward pumped by a 1480nm laser diode via a 1480/1550nm WDM coupler to provide amplifications in C-band and L-band, respectively.

The EDF (I-25) used in this study contains an Erbium ion concentration of about 2200ppm, a cut-off wavelength of 910nm, fiber diameter of 125µm, mode field diameter of 5.7µm, numerical aperture of 0.24 and peak absorption of 41.1dB/m at 1530nm. At the end of each EDF, a broadband CFBG operating at C- or L-band is incorporated to reflect the C- or L-band signals for double-pass operation. These signals are combined together by the C/L-band WDM coupler at the input port of the

amplifier before they are routed to the output port via optical circulator as shown in Figure 4.9. The insertion loss of the WDM couplers is assumed to be 0.9 and 1.8dB in the C- and L-band region, respectively. Figure 10 show the transmission spectra of both CFBGs used in both configurations. As shown in the Figure 4.10, the C-band CFBG has a reflectivity of more than 90% centred at the wavelength of 1545nm with a bandwidth of about 40nm while the L-band CFBG has a reflectivity of more than 98% centred at 1592nm with a bandwidth of about 50nm. In this experiment, the gain and noise figures of both EDFAs are characterized using a Tuneable Laser Source (TLS) and measured with an Optical Spectrum Analyzer (OSA).

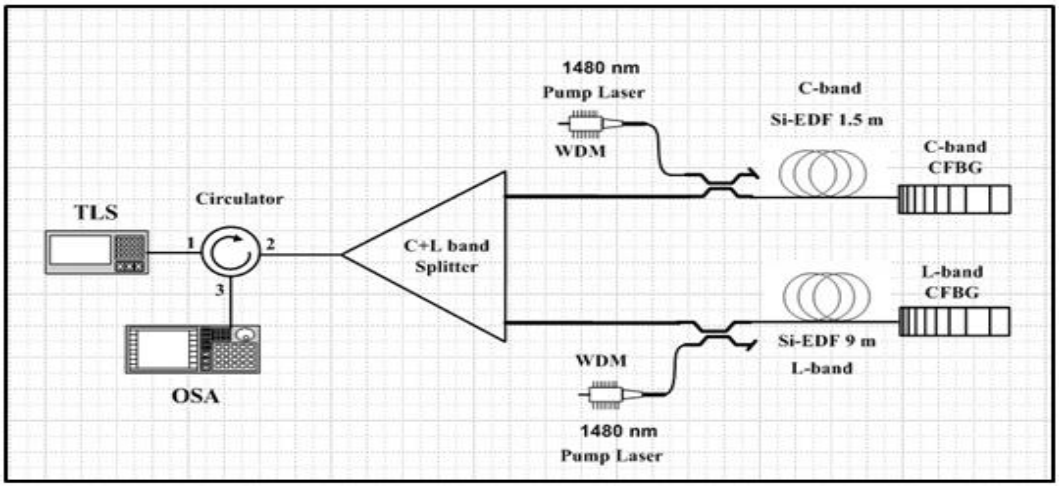

Figure 4.9: Configuration of two-stage double-pass EDFAs in parallel configurations

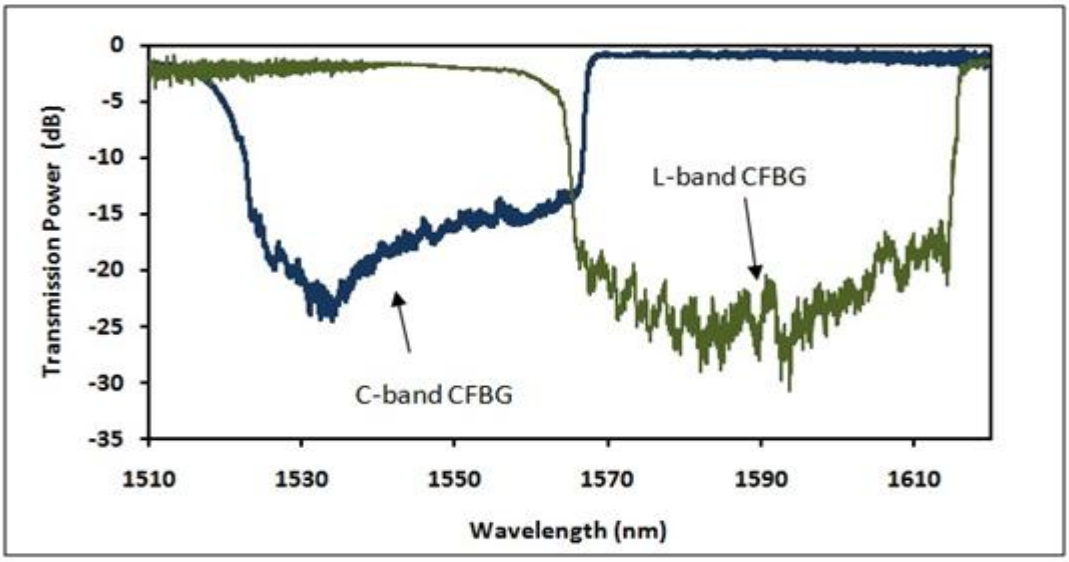

Figure 4.10: Transmission spectra of the CFBGs.

Figure 4.11 shows the gain and noise figure spectra for the parallel amplifier at various EDF lengths of the C-band. The EDF length for the L-band operation is fixed at 9m with the pump powers at 112 and 150mW for C-band and L-band operations, respectively. As shown the C-band gain increases as the EDF length increases from 1.0 to 2.2m while the L-band gain is almost unchanged. For instance, the gain increases from 17.5dB to 33.5dB at 1530nm by changing the EDF length from 1.0 to 1.5m. This is attributed to increase in the number of erbium ions, which increases the population inversion and thus gain for C-band region. However, further increase in the EDF length from 1.5 to 2.2m only increases the gain by 2dB which is due to the saturation effect. As result, Figure 4.11 shows that the C-band noise figure is the highest at 2.2m EDF. This shows that the optimum length for the C-band operation is around 1.5m. The L-band noise figure is observed to be unaffected with the change of gain and noise figure in the C-band amplifier.

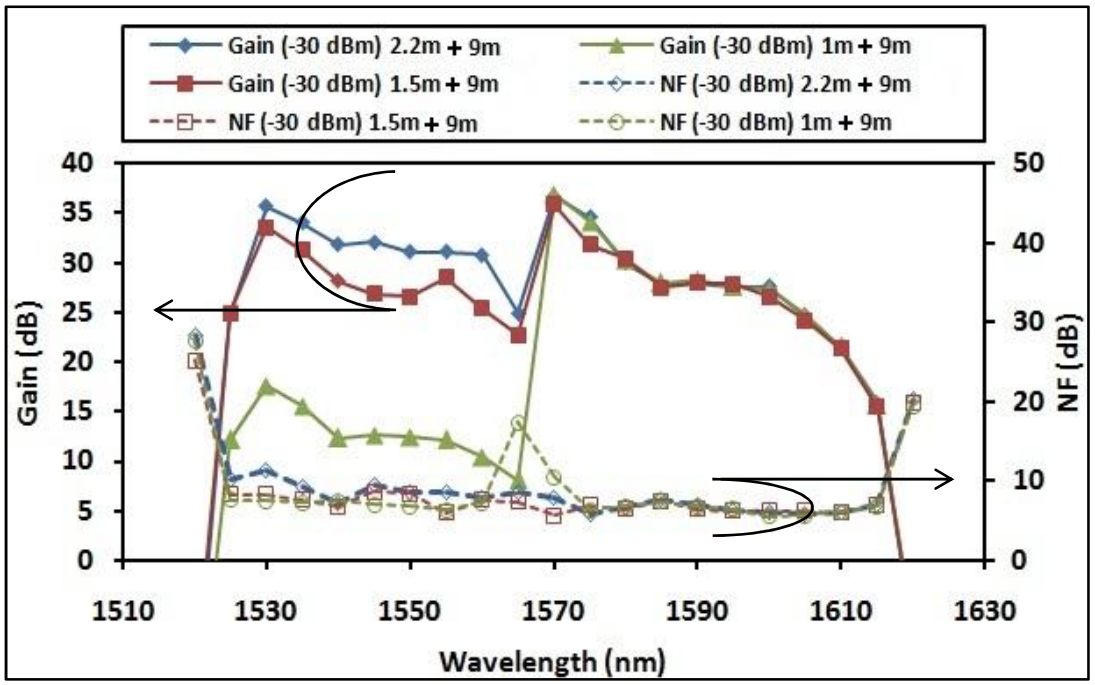

Figure 4.11: Gain and noise figure spectra of the amplifier configured in parallel setup at different EDF lengths for C-band operation

At the optimum length of 1.5m and 9m for the C-band and L-band EDFAs, wide-band operation is achieved within a wavelength ranging from 1525 nm to 1615nm. The gain of the parallel's amplifier varies from 23dB to 36dB within a wavelength region from 1530nm to 1605nm. At the wavelength 1570nm, the gain of the wide-band amplifier suddenly increases due to shift in the amplification medium from 1.5m to 9m. On the other hand, the noise figure of the parallel amplifier varies from 5.6 to 8.2dB within the wavelength region of 1530nm to 1605nm.

4.4 WIDEBAND AMPLIFIERS WITH A HYBRID GAIN MEDIUM

The amplifier consists of two stages: namely, Zr-EDF and Si-EDF. The Zirconia based Erbium-doped fiber (ZEDF) with highly doped Erbium ion concentration has been introduced for realizing an efficient and compact optical amplifier, where the combination of both Zr and Al ions are used to achieve a high erbium doping concentration of 4320ppm in the glass host without any phase separation of rare-earth

elements (Paul, 2010). In this section, a hybrid wide-band optical amplifier with a flat-gain characteristic is proposed using a combination of Zr-EDF with erbium doping concentration of 2800ppm and Si-EDF with erbium doping concentration of 2800ppm as the gain medium.

The performance of the amplifier is investigated in parallel double-pass structure of Figure 4.9 whereby a CFBG is incorporated in each stage to allow the double-pass operation. At the input of the optical amplifier, a C/L-band WDM coupler is used to separate the WDM signals into C-band and L-band. The C-band and L-band signals are amplified by a piece of 2m and 9m long for Zr-EDF and Si-EDF that are forward pumped by a 980nm and 1480nm laser diode source, respectively.

The Zr-EDF used is obtained from a fiber preform, which is fabricated in a ternary glass host, zirconia-yttria–aluminum codoped silica fiber using a Modified Chemical Vapor Deposition (MCVD) process in conjunction with a solution doping process. The peak absorption of the Zr-EDF at 978nm is measured to be 14.5dB/m, which is equivalent to the erbium ions concentration of 2800ppm. The EDF effect here is similar to what previously has been proposed by the wideband EDFA with an Erbium ion concentration of about 2200ppm. At the end of each stage, a broadband CFBG operating at C- or L-band is incorporated to reflect the C-band or L-band signals for double-pass operation. These signals are combined together by the C/L-band WDM coupler at the input port of the amplifier before they are routed to the output port via optical circulator as shown in Figure 4.9.

Figure 4.12 shows the gain and noise figure spectra of the proposed wide-band hybrid EDFA. In the experiment, the 980 nm and 1480 nm pump powers are fixed at 112 and 150mW for C-band and L-band operations respectively, while input signal power is fixed at 0dBm. As shown in the figure, wide-band operation has achieved an

amplifier, which is operating in wavelength region from 1525nm to 1615nm. The gain of the parallel amplifier is maintained at 15dB within a wavelength region from 1530nm to 1605nm with a gain variation of less than 0.5dB. The noise figure of the parallel amplifier varies from 7.4 to 11.2dB within the wavelength region of 1530nm to 1615nm.

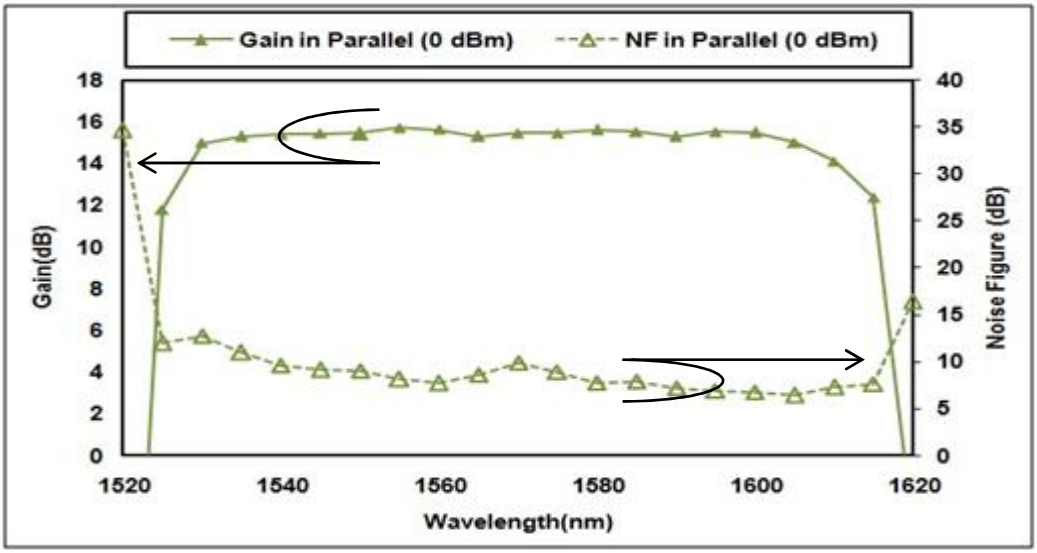

Figure 4.12: Gain (solid symbol) and Noise Figure (hollow) performances in the parallel at input signal power of (0) dBm.

Figures 4.13 (a) and (b) show the gain and noise figure spectra for the parallel amplifier at various pump power for the C-band stage. As shown in Figure 4.13 (a) at the C-band the small input signal (-30dBm) produces a gain that varies as the pump power increases from 160mW to 280mW. At input signal wavelength of 1550nm, the gain decreases from 36.5dB to 33 dB as the pump power changes from 160mW to 280mW. The small signal variation is owing to the saturation effect. The L-band small signal gain and noise figure spectra are almost unchanged. At input signal power of 0dBm, the C-band gain reduces as the pump power increases from 160mW to 280mW. The optimum pump power for flat gain is observed to be around 220mW as

shown in Figure 4.13 (b). The noise figure spectrum is seen to be unaffected by the change of pump power of the C-band amplifier.

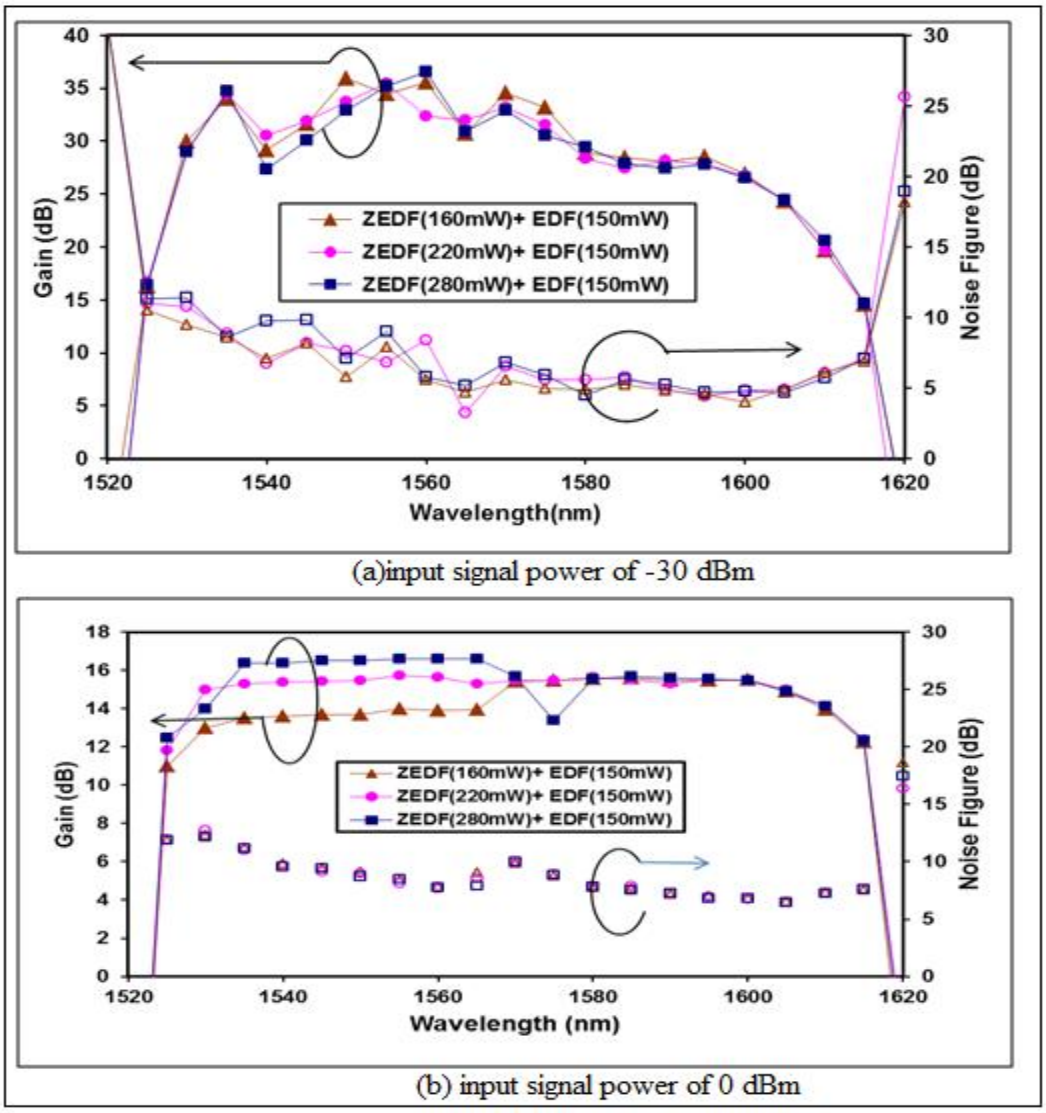

Figure 4.13: Gain and noise figure spectra of the amplifier configured in parallel setup at different pump power for C-band operation at input signal power of (a) -30dBm (b) 0dBm.

Recently a wideband optical amplifier is also demonstrated using a Bismuth-based Erbium-doped fiber (Bi-EDF) as the gain medium (Paul, 2010, Harun, 2004 a). It was shown that the Bismuth-doped glass exhibited a broadband luminescence in the near infrared region. Thus, the can become potential gain media for extending the spectral bandwidth of the current erbium-doped silica fiber amplifiers. The Bi-EDF

has Erbium ion concentration of 6300ppm. Bismuth rate glass host has the ability to be highly doped with Erbium ions to realize an ultra-compact fiber lasers and amplifiers. The Bi-EDF also has other excellent features such as wideband emission spectrum, easy refractive index control and high reliability.

In this work, a compact wide-band and flat-gain EDFA is demonstrated using a Bi-EDF as a gain medium in conjunction with double-stage double-pass configuration. The performance of the parallel amplifier is investigated and, it is found that the configuration provides a higher attainable gain from 1525 to 1620nm wavelength region. The noise figure for the configuration is maintained below 10dB in wavelength region from 1535nm to 1620nm. In the experiment, the proposed configuration, similar to Figure 4.9 uses 49 cm and 9m long Bi-EDF and Si-EDF in the first and second stages to provide C and L-band amplifications, respectively. The concentration of Si-EDF is 2200ppm while the Bi-EDF has erbium ion concentration was 6300ppm and a cut-off wavelength is 1440nm as well as a pump absorption rate was 141 dB/m at 1480nm, and they are pumped by a 1480 nm laser diode via a WDM.

Since double pass configuration provides a higher gain spectrum, this scheme is used to construct a wideband EDFA by combining the 49cm long C-band Bi-EDFA and the 9m long L-band Si-EDFA in parallel configuration. In the experiments, the 49cm and 9m Si-EDF are pumped at the optimum pump powers of 220mW and 150mW respectively. The gain and noise figures for the configuration is measured across the C and L-band wavelength regions for two input signal levels; -30dBm and 0 dBm and the results are shown in Figures 4.14 (a) and 4.14 (b) respectively. The figures show that wideband operation is achieved in both amplifiers, which covers from 1525nm to 1620nm.

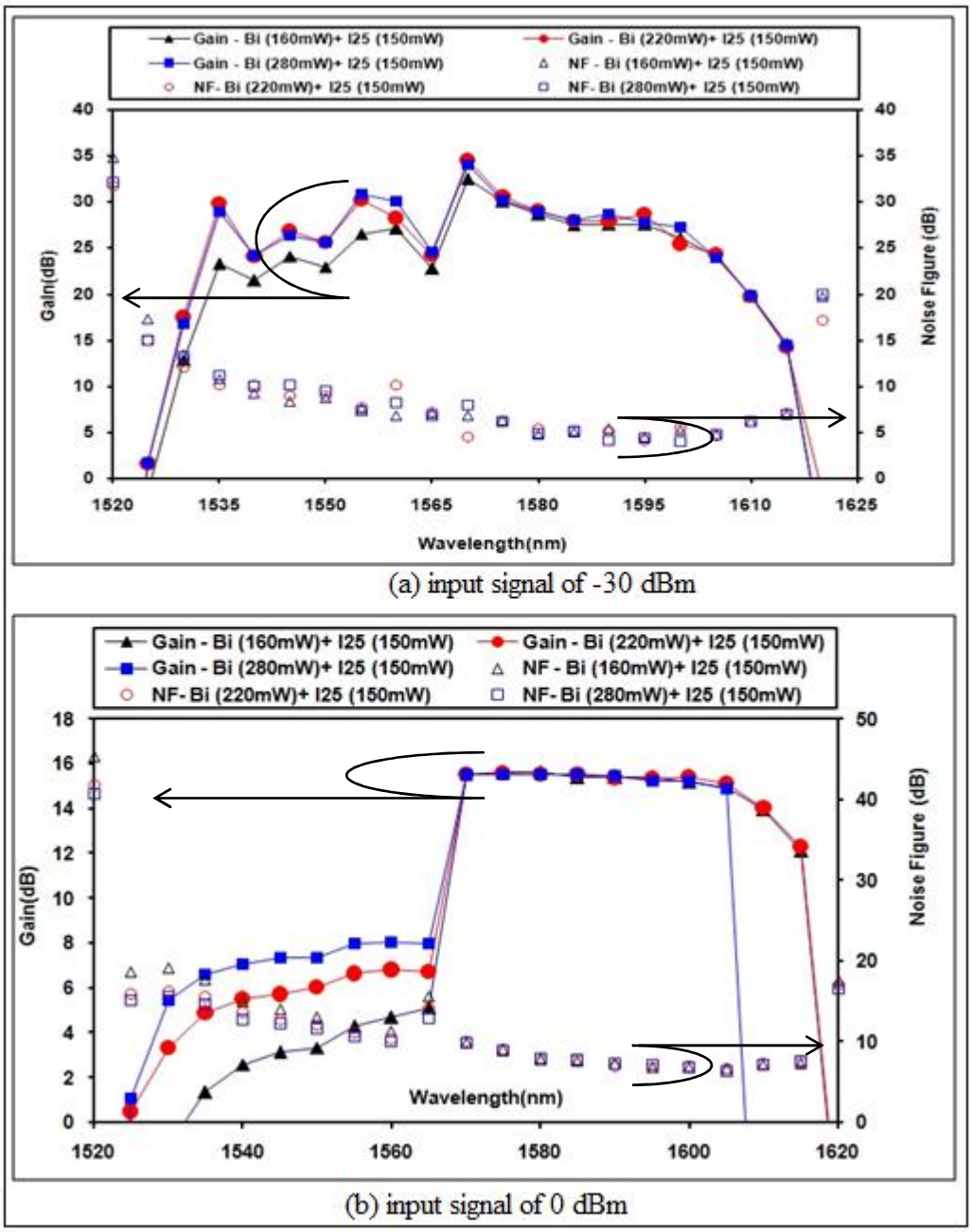

Figure 4.14: Gain and noise figure spectra of the Bi-Si-EDFA at input signal power of (a) -30dBm and (b) 0dBm.

Figures 4.14 (a) and (b) show the gain and noise figure spectra for the parallel amplifier at various pump power for the C-band stage at -30dBm and 0dBm respectively. As shown in Figure 14 (a) the C-band small signal gain (-30 dBm) varies as the pump power increases from 160mW to 280mW. Similarly, at input signal wavelength of 1550nm, the gain decreases from 32.5dB to 26dB as the pump power

changes from 160mW to 280mW, however, the small signal variation is most expected due to the saturation effect, although, the L-band small signal gain and noise figure spectra are almost same. Furthermore, for the input signal -30dBm, the average gains of the parallel Bi-Si-EDFA was obtained at approximately 22.5dB with gain variation of ± 3.5dB within the wavelength region from 1530 to 1605nm. At 1570nm, the gain suddenly increases to 35 dB due to the shift in the amplification medium from 49 cm to 9m.

The gain in the C-band region is very low for high input signal power of 0dBm compared to the values of higher gain that are obtained from the L-band as shown in Figure 4.14 (b). This is due to the high supprestion in C-band region that is due to saturation effect reducing the population inversion in the C-band region. At 1570nm, the gain suddenly increases from 6.5dB to 15dB due to the shift in the amplification medium from C-band to L-band. On the other hand, the higher L-band gain, which is attributable to the use of the standard EDF. The higher gains are obtained in the smaller input signal of -30dBm which indicates that the effect of the population inversion are larger for smaller input signals whereas the high input signals suppress the population inversion and thus reduce the attainable gain. In contrast, the noise figure values of parallel amplifier were maintained below 10dB within the L-band while they are quite high in C-band due to the lower gain in this wavelength region.

4.5 SUMMARY

In summary, the performances of the single stage EDFA in single-pass and double-pass configurations are demonstrated with EDF length of 1.5m and 9m for C-band and L-band operation, respectively. A CFBG is used to allow double-pass propagation and

increase the attainable gain. At input signal power of -30dB, the average flat gain of approximately 25dB over C-band region and the average flat gain of approximately 30dB over L-band region are achieved by the double-pass amplifier with gain variation approximately ±3dB. The corresponding noise figure is maintained at 5dB with noise figure variation ±0.5dB. The results obtained show that experimental and simulated results are in close agreement. The flat gain and bandwidth as well as noise figure of the double-pass amplifier are better, when compared to a single-pass amplifier.

A wide-band EDFA operating within a wavelength region from 1530nm to 1605 nm is also then demonstrated using a double-pass parallel configuration with CFBGs. A CFBG was used in both C-band and L-band stages to allow a double pass operation and increase the attainable gain. At an input signal power of -30dBm, the measured gain varies from 23dB to 36dB within a wideband region from 1530 to 1605nm. The corresponding noise figure varies from 5.6 to 8.2dB over this wavelength region. The optimum length for C-band operation is 1.5m for the proposed parallel amplifier. A wide-band and flat-gain optical amplifier is also demonstrated utilizing a hybrid gain media of Zr-EDF and EDF in parallel double-pass configuration. At input signal power of 0dBm, a flat gain of 15dB is achieved within a wavelength region from 1530 to 1605nm. The corresponding noise figure varies from 6.2 to 10.8dB over this wavelength region. In addition, a wide-band EDFA is demonstrated using a short Bi-EDF of 49cm and Si-EDF of 9m long for C- and L-band operation, respectively. The parallel amplifier provides a higher attainable gain at input signal of -30dBm, where average gain of approximately 22.5dB and noise figure of less than 10 dB are obtained. Whereas, at high input signal power of 0dBm, the gain is very low about 7dB with a high noise figure of 14dB at 1560nm.

CHAPTER 5

PROPOSED NEW SERIAL CONFIGURATION

5.1 INTRODUCTION

There has been tremendous grow in the traffic data rate over the internet and other internet related channels which has resulted into a huge demand for wider bandwidth optical communication systems. This has spurred the development of wideband optical fiber amplifiers which can accommodate a larger number of channels. In this study, a wide-band Erbium-doped fiber amplifiers (EDFAs) has been using a double-pass approach in parallel topology.

Beside wideband operation, the gain spectrum of the EDFA is also required to be flat for application in long haul multichannel light wave transmission systems such as the WDM. In a WDM system, the EDFA does not necessarily amplify the wavelength of each channels equally, but is often required to have equalized gain spectra in order to achieve uniform output powers and similar signal-noise ratios (SNR) (Farah, 2009). Moreover, the non-uniform gain spectrum of EDFA limits the bandwidth over which a constant gain can be achieved (Park, 1998). Therefore, several methods have been proposed to overcome this problem and designing a flat spectral gain EDFA such as controlling the doped fiber length and the pump power or proper selection of optical notch filter's characteristic, using an acousto-optic tunable filter (Loh, 1996; Sung, 1998; Chun, 2003; Seo, 2005). Recently in (Harun, 2009) proposes a new EDFA configuration for optical gain improvement by inserting an optical isolator and filter within the amplifier length to stop building-up the backward amplified spontaneous emission.

5.2 CONFIGURATION

Figure 5.1 shows the proposed compact two-stage double-pass wide-band EDFA in serial topology. It consists of two pieces of Erbium-doped fiber (EDF) which are pumped by a 1480 nm laser diode via a wavelength division multiplexer (WDM). The insertion loss of the WDM is measured to be around 0.9dB and 1.8dB in the C-band and L-band regions, respectively. A broadband Fiber Bragg Grating (FBG) is placed at the end of each EDF to reflect the signals back to the gain medium, allowing for a double propagation of the test signal. The first and second stages operate as a C-band and L-band amplifiers, respectively.

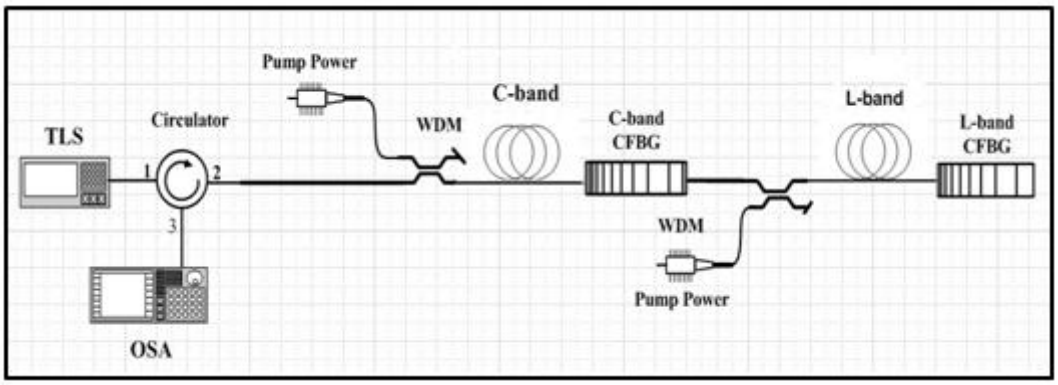

Figure 5.1: The proposal configuration of wideband dual-function double-pass EDFA

Figure 5.2(a) and (b) show the transmission spectra of the C and L-band FBGs used in the experiment. The C-band FBG (Figure 5.2a) has a reflectivity of more than 90% centered at the wavelength of 1545nm with a bandwidth of about 40nm. The L-band FBG reflects signal ranging from 1565nm to 1615nm with a reflectivity of more than 98% as depicted in Figure. 5.2(b). In the setup of Figure. 5.1, the C-band FBG is placed between the two stages to act as the reflector for the C-band EDFA. It reflects C-band signal for double-pass operation and allows the L-band signal to be transmitted. The L-band signal, above 1565nm, will go through the FBG and is

amplified by the second stage of the amplifier. The amplified signal is then reflected back into the system by the L-band FBG. An optical circulator is used in both configurations to extract the amplified output signal. A tunable laser source (TLS) is used in conjunction with an optical spectrum analyzer (OSA) to characterize the wideband EDFA**.**

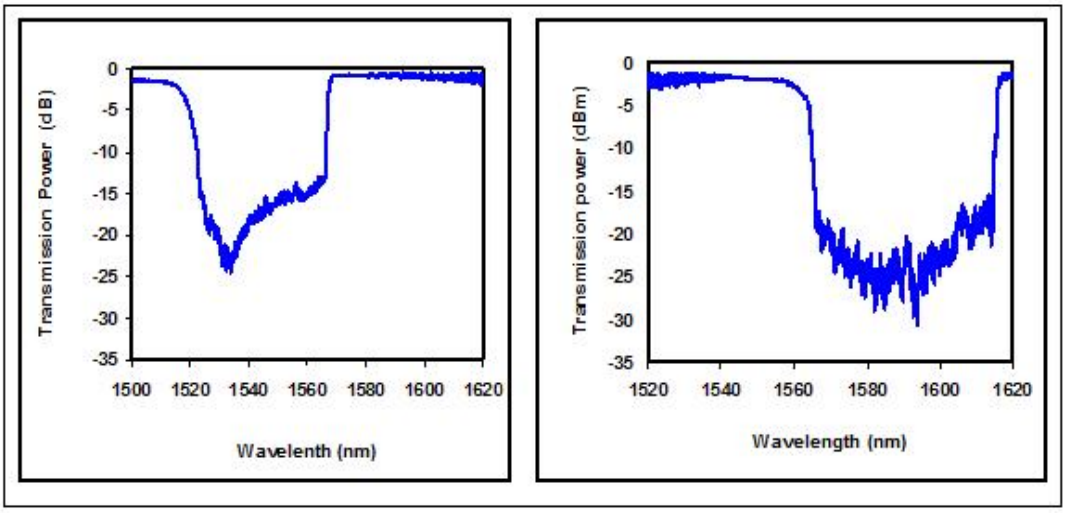

Figure 5.2: Transmission spectrum of (a) C-band FBG, (b) L-band FBG

5.3 COMPACT AND WIDEBAND EDFA WITH A BI-EDF IN A SERIAL CONFIGURATION

Many researchers, to date, have focused on the development of compact fiber amplifiers with a very short gain medium length (Qiu, 2010; Paul, 2010; Harun, 2010). To compensate for the short gain medium length, the active fiber needs to be doped with very high erbium ion concentration. However, the consequence of using high concentration erbium ion is a pair-induced quenching effect, which potentially reduces the pump power conversion efficiency and increase the noise figure for an EDFA (Delevaque,1993; Harun, 2003). In order to increase the limit of erbium doping concentration while maintaining the transmission capacity, several techniques such as

using different glass hosts like tellurite (Wang, 2008), bismuth (Dong, 2011) and co-doping the EDF with ytterbium (Tanabe, 2000; Harun, 2006) have been proposed and demonstrated. Recently, bismuth based optical fibers have gained increasing interest for fiber laser and optical amplifier applications (Li, 2010; Toney, 2010; Cheng, 2009). Bismuth glass host has the ability to be highly doped with Erbium ions to realize an ultra-compact fiber lasers and amplifiers. The bismuth-based erbium-doped fiber (Bi-EDF) also has other excellent features such as wideband emission spectrum, easy refractive index control and high reliability.

In this section, a compact, wide-band and flat-gain EDFA is demonstrated using a Bi-EDF as a gain medium in conjunction with the proposed two-stage double-pass serial configuration. The experiment is conducted based on Figure 5.1 using Bi-EDFs as the gain medium. 21cm and 46cm long Bi-EDFs were used in the first and second stages to provide C and L-band amplifications, respectively. Both Bi-EDFs have erbium ion concentration of 6300ppm and a cut-off wavelength of 1440nm as well as a pump absorption rate of 141dB/m at 1480nm. Thus, 1480nm laser diodes are used as the pump source for both Bi-EDFs.

First, the gain and noise figure characteristics of both the C-band and L-band Bi-EDFAs are individually investigated for both single-pass and double-pass configurations. In the experiment, the Bi-EDF lengths are fixed at 21cm and 46cm for C-band and L-band operations, respectively while input signal and pump powers are set at -30 dBm and 150 mW, respectively. The results are as illustrated in Figures 5.3(a) and 5.3(b) for C-band and L-band Bi-EDFAs respectively. In the double-pass amplifier, the signals are doubly propagated through the Bi-EDF, which increases the population inversion resulting in a double increment of the gain as shown in both figures. For instance, the gain increases from 12.8 dB to 24.7dB at 1535nm for the C-

band Bi-EDFA due to the double-propagating of the signal as shown in Figure 5.3 (a). A flat-gain of around 23dB, with double-pass configuration,was obtained with gain variation of ± 3.5dB within the wavelength region from 1530 to 1565nm.

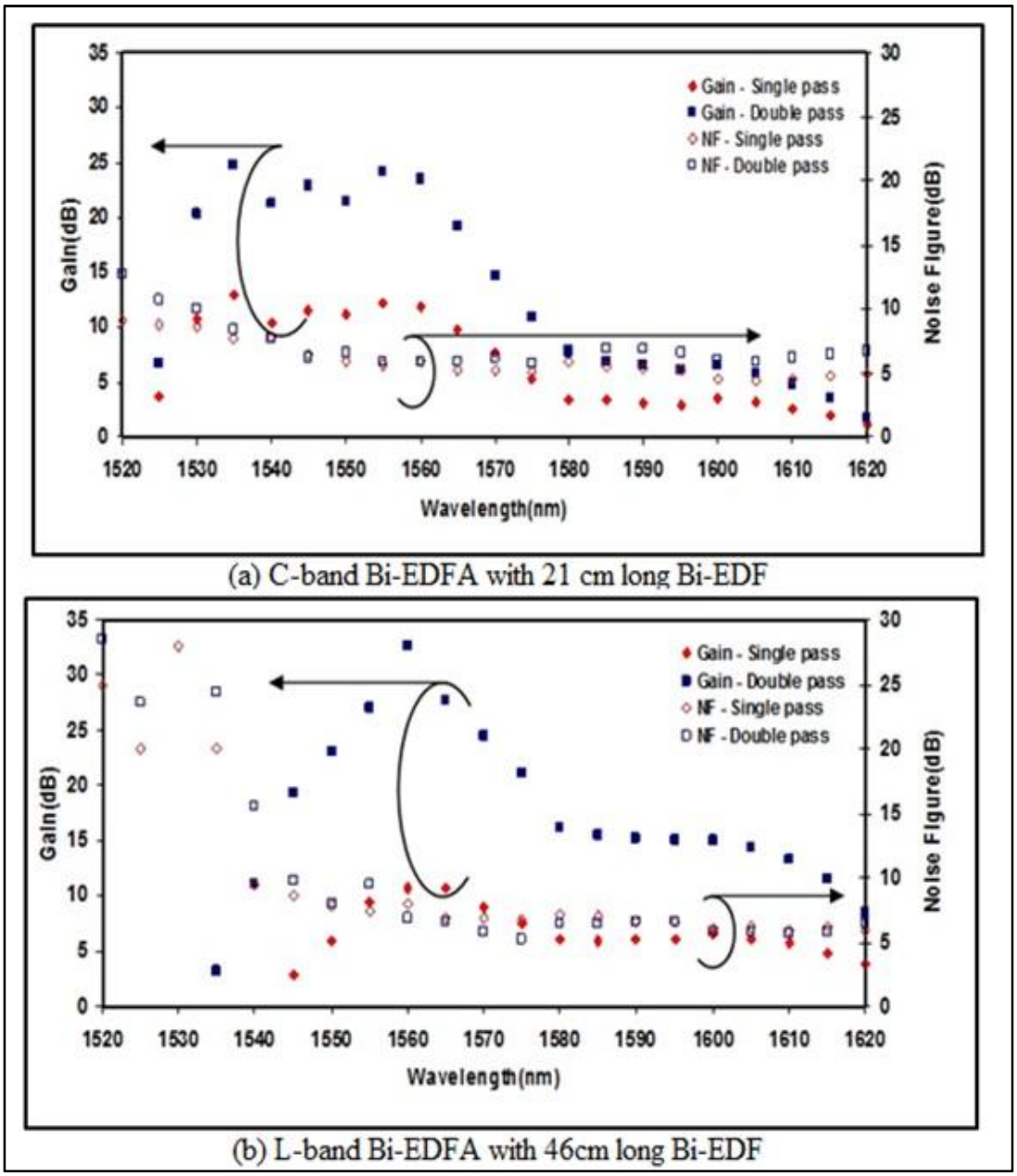

Figure 5.3: Gain and noise figure spectra of the Bi-EDFA at input power of -30dBm

Meanwhile, for L-band amplifier, the gain increases from 6.0dB to 16.2dB at 1580nm due to the increase in the effective gain medium length increment as shown in

Figure 5.3(b). It is also observed in both figures that the noise figure for the double pass Bi-EDFA is reasonably higher by an average of 2dB when compared to that of the single pass configuration. This is attributed to the higher counter propagating ASE at the input part of the amplifier which reduces the population inversion and therefore increases the noise figure. Consequently, the noise figure is relatively higher for shorter wavelength which is attributed to the lower gain and higher loss characteristics associated with the shorter wavelength.

Since double pass configuration provides a higher gain, this scheme is used to construct a wideband EDFA by combining the 21cm long C-band Bi-EDFA and the 46cm long L-band Bi-EDFA in serial configuration. In the experiment, the 21cm and 46cm Bi-EDF are pumped at the optimum pump powers of 150mW and 100mW respectively. The gain and noise figures for configuration are measured across the C and L-band wavelength regions for two input signal levels, such as small input signal power (-30dBm) and high input signal power (0 dBm)and the results are shown in Figure 5. 4 (a) and (b) respectively.

Wideband operation is achieved in the amplifier, which covers from 1525nm to 1620nm as shown in the figures. For input signal of -30dBm, the average gains of the linear Bi-EDFA are obtained at approximately 15dB with gain variation of ±3 dB within the wavelength region from 1530 to 1605nm. Additionally, in this configuration, the gain is slightly less than L-band due to the gain saturation effect in the C-band region. The unused L-band ASE from the second stage passes through the C-band CFBG and was amplified by the first stage amplifier, which in turn suppresses the amplifier's gain in the C-band region. For input signal of 0dBm, the average gain of approximately 10dB with a gain variation of ±2dB within 1540nm to 1620nm region is obtained for linear Bi-EDFA. Furthermore, a higher L-band gain is observed

in the linear Bi-EDFA, which due to the L-band signals travelling a longer effective gain medium length in the linear configuration. This causes the amplification region shifting to a longer wavelength; however, the C-band gains are lower in the linear Bi-EDFA due to the gain saturation effect which reduces the population inversion in the C-band region.

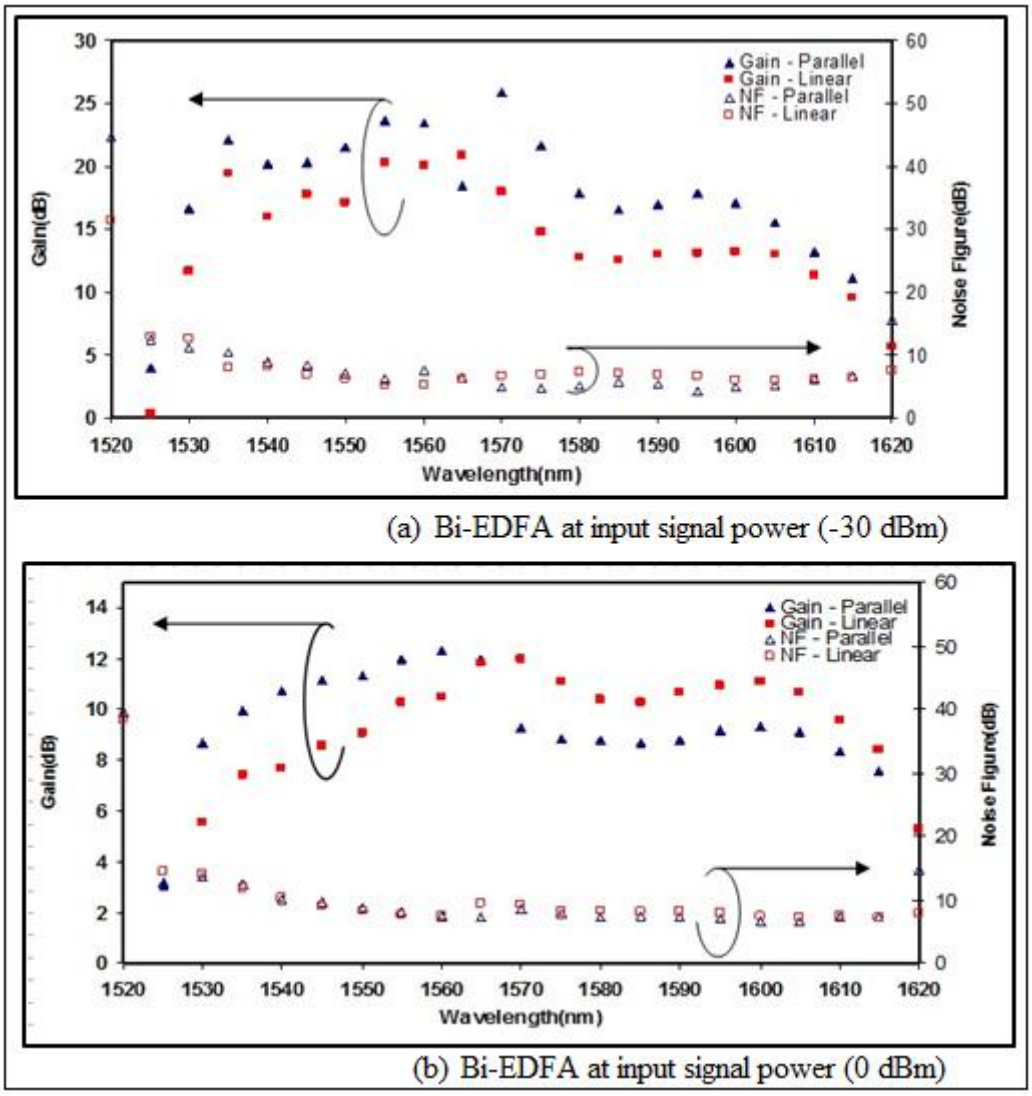

Figure 5.4: Gain and noise figure spectra of the Bi-EDFA at input signal power of (a) -30dBm and (b) 0dBm

The higher gains are obtained in the smaller input signal of -30dBm and this indicates that the effects of the population inversion is larger for smaller input signals whereas the high input signals suppress the population inversion and thus reduce the attainable gain. On the other hand, the noise figures of the amplifier is maintained below 10 dB within the wavelength region from 1535nm to 1620nm for these input signal powers as shown in Figure 5.4(b).

5.4 OPTICAL AMPLIFIER WITH FLAT-GAIN AND WIDE-BAND OPERATION UTILIZING A HIGHLY CONCENTRATED EDF

It is very difficult to splice a Bi-EDF with a standard SMF due to the difference in melting temperature. The Bi-EDF has a lower melting compared to that of silica fiber. Therefore, the interest of silica–based EDF (Si-EDF) is growing up especially for a compact, flat-gain and wide-band operations. Here, the performance of new flat-gain wideband optical amplifier is demonstrated by utilizing a highly concentrated EDF as the gain media in a serial configuration. The performance of the amplifier is investigated for two different gain media, namely Si-EDF and Bi-EDF, for operating in the C-band region for the firststage. The second stage employs a forward pumped 9m long Si-EDF for operationin the L-band region. A chirp fiber Bragg grating (CFBG) is incorporated in each stage to allow for the double-pass operation. The proposed configuration is similar to Fig. 5.1 using a two-stage setup and two CFBGs. The C-band and L-band signals are amplified by using 49cm Bi-EDF and a 9m Si-EDF respectively which were forward pumped by a 1480nm laser diode for a flat-gain and wide-band operation.

The Si-EDF has an erbium ion concentration of 2200ppm and a cut-off wavelength of 910nm with peak absorption rate of 41dB/m at 976nm. On the other

hand, the Bi-EDF has a higher erbium ion concentration of 3250 ppm and a cut-off wavelengthof 1440nm, as well as a pump absorption rate of 141dB/m at 1480nm. The C-band CFBG is placed between the two stages to act as a reflector for the C-band EDFA.It reflects C-band signal for double-pass operation and allows the L-band signal to be transmitted so that it can be amplified by the second stage of the amplifier.

The amplified signal is then reflected back into the system by the L-band CFBG. An optical circulator is used to route the amplified signal into the output port. The gain and noise figures of the proposed amplifier are characterized by using a TLS in conjunction with an OSA. The experiment is also repeated for all-silica optical amplifier, which is obtained by replacing the 49cm Bi-EDF with 1.5m long Si-EDF.

Fig. 5.5 compares the ASE spectrum for both amplifiers when the pump powers of 112mW and 150mW are used for the firstand second stages respectively. As shown in both ASE spectra, they are almost flat within a wide wavelength range covering both C- and L-band regions. A strong lasing wavelength between the C- and L-band regions is also observed due to the overlapping reflection spectral between the C- and L-band CFBG. Which suppressed and clamps the gain ,so that flat-gain operation is achieved. It is also observed that the use of Bi-EDF in thefirst stage to produce an ASE spectrum with stronger intensity, especially in the longerwavelength region.

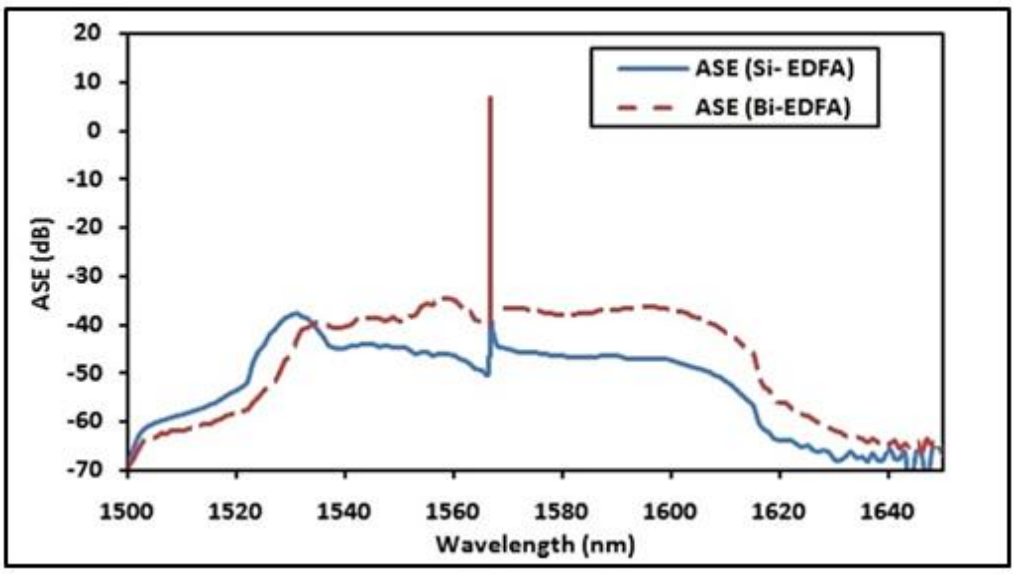

Figure 5.5: ASE spectra of the proposed serial two-stage amplifiers configured with different EDFs at the first stage.

Figure 5.6 compares the measured gain and noise figure characteristics for both amplifiers at small input signal power of -30dBm. In the experiment, the pump powers are fixed at 112 and 150mW for C-band and L-band operations respectively while input signal power is fixed at -30dBm. As shown in the figure, wide-band and flat-gain operation are achieved in both amplifiers. For instance, a flat-gain of around 16dB is achieved within a wavelength region from 1525nm to 1600nm with the all-silica optical amplifier. It is also observed that the gain produced by the hybrid amplifier (Bi-EDF + Si-EDF) is slightly higher than that produced by the all-silica amplifier, especially in longer wavelength region from 1565nm 1615nm. However, all-silica amplifier has better flatness compared to the hybrid one. A small signal gain of more than19dB is obtained within a wavelength region from 1545 to 1605nm with the use of Bi-EDF at the first stage in the hybrid amplifier.

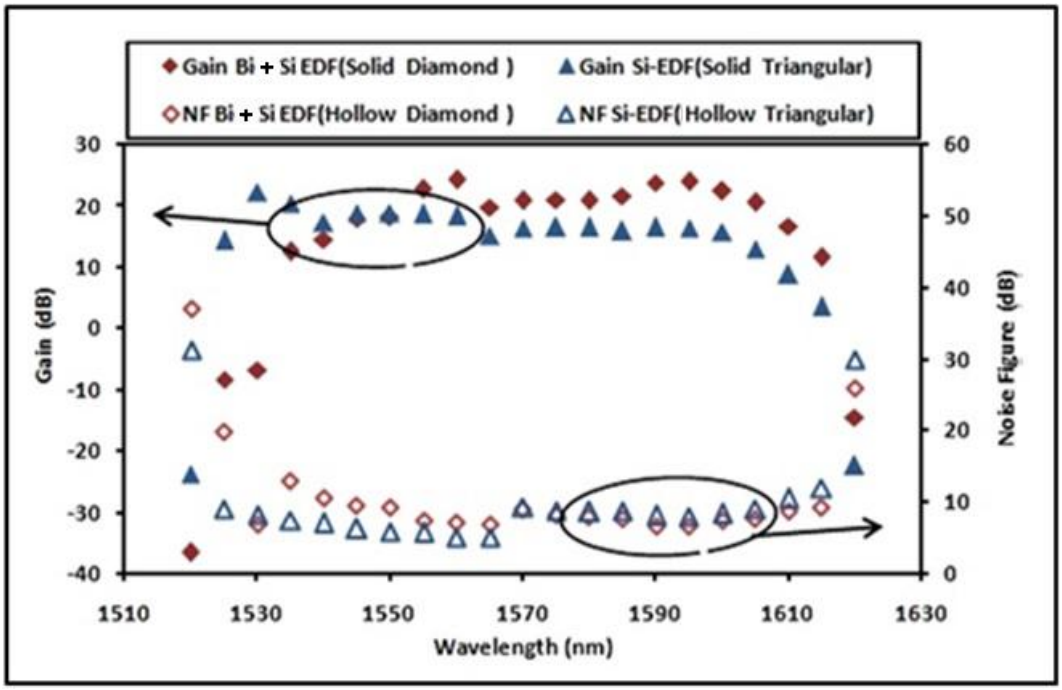

Figure 5.6: Gain and noise figure spectra for all-silica and hybrid amplifiers at input signal of -30dBm.

Compared to the hybrid amplifier, all-silica amplifier has lower noise figure especially at a shorter wavelength region. This is attributed to the gain of all-silica amplifier which is more pronounced in the shorte rwavelength region. Since the gain of the hybrid amplifier is so much higher at wavelength above 1590nm region, the noise figure of this amplifier is better at this region. Figure 5.7 shows the gain and noise figure spectra for both amplifiers at a higher input signal power of 0dBm. Both amplifiers show a flat-gain at around 10dB with a wide-band wavelength operation ranging from C-band to L-band region. Thegain spectrum exhibits a shift toward a longer wavelength region with theuse of Bi-EDF in the first stage. This is attributed to the forward ASE which isstronger with the use of Bi-EDF, compared to that produced with Si-EDF as shownin Figure. 5.3. The forward C-band ASE shifts the amplification region from C-band toL-band region while the L-band ASE reduces the loss of L-band signal and thus increases the gain in this region. With a Si-EDF, the flat gain spectrum

ranged between a wavelength region from 1535nm to 1605nm with a gain variation of less than 2dB. Compared to the amplifier with Si-EDF, the C-band noise figure in the amplifier with Bi-EDF is higher due to the relatively higher C-band ASE from the second stage which was reflected back to the gain medium and thus reducesthe population inversion at the input part of the C-band EDFA. The L-band noise figure is almost similar for both amplifiers; however, the noise figures for both amplifiers arealso maintained below 12dB in the flat-gain region. In an ideal amplifier, all signals with different wavelengths should be amplified equally which means that the gain spectrum of this amplifier should be flat. Comparing the results work with those from parallel configuration, the new proposed amplifier shows a better gain flatness, especially at the boundary between 1535nm to 1575nm.

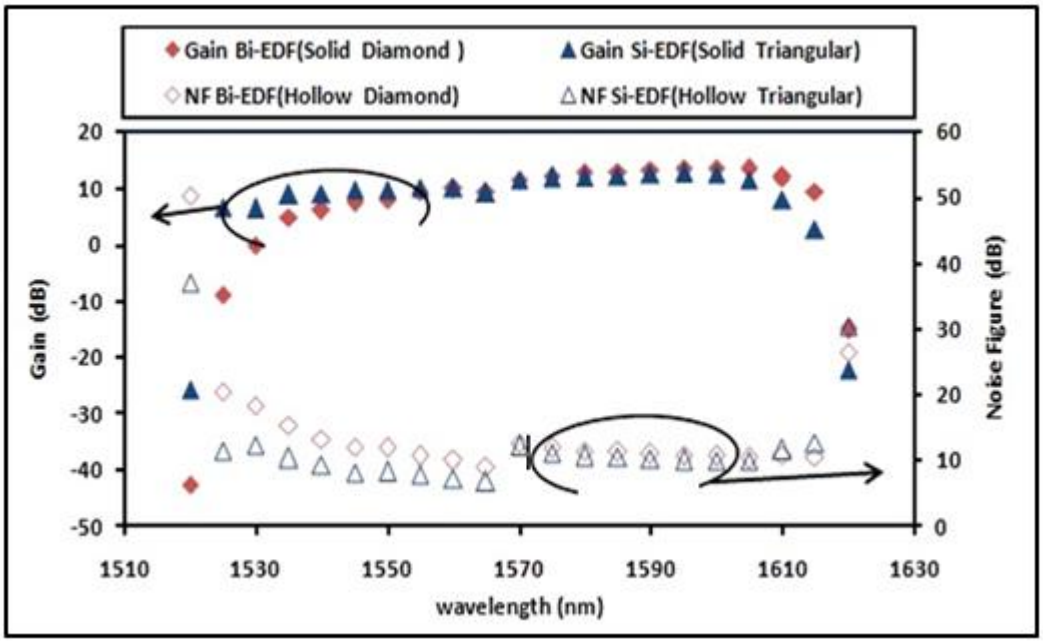

Figure 5.7: Gain and noise figure spectra for both amplifiers at a higher input signal Power of 0dBm.

5.5 WIDEBAND EDFA IN SERIAL DOUBLE-PASS CONFIGURATION

5.5.1 Analytical analysis for Silica-based EDFA

Here, an analytical evaluation of a silica-based EDF is presented for both C- and L-band operations. Since the EDFA uses pump wavelength of 1480nm, the two energy levels systems are considered. The Er^{3+} ions densities of upper state population (N_2) and ground state population (N_1) are calculated as follow (Desurvire, 1994):

$$N1 = \circ \frac{1 + W_{21}^{2}}{1 + (W_{12} + W_{21})^{2} + R^{2}} \tag{5.1}$$

$$N2 = \circ \frac{R^{2} + W_{12}^{2}}{1 + (W_{12} + W_{21})^{2} + R^{2}} \tag{5.2}$$

Where W_{12} and W_{21} are stimulated absorption rate and stimulated emission rate respectively, R is the pumping rate, τ is the fluorescence lifetime and $\rho = N_1 + N_2$ is the Er^{3+} ions density per unit volume. The value of W_{12}, W_{21} and R can be calculated as:

$$W12 = \frac{\pm_{SA}\Gamma_S}{hV_S A}\left[P_S^{+} + P_S^{-} + P_a^{+} + P_a^{-}\right] \tag{5.3}$$

$$W21 = \frac{\pm_{SE}\Gamma_S}{hV_S A}\left[P_S^{+} + P_S^{-} + P_a^{+} + P_a^{-}\right] \tag{5.4}$$

$$R = \frac{P_P \Gamma_P \pm_P}{hV_P A} \tag{5.5}$$

Where $\pm_{SE}$ and $\pm_{SA}$ are the emission and absorption cross sections of the signal, while $\pm_{PE}$ and $\pm_{PA}$ are the emission and absorption cross sections of the pump. V_S and V_P are the signal and pump frequencies respectively. Γ_S and Γ_P are the overlap factors of the signal and the pump respectively. It represents the overlap of the erbium ions with the mode of the signal light field and pump light field respectively.

Here, A is the effective cross-sectional area of the distribution of erbium ions, where h is the Planck constant, P^{+}_{S} is the forward signal power, P^{-}_{S} is the backward signal power which is equal to the final signal output power of EDFA and P_P is the pump power of EDFA. P^{+}_{ase} and P^{-}_{ase} are the forward and backward spontaneous emission powers of EDFA respectively. The values of all the above parameters are shown in Table 5.1.

Table 5.1
EDF parameters for C-band

a_S = 1550 nm.	$\pm_{SA}(a_S)$ = 2.85 X 10-25 m2
a_p = 1480 nm.	$\pm_{SE}(a_S)$ = 4.03 X 10-25 m2
d_S = 0.43	$\pm_{PA}(a_P)$ = 2.86 X 10-25 m2
d_P = 0.40	$\pm_{PE}(a_P)$ = 0.32 X 10-25 m2
A = 19.8 X 10-8 m2	Δv = 3100 GHz (25 nm)
= 440 ppm	= 0.011 seconds
$\sim_S$ = 0.20 dB/Km	$\sim_P$ = 0.24 dB/Km

Figure 5.8 shows the upper state population and ground state population N_1 and N_2 respectively as a function of fiber length correspond to 150mW pump power, -30 dBm signal power and λ=1550nm. As N_1 and N_2 intersect at 1.5m, so the optimum EDF length for C-band operation is 1.5m. As the EDF length further increases, the gain gets saturated and the use of pump power becomes inefficient.

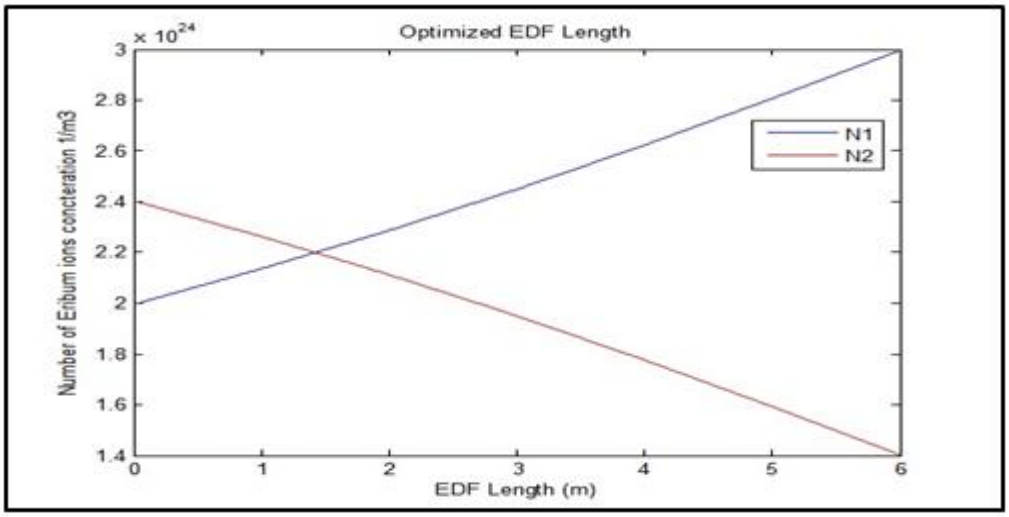

Figure 5.8: Optimization the EDF length for C-band operation

Table 5.2
EDF parameters for L-band

a_S = 1590 nm.	$\pm_{SA}(a_S)$ = 421 X 10^{-25} m^2
a_P = 1480 nm.	$\pm_{SE}(a_S)$ = 1.297 X 10-25 m^2
d_S = 0.43	$\pm_{PA}(a_P)$ = 2.86 X 10-25 m^2
d_P = 0.40	$\pm_{PE}(a_P)$ = 0.32 X 10-25 m^2
A = 19.8 X 10-8 m^2	Δv = 3100 GHz (25 nm)
= 2200 ppm	= 0.011 seconds
$\sim_S$ = 0.20 dB/Km	$\sim_P$ = 0.24 dB/Km

On the other hand, for the L-band operation is optimized based on Figure. 5.9. The figure shows the upper state population (N_2) and ground state population (N_1) against EDF length, which is obtained when the pump power, input signal power and input signal wavelength were fixed at 60mW pump power, -30dBm and 1590 nm, respectively . Table 5.2 shows all the parameters that is used in this analysis

N_1 and N_2 intersect at 9m (Figure 5.9) whereby the pump power is fully absorbed and further increase in the length supports an increment of stimulated emission. Moreover, for an EDF length of longer than 9m, the stimulated emission

process starts to take power from the input signal power and thus degrades the attainable gain and increases the noise figure. Furthermore, if the selected length is less than 9m, some pump power will not be used efficiently to improve gain. This shows that the optimum EDF length for L-band operation is 9m at the pump power of 60mW.

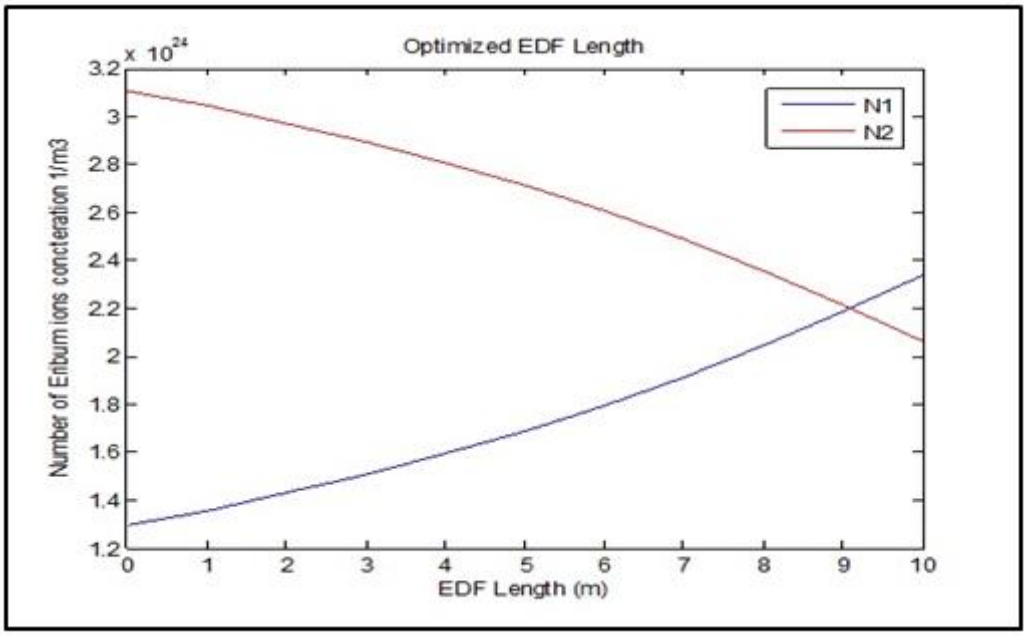

Figure 5.9: Optimization the EDF length for L-band EDFA operation

As shown in Figure 5.9, N_1 and N_2 intersect at 9m whereby the pump power is fully absorbed and further increase in the length will not support an increment of stimulated emission. Moreover, at EDF length of longer than 9m the stimulated emission process starts to take power from the input signal power and thus degrades the attainable gain and increases the noise figure. Furthermore, if the chosen length is less than 9m, some pump power will not be used efficiently to improve gain. This shows that the optimum EDF length for L-band operation is 9m at the pump power of 60 mW.

The forward signal power, backward signal power, pump power, forward ASE and backward ASE are represented by P_S^+ , P_S^- , P_p , P_a^+ and P_a^- respectively. The values of all the powers can be calculated by the following equations (Nadir, 2007c):

$$\frac{dP_{ASE}^+}{dz} = P_{ASE}^+ \mathrm{d}_S(\pm_{SE}N_2 - \pm_{SA}N_1) + 2\pm_{SE}N_2\mathrm{d}_S h\nu_S \mathrm{a}\nu - \sim_S P_{ASE}^+ \quad (5.6)$$

$$\frac{dP_{ASE}^-}{dz} = -P_{ASE}^- \mathrm{d}_S(\pm_{SE}N_2 - \pm_{SA}N_1) - 2\pm_{SE}N_2\mathrm{d}_S h\nu_S \mathrm{a}\nu + \sim_S P_{ASE}^- \quad (5.7)$$

$$\frac{dP_p^+}{dz} = P_p^+ \mathrm{d}_p(\pm_{PE}N_2 - \pm_{PA}N_1) - \sim_p P_p^+ \quad (5.8)$$

$$\frac{dP_S^+}{dz} = P_S^+ \mathrm{d}_S(\pm_{SE}N_2 - \pm_{SA}N_1) - \sim_S P_S^+ \quad (5.9)$$

$$\frac{dP_S^-}{dz} = -P_S^- \mathrm{d}_S(\pm_{SE}N_2 - \pm_{SA}N_1) + \sim_S P_S^- \quad (5.10)$$

Where $\Delta\nu$ is the bandwidth of the ASE and z is the organize along the DFA. The gain of the EDFA can be obtained from the organize analytical solutions of Equations (5.6) - (5.10) with the help of Equations (5.1) to (5.5).

On the other hand, the noise figure is generated by spontaneous emission; the number of spontaneous photons is given by (Becker, 2002).

$$\dagger_{SP} = \frac{\dagger N_2}{\dagger N_2 - N_1} \quad (5.11)$$

where the (z) is the coordinate along the EDFA fiber and $\dagger$ defined as following;

$$\dagger = \frac{\pm_{SE}}{\pm_{SA}} \quad (5.12)$$

As a result, NF of the high gain DP-EDFA at signal wavelengths (a_S) is calculated as following:

$$NF(\text{a}S) = \frac{1 + 2\text{¦}_{SP}[G_{EDFA} - 1]}{G_{EDFA}} \tag{5.13}$$

For high gain condition (Gain>20 dB) the noise figure equation (Desurvire, 1994) can be written as:

$$\text{NF}(\text{a}_S) \approx 2\text{¦}_{SP} \tag{5.14}$$

The gain and noise figure spectra of all-silica wide-band EDFA were simulated at optimized parameters using MATLAB software. For C- and L-band operations, the optimized length are obtained 1.5m and 9m at the optimized pump powers of 150mW and 60 mW respectively for small input signal operation at -30dBm. The experiment is conducted in order to verify the theoretical analysis. Figure 5.10 shows the simulation and experimental results depict the flat-gain and wide-band operations. As shown in the figure, the highest simulated gain of 26.2dB is obtained at 1530nm while the minimum simulated gain of 13.5 was obtained at 1615nm. The average simulated gain of 23dB was obtained within the wavelength region from 1525nm to 1610nm with gain variation of ± 3.5. The corresponding simulated noise figure was less than 5dB within this wavelength region. As also shown in Figure 5.10, the experimental result is in good agreement with the simulation result.

The experimental gains are slightly lower than the simulation one due to the insertion loss of the components, which have been ignored in the theoretical analysis. The experimental noise figure was higher compared to the simulation at L-band region due to effect of forward ASE from C-band, which was ignored.

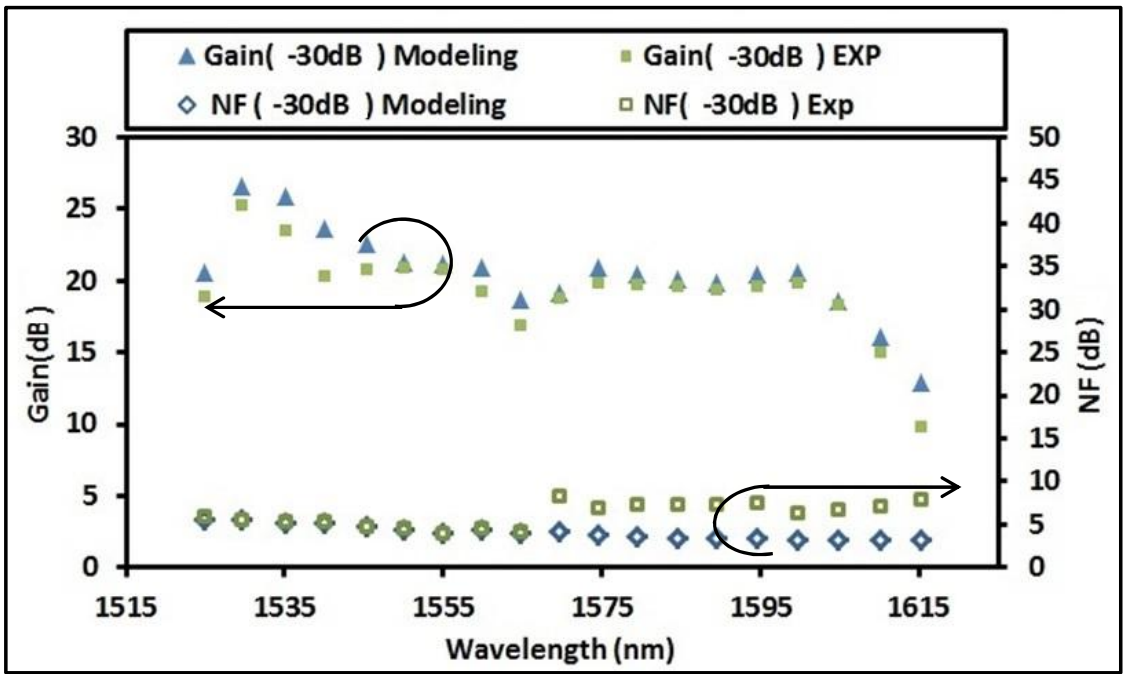

Figure 5.10: The simulated gain and noise figure spectra at small input signal power of -30dBm. The experimental result is also shown for comparison purpose.

5.5.2 Bench-marking of the proposed configuration

The major criterions of the compact optical fiber amplifiers are: gain, noise, bandwidth, and gain spectrum flatness. These parameters are reported more or less in the following range: NF < 08dB, Higher gain more then > 20dB, Flatter gain variation ±03dB and Wider bandwidth (C and L-band together). In this section, the performance of the proposed two stage-silica EDFA is compared with two different serial configurations. In this proposed, gain medium is a highly doped fiber with Erbium ion concentration of 2200ppm, which the length is fixed at the optimized values of 1.5m and 9m for C-band and L-band operation, respectively. Two forward pump laser at 1480nm with optimum output power of 150 mW and 60mW were deployed in C-band and L-band stages respectively. A WDM coupler was used to combine the pump light with the signal at each stage. The C-band chirp fiber Bragg grating (CFBG) is placed midway the two stages to act as a reflector for the C-band

EDFA. It reflects C-band signal for double-pass operation and pass-through the L-band signal to be transmitted so that it can be amplified by the second stage of the amplifier. The amplified signal is then reflected back into the system by the L-band CFBG as shown in Figure 5.11(a). The performance of the wideband amplifier with serial configuration of Figure 5.11(b) is also investigated for comparison purpose.

In this amplifier (Sinivasagam, 2004) is serial configuration C-plus L-band EDFA with over 70nm operating range is obtained (Sinivasagam, 2004). The design consists of two 980/1590 wavelength selective couplers: WSC1 and WSC2, two silica based erbium doped fibers (EDF) of different lengths: EDF I (4.2m) and EDF II (8m) and both pumped by 978nm pump lasers. The pump I and pump II pump powers were fixed at 62.3mW and 90.3mW respectively throughout the experiment. Both pump power could deliver a maximum pump power of 100mW and the actual pump coupled to WDM I and WDM II experienced about 0.5dB loss due to insertion loss, splice loss and difference in numerical aperture (NA). The two EDFs have the same properties with a cutoff wavelength of 831nm, 16.2dB/m peak absorption at 1530nm. The EDFA was characterized from 1530 to 1605 at 5nm steps using a tunable C to L-band laser source as the input signal (Ando Model: AQ4321D) and the output signal was monitored via an optical spectrum analyzer (OSA) (AndoModel: AQ6317B). The performance parameter such as gain, NF and output power was taken at 10nm span with 0.2nm resolution for input 30dBm as shown in Figure 5.11(b).

The components used in this EDFA design were optimized at L-band with a 7dB insertion loss at the C-band. These components were selected due to the unavailability of components that have low insertion loss in both the C- and L-band region. Besides, the gain of C-band signal in an EDFA is normally higher than that of a L-band signal which could compensate the high insertion loss of the L-band

components used in the design. The selection of L-band WDM especially WDM II could prevent backward ASE from Stage II from undesired ASE induced population inversion that could cause gain depletion in Stage I of the EDFA design.

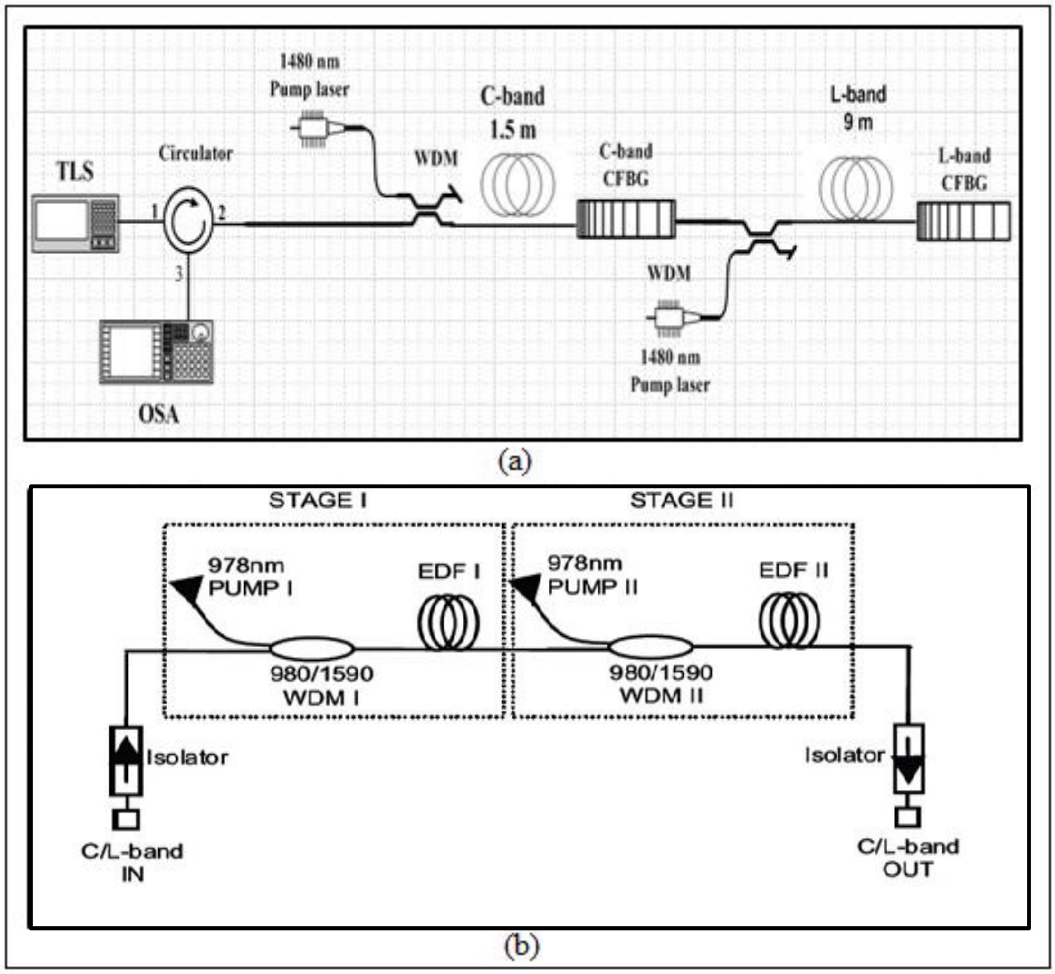

Figure 5.11: Configuration of two-stage double-pass EDFAs in (a) proposed and (b) (Sinivasagam, 2004).

For the combination purpose, the gain and noise figure characteristics for the proposed and the (Sinivasagam, 2004) are obtained for the C-band and L-band stages as shown in Figure 5.12. The measured gain and noise figure characteristics for both amplifiers are at the small input signal power of -30dBm. As shown in the figure, wideband and flat-gain operation are achieved in both amplifiers. For instance, a flat-gain of around 22dB is achieved within a wavelength region from 1540nm to 1610nm

for the proposal amplifier. It is also observed that the gain produced by the another serial amplifier (EDF 4.2m + EDF 8m) is all less than the proposal amplifier for all the wideband, for example the 18.5dB at wavelength 1530nm while at the same wavelength of the prposal amplifier the gain is higher by 10dB. This is due to the high concentration of the proposal configuration compare to the serial amplifier. Moreover, the proposal amplifier has better flatness compared to the another one. Compared to serial amplifier the higher gain is obtained also in the L-band for the proposal amplifier which indicates that the effect of the population inversion is larger. While the gain in the serial amplifier suppress the population inversion and thus reduce the attainable gain. In contrast, the noise figure for both amplifiers were maintained below 10dB within the C- and L-band.

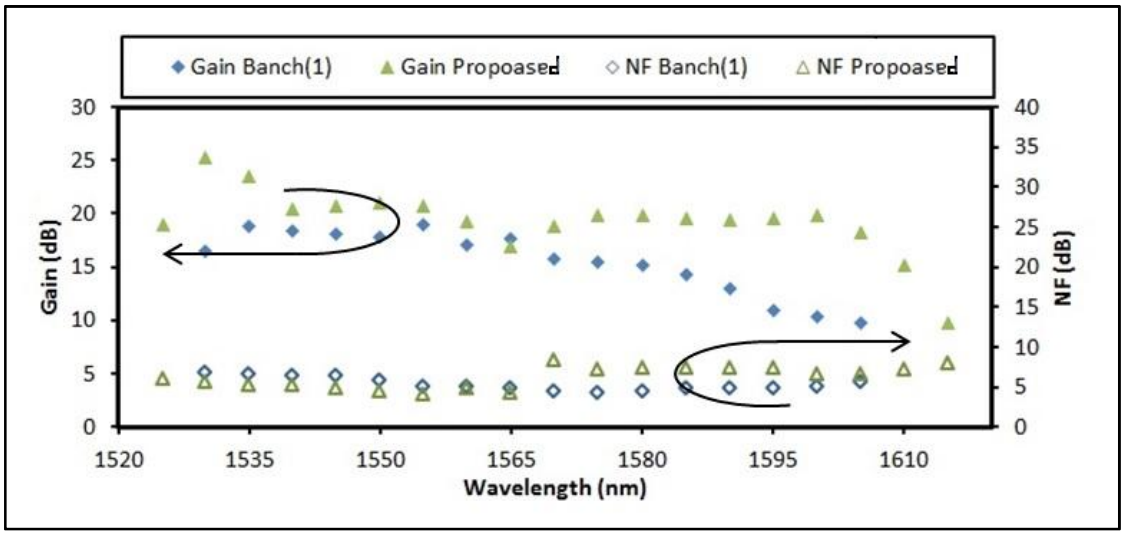

Figure 5.12: comparing the gain and noise in C- and L-band spectra for proposed and as bench mark (Sinivasagam, 2004).

Wide-band bismuth-based er8bium-doped fiber amplifier with a flat-gain characteristic is prposed by (Cheng, 2009). In this amplifier, a broadband FBG is incorporated in between the stages to prevent the gain saturation at C-band, to flatten

the overall gain spectrum and to reduce the noise figure especially for C-band. The advantage of the Bi-EDFA, in comparison with the other type of EDFA, is that its gain bandwidth can cover the C and L-band region. The configurations consist of two pieces of Bi-EDF sections as gain media, a broadband fiber Bragg grating (FBG) and optical circulators. The FBG is placed in between the two stages to act as a reflector for the C-band Bi-EDFA. It reflects C-band signal and allows the L-band signal to be transmitted. the transmission spectrum of the FBG has a reflectivity of more than 98% centered at a wavelength of 1545 nm with a bandwidth of about 40 nm. The Bi-EDF has an erbium ion concentration of 3250ppm and a cutoff wavelength of 1440 nm, as well as a pump absorption rate of 83 dB/m at 1480 nm. The Bi-EDF's length is set at 49 cm and 215cm for the first and second stages, respectively. Both 49-cm and 215-cm-long Bi-EDFs are pumped by a 1480-nm laser diode to provide amplifications in C-band and L-band, respectively.

The C-band signal, ranging from 1520 nm to 1565 nm, is amplified in the first stage, and reflected back by using broadband FBG to the first stage to undergo amplification for the second time. The L-band signal, which start from the above 1565nm will go through the FBG and is amplified in the second stage of the amplifier. Then the amplified signal is reflected back into the system by a loop mirror that is constructed using an optical circulator. The loop mirror is constructed by connecting port 3 with port 1 so that the light from port 2 is routed back into the same port. A tunable laser source (TLS) is used in conjunction with an optical spectrum analyzer (OSA) to characterize the Bi-EDFA as shows inn the figure 5.13(b). Whereas the proposed amplifier is explained early in Figure 5.11(a).

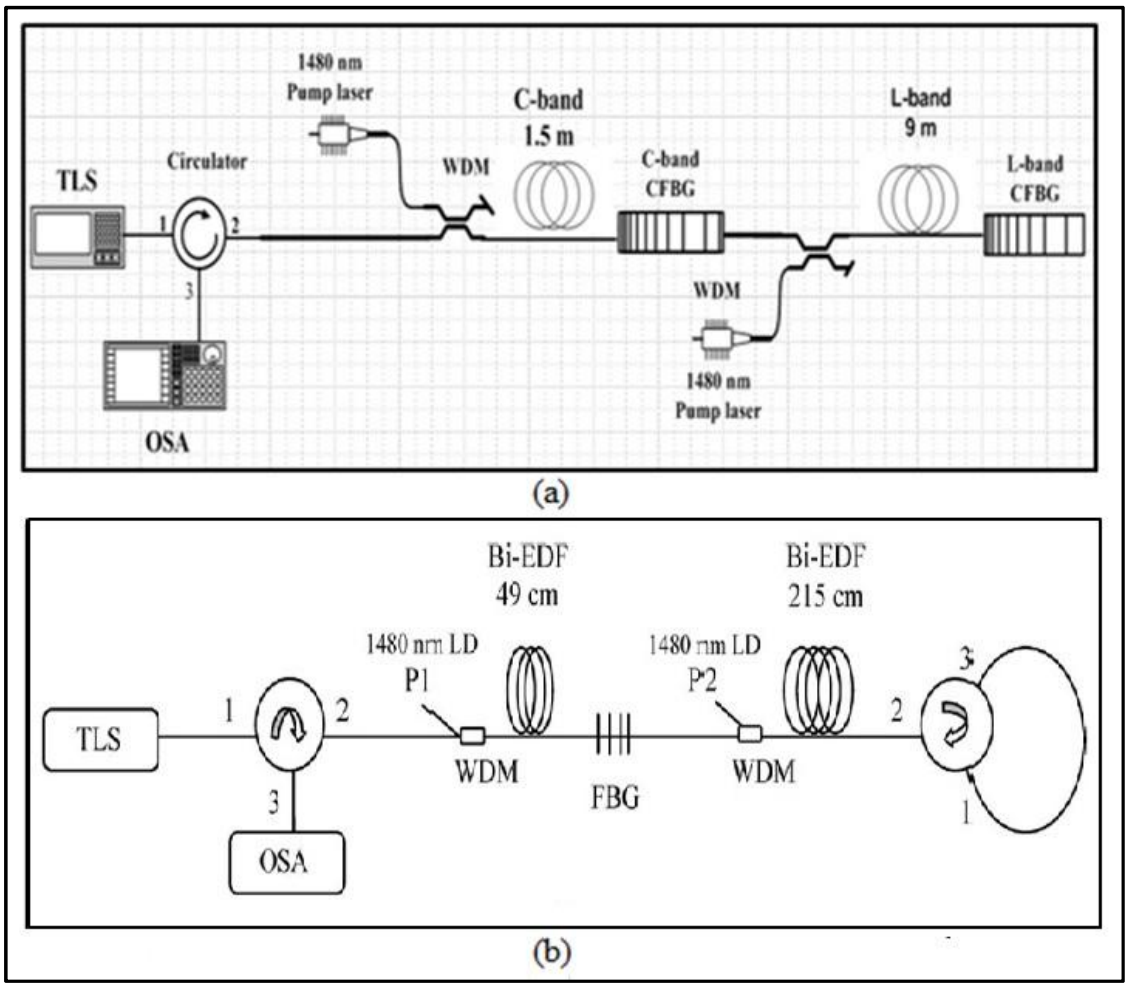

Figure 5.13: Configuration of two-stage double-pass EDFAs in (a) proposed and (b) (Cheng, 2009).

For the combination purpose, the gain, noise figure and flatness characteristics for the proposed amilifier and the second serial amplifier are obtained for the C-band and L-band stages as shown in Figure 5.14. The slow gain and noise figure characteristics for the proposed and the second serial amplifiers are at the small input signal power of -30dBm. As shown in the figure, wideband and flat-gain operation are attained in both amplifiers. It is observed that the gain produced by the second serial amplifier (EDF 49cm + EDF 215cm) for the C and L band respectively is higher than the proposal amplifier over the bandwidth. For instent at 1550nm and 1605nm the gain is close to 33.5dB while at the same wavelength of the prposal amplifier the gain

is lower by 12.5dB and 16.5 dB for C and L-band correspondingly. This is attributable to the high concentration of the serial amplifier compare to the proposal configuration. However, it observed the second serial amplifier is unflatness over bandwidth which can not avoiding transmission impairments that causes by heterogeneous amplification. The proposal amplifier has better flatness compared to the second serial amplifier where it is given a wider flat gain (1540nm to 1610m), average gain (22dB) with variation of ±3dB and low noise figure less than (6.5dB) at low input signal power (-30dBm). At the wavelength 1570nm, the gain of the wide-band amplifier suddenly increases due to shift in the amplification medium from 1.5m to 9m. The corresponding noise figure of the second serial amplifier is around 9dB in the C-band, which is much different compared to the proposed amplifier due to the effect of the back amplification of ASE as shown in the Figure 5.14. On the other hand, both amplifiers have all most same noise figure noise which around 8dB. Table 5.3 shows the compering of the three amplifiers in terms of maximum gain, maximum noise figure, flatness gain and bandwidth.

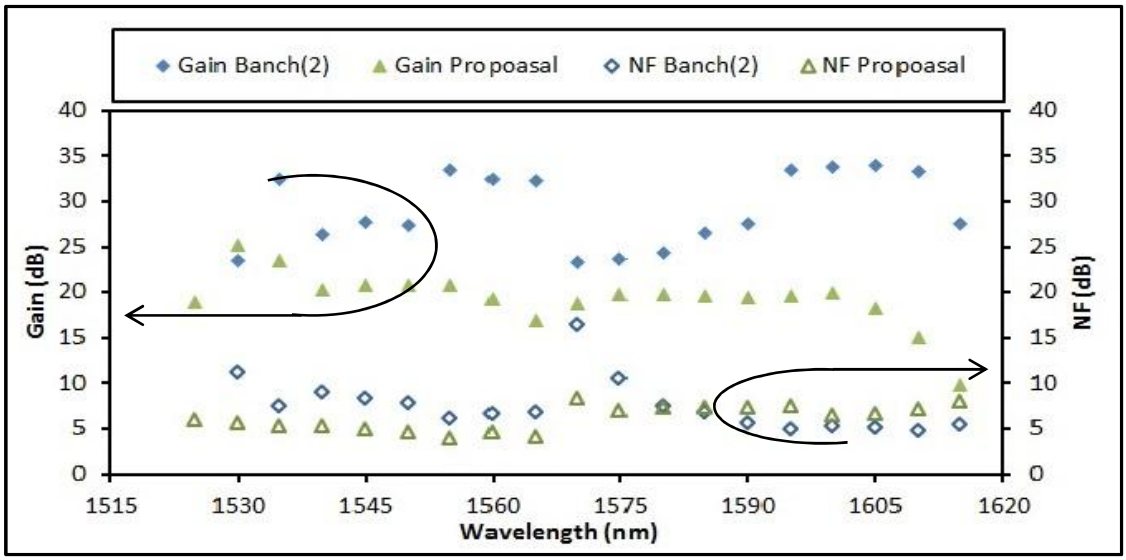

Figure 5.14: Comparing the gain and noise figure for proposed and bench mark (Cheng, 2009) in C- and L-band spectra.

Table 5.3

Comparing the three amplifiers

Amplifier	Max Gain	Max NF	Flatness Gain	Bandwidth
Sinivasagam, 2004 Normal Concentration (440ppm)	19dB	6.6dB	(1535-1575nm) 40nm	(1530-1605nm) 75nm
(Cheng, 2009) High Concentration (6300ppm)	34dB	16dB	(1535-1575nm) 40nm	(1530-1615nm) 85nm
Proposal Amplifier (2011) High Concentration (2200ppm)	25dB	7.5dB	(1540-1610) 70nm in C & L band	(1525-1615nm) 90nm

5.6 **SUMMARY**

Compact, wideband and flat-gain optical amplifiers are demonstrated using a new serial configuration. A broadband CFBG is used in both the C-band and L-band stages to allow a double pass operation and increase the attainable gain. First, a wide-band operation of a Bi-EDFA was demonstrated using a short Bi-EDF with a total length of 67cm. At high input signal power 0 dBm, the average gain of approximately 10dB with a gain variation of ± 2dB is obtainedwithin 1540nm to 1620nm region with aserial configuration. The noise figure in this configuration is maintained below 10 dB within wavelength region from 1535 nm to 1620nm.

A flat-gain and wideband EDFA is also demonstrated using a hybrid gain medium and all-silica gain medium. The application of Bi-EDF in the first stage

improved the small signalgain as well as shifts the gain spectrum slightly to longer wavelength region but atthe expense of noise figure penalty at C-band region. The small signal gain of more than 19dB is obtained within a wavelength region from 1545 to 1605nm with theuse of Bi-EDF. In the proposed amplifier, the flat gain spectrum is observed, ranging from wavelength region from 1535nm to 1605nm with a gain variation of less than 2dBat the input signal of 0dBm.

The proposed amplifier is bench-marked with the two different serial amplifier at the end of this chapter. At input signal power of -30dBm, the average flat-gain of 22dB with variation of ±3dB is achieved within wavelength spectra from 1530nm to 1600nm. The corresponding noise figure varies from 4 to 8dB over this wavelength spectra. Compared to the benchmark work mentioned earlier, the flat-gain and bandwidth as well as noise figure of the proposed amplifier are demonstrated to be better.

CHAPTER 6

CONCLUSION AND FUTURE WORK

6.1 CONCLUSION

This research work has presented the development of an enhanced wide-band high concentration optical amplifier using experimental and analytical approaches. An extensive investigation of the theoretical background of EDFA is carried out in the form of a critical review of contemporary research works. From the investigation of the impact of increasing the doping concentration on the EDF, it is found that the I-25 fiber gives better performance when compared to I-6 fiber. The results obtained show enhanced values of gain-coefficient-efficiency (GCE) and figure-of-merit (FOM) verifying the effectiveness of the analysis and performance evaluation carried for both amplifiers.

In addition, the performance of a single stage EDFA as single-pass and double-pass configurations is presented with EDF length of 1.5m and 9m for operations in C-band and L-band respectively. A CFBG is used to allow double-pass propagation leading to an increased attainable gain. At input signal power of -30dB, an averaged flat gain of approximately 25dB over C-band region and an averaged flat gain of approximately 30dB over L-band region are achieved by the double-pass amplifier with ±3dB gain variation of approximately. Compared to a single-pass amplifier the flat gain wider bandwidth as well as noise figure of the double-pass amplifier have been shown to be better results in terms of gain, noise figure and flatness than other contemporary research works.

A wide-band EDFA operating within a wavelength region from 1530nm to 1605nm is then demonstrated using a double-pass parallel configuration with CFBG. A CFBG is used in both C-band and L-band stages to allow a double pass operation for increasing the attainable gain. At an input signal power of -30dBm, the measured gain varies from 23dB to 36dB within a wideband region from 1530nm to 1605nm.

Wideband and flat-gain optical amplifiers are investigated using a new serial double-pass configuration. A broadband CFBG is used in both the C-band and L-band stages to allow a double-pass operation which increases the attainable gain, the flat gain spectrum is observed, ranging from wavelength region 1535nm to 1605nm with a gain variation of less than 2dB at the input signal of 0dBm. The proposed serial configuration is benchmarked with the conventional parallel configuration for all-silica amplifier. At input signal power of -30dBm with an average flat-gain of 22dB with variation of ±3 dB is achieved within wavelength spectra ranging from 1530nm to 1600nm.

6.2 RESEARCH CONTRIBUTION

The contribution of this research work lies in the development of an enhanced EDFA which is able to increase the amplification bandwidth, thus supporting more channels for use in DWDM networks. An enhancement of such a level contributes towards overcoming the current limitations of band gain flattening features besides maintaining the original phase of the signal compared to the current EDFAs already in use in the markets. In addition, wide band dispersion compensation technique is embedded in the proposed configuration to overcome the dispersion of the link, hence, it is hoped that the findings in this research will spark more light into more research initiatives aimed at integrating dispersion compensating modules with optical

amplifiers. The resulting proposed amplifier leads to enhancing the broad-band applications in wavelength division multiplexed long-haul communication systems as well as local optical networks.

6.3 RECOMMENDATION FOR FUTURE WORK

In addition to the attenuation compensation, the proposed amplifier has the capability to compensate for dispersion as well. Hence, an extensive research is needed to model the dispersion compensation effects more precisely. Also further studies could be extended to add a polarization controller on to the proposed design in the effort of improving the overall performance. Finally, as the proposed amplifier is designed to be locally pumped, a further study on a dual amplification technique in the form of a hybrid of Raman amplifier and remotely-pumped EDFA is needed to increase the transmission span.

REFERENCES

Abd El–Naser and Ahmed Nabih (2010). Comparison performance evolution of different transmission techniques with bi-directional distributed Raman gain amplification technique in high capacity optical networks. Inter. *J. P. Sci*., 5(5), 484-495.

Alexander Graham Bell (1880). On the Production and Reproduction of Sound by Light. *American Journal of Science* 118, 305–324.

Agrawal, G.P. and Headley C.(2005). *Raman amplification in fiber optical communication system*. Academic Press.

Ahmed M.H., et al (1998). Combined Erbium and Raman amplification at 1.55 µm in submarine links using backward pumping at 1.48 µm. *Pure and Applied Optics Journal of the European Optical Society Part A*, 659-666.

Arumugam (2001). Optical fiber communication - An overview. *Pramana- Journal of Physics*, 57(5) 849–869.

Agrawal, G.P. (1992). *Fiber-optic communication systems*.Wiley.

Armitage, J.R. (1988). Three-level fiber laser amplifier: *A theoretical model. Applied Optics* 27(23), 4831-4836.

Armitage, J.R. (1991). Introduction to glass fiber lasers and amplifiers. *Optical Fiber Lasers and Amplifiers*.

Bonada, et al (2007). Noise Figure Characterization in Erbium Doped Fibers for Remotely Amplified PONs. Transparent Optical Networks, *International Conference on Digital Object Identifier* 4, 219 - 222.

Becker, P.C., et al. (1999). *Erbium-Doped Fiber Amplifiers: Fundamentals and Technology*. Academic Press.

Becker, et al (2002). *Erbium doped fiber amplifiers fundamentals and technology*. Academic Press.

Buet, L., et al (2001). Error-free 100×10 Gbit/s unrepeatered transmission over 350 km . *Proceedings of the Optical Fiber Communication Conference and Exhibit* 2, 5-1 – 5-3.

Berkdemir and Ozsoy (2009). On the Temperature-Dependent Gain and Noise Figure Analysis of C-Band High-Concentration EDFAs with the Effect of Cooperative up Conversion. *Lightwave Technology Journal*27(9), 1122 – 1127.

Baris Altiner, and Ozlem Unverdi. (2009). Modelling - Simulation and Gain Flattening Improvements for an Erbium Doped Fiber Amplifier. *International Symposium Optomechatronic Technologies, 451 – 454.*

Belloui et al. (2003). A High-Gain EDFA Design Using Double-Pass Amplification with a Double-Pass Filter. *IEEE photonics technology letters* 15(9), 1195-1197.

Bijan G.and Sourangshu M. (2011). All-Optical Wavelength Encoded Nand And NorOperations Exploiting Semiconductor Optical Amplifier Based Mach-Zehnder Interferometer Wavelength Converter And Phase Conjugation System. *Optics and Photonics Letters*4(2), 47–55.

Bisson J.-F., and Kouznetsov D. (2008). Study of the Complex Atomic Susceptibility of Erbium-Doped Fiber Amplifiers. *Journal Of* Lightwave Technology 26, (4),457-459.

Boumaza N, et al (2009). Numerical simulation of nonlinear pulses propagation in a nonlinear optical directional coupler Intl. *Journal Physical Science.* 4 (9),505-513.

Bolshtyansky, et al (2000). Model of temperature dependence for gain shape of erbium-doped fiber amplifier. *J.LightwaveTechno* 18(11), 1533–1540.

Bjarklev, A.S., et al (1989). Large signal modeling of an Erbium-doped fiber amplifier. *Proceedings of SPIE, Fiber Laser Sources and Amplifiers Optic*1171, 118-129.

Chun, et al. (2003). Optical automatic gain control of EDFA using two oscillating lasers in a single feedback loop. *Optics Communications,* 157–162.

Connelly and T Damhus (2005). Nomenclature of Inorganic Chemistry: IUPAC

Chaudhry, et al (1994). Unrepeatered transmission at 2.5 Gbit/s over 410 km with a single remote amplifier and dispersion compensation. *Electronics Letters* 30(24), 2061-2063.

Choi, S., et al (2002). Higher-order-mode dispersion compensation technique based on mode converter using hollow optical fiber. *Proceedings of Optical Fiber Communication Conference*, 177-178.

Chesnoy, J. (2002). *Undersea Fiber Communication Systems*. Academic Press.

Chang , et al. (2006). A dual pumped double-pass L-band EDFA with high gain and low noise. *Optics Communications* 267, 108-112.

Chin-Feng Sand Likarn W (2007). Gain enhancement of L-band EDFA by using residual pump power in a three-stage configuration. *Optics Communication* 280,412– 416.

Chang and Kamikawa. (1989). Losses in small-radius bends in single-mode fibers**.** *Electronics Letters* 25(15), 947 -949.

Carmelo, et al. (2005). Influence of Pump Direction in All-Optical Gain-Clamped EDFA. *SBMO/IEEE MTT-S International Microwave & Optoelectronics Conference, 550 – 554.*

Chien, et al. (2004). S- plus C-band erbium-doped fiber amplifier in parallel structure. *Optics Communications* (241), 443–447.

Djafar, et al (2001). *Fiber-optic communication technology*. Prentice Hall

Desurvire (1987). High-gain Erbium dope traveling-wave fiber amplifier. *Optics Letters* 12 (11), 888-890.

Delevaque, E., et al. (1993). Modeling of pair-induced quenching in erbium-doped silicate fibers. *IEEE Photonics Technol. Lett.* 5, pp. 73–75

Desurvire, E. and Simpson J.R. (1989). Amplification of spontaneous emission in Erbium-doped single-mode fibers. *Journal of Lightwave Technology* 7(5), 835-845.

Desurvire (1994). *Erbium-doped fiber amplifiers, principles and applications*. Wiley.

Ellison, et al.,(1999). Hybrid erbium silicate conventional-band fiber amplifier with ultra low gain ripple. *Opt Amplifiers and their amplifications*, 51-56.

Franz, J.H. and V.K. Jain. (2000). *Optical communications: components and systems*. Alpha Science.

Farah et al. (2009). EDFA Gain Optimization for WDM System. *ELEKTRIKA*, 11(1), 34-37.

Gabla, et al. (1992). 401 km, 622Mb/s and 357km, 2.488Gb/s IM/DD repeaterless transmission experiences using Erbium-doped fiber amplifiers and error correcting code. *IEEE Photonics Technology Letters*, 4 (10), 1148-1151.

Giles, H. and Coupland, N. (1991). Language: Contexts and Consequences. Keynes: Open University Press 60-61.

Gordon, J.P. and Mollenauer L.F. (1991). Effects of fiber nonlinearities and amplifierspacing on ultra-long distance transmission. *Journal of Lightwave Technology* 9(2), 170-173.

Harry, J. and R. Dutton. (1998). *Understanding optical communications*. Prentice Hall

Hansen, P.B., et al. (1995). 2.488 Gbit/s unrepeatered transmission over 423 Km employing remotely-pumped post- and pre-amplifiers. *Electronic Letters31(6) 466-467.*

Hamida B. A., et al (2012). Wideband and compact erbium-doped fiber amplifier using parallel double-pass configuration. *Microwave and Optical Technology Letters* 54(3), 629-631.

Holton, C. and S. Henderson. (2003). *Lasers focus world magazine*. PennWell.

Harun, et al. (2010). Experimental and theoretical studies on a double-pass C-band bismuth-based erbium mdoped fiber amplifier. *Opt. Laser Technology* 42, 790–793.

Harun, et al., (2009). Experimental and theoretical studies on a double-pass C-band bismuth based erbium-doped fiber amplifier. *Optics & Laser Technology* 3(10), 971-974.

Harun, et al. (2003).Effect of injection of C-band ASE on L-band erbium-doped fiber amplifie. *JETP Letters*, 77(9) 461-463.

Harun and H. Ahmad (2004 a). Gain clamping in double-pass L-band EDFA using a broadband FBG. J.*phy*., 62 (4), 893-897.

Harun, et al. (2004 b). All-Optical gain clamped Double–pass L-band EDFA based on partial reflection of AES. *IEICE Elect. Exp*1(7)171-175.

Harun and Harith (2004 c). Gain Clamped Two-Stage Double-Pass L-Band EDFA With A Single Fiber Bragg Grating. *Chinese Phys Lett 21(10), 1954-1957.*

Harun and H. Ahmad, (2004 d). Demonstration of Highly Efficient Flat-Gain L-band EDFA With Two-Stage Double- Pass Configuration. *ECTI Transactions on Electrical Eng., Electronics and Communications 2, (1), 36-39.*

Harun, et al. (2005). Gain enhancement in partial double-pass L-band EDFA system using a band-pass filter. *Laser Phys. Lett*. 2(1) 36-38.

Harun, et al. (2006). Gain-clamping techniques in two-stage double-pass L-band EDFA. *J. Phys.* 66 (3)539-545.

Faustini and Martini. (1997). Bend loss in single-mode fibers. *Journal of Lightwave Technology* 15(4), 671-679.

Haugen, et al. (1992). Bidirectional transmission at 622 Mb/s utilizing erbium-doped fiber amplifiers. *IEEE Photonics Technology Letters*, 4(8), 913-916.

Hao et al., (2005). Noisefigure improvement of a double-pass erbium-doped fiber amplifier by using a HiBi fiber loop mirror as ASE rejecter. *Opt. Comm*., 244,383-38.

Hagimoto, et al (1989). 250 km nonrepeated transmission experiment at 1.8Gb/s using LD pumped Er^{3+}- doped fiber amplifiers in IM/Direct detection system. *Electronics Letters* 25(10), 662-663.

James, B.A. (1991). A review of the fabrication and properties of Erbium-doped fibers for optical amplifiers. *Journal of Lightwave Technology*, 9(2) 220-227.

Jeunhomme, L. (1990). *Single-mode fiber optics principles and application*. Marcel Dekker.

Ji, J.H., et al (2005). Low noise-figure gain-clamping L-band double-pass doped fiber ring lasing amplifier with interleaver. *Journal of Lightwave Technology*,23(3), 1375-1379.

Jouinia (2002). Spectroscopic investigations of neodymium cyclotripho sphates. *J.Luminescence*, 99(4), 365-372.

Juhan Lee, et al. (1999). Enhancement of Power Conversion Efficiency for an L-Band EDFA with a Secondary Pumping Effect in the Unpumped EDF Section. *IEEE Photonics Technology Letters*, 11(1)

John (1996).*Optic fiber and light-abrilliant combination*, p (1).

Jerrard (1980). Optical fiber communications. *Optics & Laser Technology* 12 (4) 221

Keiser and Gerd.(2000). *Optical fiber communications*. McGraw-Hill Higher Education

Kaur and Gupta (2010). Enhancing the Performance of WDM Systems by using TFF in hybrid amplifiers. *IEEE Advance Computing Conference (IACC*), 106 – 109.

Liaw, et al. (1997). Chirped-fiber-grating integrated optical limiting amplifier for dispersion compensation. *Proceedings of the IEEE Lasers and Electro-Optics Society Annual Meeting*1, 26-27.

Mrinmay et al. (2007). Investigation of the optical gain and noise figure for multi-channel amplification in EDFA under optimized pump condition. *Optics Communications* 273, 407– 412.

Mears, et al. (1987). High gain rare-earth-doped fiber amplifier at 1.54 μm. *Proceedings of the Optical Fiber Communication Conference, 3(12), 167-169.*

Mears, et al. (1988).Optical fiber amplifiers for 1.5 μm operation. *Proceedings of the Optical Fiber Communication Conference, 3-5.*

Miyakawa, et al (2002).40 Gbit/s×25 WDM unrepeatered transmission over 362 km. *Electronics Letters*, 38(14), 726-727.

Ma, M.X., et al (1998). 240 km repeater spacing in a 5280 km WDM system experiment using 8 2.5 Gb/s NRZ transmission. *IEEE Photonics Technology Letters* 10(6), 893-895.

Nagaraju , M.C. and Paul, M. Pal(2009). Design and fabrication of an intrinsically gain flattened Erbium doped fiber amplifier. *Optics Communications* 282, 2335-2338.

Naji, et al. (2004). Efficient 1480 nm Er^{3+} doped fiber amplifier using narrow-band filtering in double-pass amplification. *International Symposium on Information and Communication Technologies* 4, 11-14.

Naji AW, et al. (2006 a). Dual-function remotely-pumped Erbium-doped fiber amplifier Loss and dispersion compensator. *Optics Express*, 14(8) 8054-8059.

Naji AW, et al. (2006 b). Repeaterless Transmission Incorporating Enhanced Remotely-Pumped EDFA and Distributed Raman Amplifier. *Laser and Electro-Optic Seminar:* SP24.

Naji AW, et al. (2006 c). Dual-function remotely-pumped Erbium-doped fiber amplifier: Loss and dispersion compensator. *J. Opt. Express, OSA*, 14(18)8054-8059.

Naji, et al. (2011). Review of Erbium-doped fiber amplifier, *International Journal of the Physical Sciences*, 6(20) 4674-4689.

Nadir H, et al (2007a).A Numerical Analysis of R-EDFA for Long Haul Optical Fiber Communication System. 4th International Conference: Sci. *Electr. Technol. Info. Telecomm*,25-29.

Nadir H, (2007b). Modeling of Hybrid EDFA/DRA for Long Haul Optical Fiber Commuication System. Msc dissertation, Malaysia.

Nadir H, et al (2007c). Modeling Optimization and Experimental Evaluation of Remotely Pumped Double Pass EDFA. *Microw. Opt. Technol. Lett*., 49(9) 2257-2261.

Nadir H, et al (2007d).Numerical Analysis and Optimization of Remotely Pumped Double Pass Erbium Doped Fiber Amplifier. *IEICE Electronics Express* 4(5), 172-178.

Peter, et al. (1989).Bit Error Rate Performance for Optical Fiber Systems with modal noise. *Journal of Light wave Technology*7 (9), 1285-1289.

Palais, J.C. (1998) . *Fiber optic communications*. New York: Prentice Hall.

Park, et al. (1996). Doped fiber length and pump power of gain- flattened EDFAs. *Elect.Lett*.32, 2161.

Papannareddy, R. (1997). *Introduction to lightwave communications systems*. Artech House.

Park, et al. (1998). A gain-flattened two-stage EDFA for WDM optical networks with a fast link control channel, *Optics Communications*, 153,23–26

Paul, et al. (2010). Wideband EDFA based on erbium doped crystalline zirconia yttriaalumino silicate fiber. *J. LightwaveTechnol*28 , 2919-2924.

Kazovsky, et al., (1996). *Optical fiber communication system*.Artech House.

Kunihiko,(1998).1.3-μm Pr-doped In-Ga-based Fluoride fiber amplifiers pumped by grating-fiber-pigtailed 0.98-μm-band laser diodes with a detuned wavelength of 1 μm. *IEEE Photonics Technology Letters* 10(8), 1112-1114.

Khairi, et al. (2004 a) High gain triple-pass amplification in two-stage optical amplifier architecture. *Microw. Opt. Techn. Let*, 41(4) 317-318.

Khairi, et al. (2004 b). Optimum pumping scheme of dual-stage trple-pass erbium – doped fiber amplifier. *Microw Photonics Techn. Leterst* 16(2), 419-421.

Kuntze Scott. B. and Aaron J. Zilkie (2008). Nonlinear State–Space Model of Semiconductor Optical Amplifiers With Gain Compression for System Design and Analysis. *Journal of Light wave Technology, vol. 26(14), 2274-2280*.

Loh, et al. (1996). Dispersion Compensation over Distances in Excess of 500 km for *Microw* l0-Gb/s Systems Using Chirped Fiber Gratings. *IEEE Photonics Technology Letters* 8(7) 944-946.

Qiang et al., (2004). A novel 3-stage structure for a low-noise, high-gain and gain-flattened L-band erbium doped fiber amplifier. J. Zhejiang Uni. Sci., 5(9)1130-1134.

Qiu, Y.Q., et al (2010). Spectral characteristics of the erbium-bismuth co-doped silica fibers and its application in single frequency fiber laser. *Laser Phys*. 20, 1418–1424.

Rosolem JB and Juriollo AA (2008).S Band EDFA Using Standard Erbium Doped Fiber, 1450 nm pumping and Single Stage ASE Filtering. *International ConferenceOptical Communication*.Netw.1-3.

Shih et al.,(2002). Optically gain-clamped wideband erbium-doped fiber amplifier using acommon figure-eight feedback-loop lasing light. *Optics Communications*205, 293–298.

Seongtaek et al. (2001). Broad-Band Erbium-Doped Fiber Amplifier with Double-Pass Configuration. *IEEE Photonics Technology Letters, 13(12).*

Senior, J.M (1992). *Optical fiber communications: principles and practice*. Prentice.

Sung Cho, et al. (1998). Dynamically gain –flattened hybrid optical amplifier utilizing erbium doped fiber amplifier semiconductor optical amplifier. *ECOC*, 363-364.

Smith and McGreer.(1999). Diffraction gratings utilizing total internal reflection facets in littrow configuration. *IEEE Photonics Technology Letters*, 11(1) 84-86.

Sun,et al. (1998). A Gain-Flattened Ultra Wide Band E for High Capacity WDM Optical Communications Systems , *ECOC*.

Seo, et al., (2005).A Novel Hybrid Silica Wide-Band Amplifier Covering S + C + L Bands with 105-nm Band-width. *IEEE Photonics Technology Letters* 17(9), 1830-1832.

Sinivasagam, et al., (2004). C-plus l-band EDFA with over 70nm operating range. *IEEE*, 3, 78 – 81.

Surinder Singh and R. S. Kaler, (2006). Gain flattening approach to physical EDFA for 16 × 40 Gb/s NRZ-DPSK WDM optical communication systems. *Fiber and Integrated Optics*, 25(5), 363-374.

Tamechika (2006). 14 Tbit/s over a single optical fiber: successful demonstration of world's largest capacity. *News release (NTT) Science and Core Technology Laboratory Group.*

Tsair and Shih H (2008). The L-band EDFA of high clamped gain and low noise figure implemented using fiber Bragg grating and double-pass method. *Opt. Comm.*, 281(5)1134-1139.

Tsair, et al. (2000). Optimum configuration and design of 1480-nm pumped L-band gain-flattened EDFA using conventional erbium-doped fiber. *Optics Communication*183, 51–63.

Tanabe, et al. (2000). Broad band 1.5um emission of Er^{3+} ion in bismuth based glasses for potential WDM amplifier. J. Luminescence87,670-672.

Urquhart, P. (1988). Review of rare earth doped fiber lasers and amplifiers. *IEEE Proceedings of Optoelectronics*, 135(6) 385-407.

Wilczewski, et al. (1996). Determination of the field radius from bending loss measurements of optical fibers with arbitrary index profile**.** *IEEE Photonics Technology Letters* 8 (1), 90-91.

Yoshida, S. Kuwano, and K. Iwashita (1995), *Electron, Lett*,.

Zhi et al., (2003).Optimal design of L-band EDFAs with high-loss inter-stage elements.*Opt. Comm*., 224, 63-72.

APPENDIX A

MATLAB PROGRAM

```
function C-band
LambdaP   = 1480 * 10^(-9);
h         = 6.626 * 10^(-34);
C         = 3 * 10^8;
Tau       = 0.011;
AlphaP    = ( (0.24)/  (10 * log10 (exp(1))) ) * 10 ^ (-3);
AlphaS    = ( (0.20)/  (10 * log10 (exp(1))) ) * 10 ^ (-3);
dv        = 3100 * 10 ^ (9);
Length    = 8;
SigmaPA   = 2.787671233 * 10^(-25);
SigmaPE   = 0.810563905 * 10^(-25);
GammaP    = 0.43;
GammaS    = 0.40;
Ro        = 4.4 * 10^(24);
PPa = [ 5 ] ;

lambda = [  1520 * 10^(-9)      4.54835*10^(-25)    3.454733*10^(-25);
          1521 * 10^(-9)      4.7776*10^(-25)     3.718083*10^(-25);
          1522 * 10^(-9)      5.04271*10^(-25)    4.020069*10^(-25);
          1523 * 10^(-9)      5.32998*10^(-25)    4.35097*10^(-25);
          1524 * 10^(-9)      5.62611*10^(-25)    4.692887*10^(-25);
          1525 * 10^(-9)      5.90693*10^(-25)    5.02889*10^(-25);
          1526 * 10^(-9)      6.14827*10^(-25)    5.335156*10^(-25);
          1527 * 10^(-9)      6.33159*10^(-25)    5.592383*10^(-25);
          1528 * 10^(-9)      6.44239*10^(-25)    5.782373*10^(-25);
          1529 * 10^(-9)      6.4722*10^(-25)     5.905457*10^(-25);
          1530 * 10^(-9)      6.42063*10^(-25)    5.955165*10^(-25);
          1531 * 10^(-9)      6.28243*10^(-25)    5.931096*10^(-25);
          1532 * 10^(-9)      6.06044*10^(-25)    5.830345*10^(-25);
          1533 * 10^(-9)      5.75987*10^(-25)    5.653245*10^(-25);
          1534 * 10^(-9)      5.39887*10^(-25)    5.409713*10^(-25);
          1535 * 10^(-9)      5.01088*10^(-25)    5.131305*10^(-25);
          1536 * 10^(-9)      4.3682*10^(-25)     4.864009*10^(-25);
          1537 * 10^(-9)      4.2772*10^(-25)     4.612518*10^(-25);
          1538 * 10^(-9)      4.10073*10^(-25)    4.507026*10^(-25);
          1539 * 10^(-9)      3.944*10^(-25)      4.433733*10^(-25);
          1540 * 10^(-9)      3.83521*10^(-25)    4.407568*10^(-25);
          1541 * 10^(-9)      3.75302*10^(-25)    4.404659*10^(-25);
          1542 * 10^(-9)      3.67768*10^(-25)    4.408823*10^(-25);
          1543 * 10^(-9)      3.5975*10^(-25)     4.401749*10^(-25);
          1544 * 10^(-9)      3.50806*10^(-25)    4.380954*10^(-25);
          1545 * 10^(-9)      3.40935*10^(-25)    4.344712*10^(-25);
          1546 * 10^(-9)      3.3058*10^(-25)     4.303382*10^(-25);
```

```
        1547 * 10^(-9)     3.20105*10^(-25)   4.257337*10^(-25);
        1548 * 10^(-9)     3.10032*10^(-25)   4.206963*10^(-25);
        1549 * 10^(-9)     3.00322*10^(-25)   4.162752*10^(-25);
        1550 * 10^(-9)     2.91056*10^(-25)   4.118853*10^(-25);
        1551 * 10^(-9)     2.82434*10^(-25)   4.082463*10^(-25);
        1552 * 10^(-9)     2.74577*10^(-25)   4.054906*10^(-25);
        1553 * 10^(-9)     2.67325*10^(-25)   4.032823*10^(-25);
        1554 * 10^(-9)     2.60475*10^(-25)   4.010286*10^(-25);
        1555 * 10^(-9)     2.53707*10^(-25)   3.991122*10^(-25);
        1556 * 10^(-9)     2.46777*10^(-25)   3.964253*10^(-25);
        1557 * 10^(-9)     2.39726*10^(-25)   3.933061*10^(-25);
        1558 * 10^(-9)     2.32272*10^(-25)   3.888089*10^(-25);
        1559 * 10^(-9)     2.24174*10^(-25)   3.831779*10^(-25);
        1560 * 10^(-9)     2.15471*10^(-25)   3.758389*10^(-25);
        1561 * 10^(-9)     2.06084*10^(-25)   3.668944*10^(-25);
        1562 * 10^(-9)     1.96535*10^(-25)   3.569296*10^(-25);
        1563 * 10^(-9)     1.86583*10^(-25)   3.458282*10^(-25);
        1564 * 10^(-9)     1.76793*10^(-25)   3.33918*10^(-25);
        1565 * 10^(-9)     1.66922*10^(-25)   3.213979*10^(-25); ] ;

      lambda1 = lambda(:,1) ;

Vp      = (C) / LambdaP;
Vs      = (C) / lambda(1,1);
A       = 19.8 * 10^(-12);

len = length(lambda) ;
Pinput = zeros(1,len) ;
Poutput = zeros(1,len) ;
gain = zeros(1,len) ;
NF = zeros(1,len) ;
NF_dB = zeros(1,len) ;

figure
hold on
for L = 1 :
for k = 1 : len

Xi     = zeros(1,Length+1);
Pp     = zeros(1,Length+1);
PaF    = zeros(1,Length+1);
Ps     = zeros(1,Length+1);
Ps_neg = zeros(1,Length+1);
N1     = zeros(1,Length);
N2     = zeros(1,Length);
% _____________________________________________________________
```

```
%  5. Calculation of Forward signal and Forward ASE from forward direction.
%_____________________________________________________________

PaF(1)  = 0;
Xi(1)   = 1;
Ps(1)   = 10 ^ (-35/10)*(10 ^ -3) ;
Pp(1)   = PPa(L) * (10 ^ -3);
Rx      = ( Pp(L) * SigmaPA * GammaP) / (h * Vp * A);
W12     = ( (Ps(1) + PaF(1)) * lambda(k,2) * GammaS) / (h * Vs * A);
W21     = ( (Ps(1) + PaF(1)) * lambda(k,3) * GammaS) / (h * Vs * A);
N1(1)   = Ro * (   (1 + (W21*Tau) )   / (1 + ((W21+W12)*Tau) + (Rx*Tau)) );
N2(1)   = Ro * (   ((W12 + Rx)*Tau)   / (1 + ((W21+W12)*Tau) + (Rx*Tau)) );

for i = 1 : Length

  Xi(i+1)  =  i + 1;
  Pp(i+1)  =  Pp(i) * (exp (GammaP * (SigmaPE*N2(i) - SigmaPA*N1(i))) )* (exp(-
AlphaP)) ;
  Ps(i+1)  =  Ps(i) * (exp (GammaS * (lambda(k,3)*N2(i) - lambda(k,2)*N1(i))) )*
(exp(- AlphaS)) ,
  PaF(i+1) =  PaF(i)* (exp (GammaS * (lambda(k,3)*N2(i) - lambda(k,2)*N1(i))) )*
(exp(- AlphaS))+ 2*lambda(k,3)*GammaS*N2(i)*h*Vs*dv ;
  Rx       = ( Pp(i+1) * SigmaPA * GammaP) / (h * Vp * A) ;
  W12      = ( (PaF(i+1) + Ps(i+1)) * lambda(k,2) * GammaS) / (h * Vs * A);
  W21      = ( (PaF(i+1) + Ps(i+1)) * lambda(k,3) * GammaS) / (h * Vs * A);
  N1(i+1)  =  Ro * (   (1 + (W21*Tau))    /  (1 + ((W21+W12)*Tau) + (Rx*Tau)) );
  N2(i+1)  =  Ro * ( ((W12 + Rx)*Tau)     /  (1 + ((W21+W12)*Tau) + (Rx*Tau)) );

end
%
_____________________________________________________________
% 6.Calculation of Backward signal and Backward ASE from backward direction.
% _____________________________________________________________

Ps_neg(Length+1) = 0.9 * Ps(Length);
   PaB(Length+1) = 0;

for i = Length: -1: 1

   Ps_neg(i)      =      Ps_neg(i+1)  *  (exp  (GammaS  *  (lambda(k,3)*N2(i)  -
lambda(k,2)*N1(i))) )  * (exp(- AlphaS)) ;
     PaB(i)      =           PaB(i+1)  *  (exp  (GammaS  *  (lambda(k,3)*N2(i)  -
lambda(k,2)*N1(i))) ) * (exp(- AlphaS)) + 2*lambda(k,3)*GammaS*N2(i)*h*Vs*dv ;

end
```

```
% 7. Stabilization of the system using relaxation method.
% _____________________________________________________________

for j = 1: 200

   Rx      =  ( Pp(1) * SigmaPA * GammaP)  / (h * Vp * A) ;
   W12     = (( Ps(1)+ PaF(1) + PaB(1) + Ps_neg(1)) * lambda(k,2) * GammaS) / (h *
Vs * A) ;
   W21     = (( Ps(1)+ PaF(1) + PaB(1) + Ps_neg(1)) * lambda(k,3) * GammaS) / (h *
Vs * A) ;
   N1(1)   =  Ro * (   (1 + (W21*Tau))     / (1 + ((W21+W12)*Tau) + (Rx*Tau)) );
   N2(1)   =  Ro * ( ((W12 + Rx)*Tau)      /  (1 + ((W21+W12)*Tau) + (Rx*Tau)) ) ;

   for i = 1 : Length

      Xi(i+1)     =  i + 1;
      Pp(i+1)      =  Pp(i) * (exp (GammaP * (SigmaPE*N2(i) - SigmaPA*N1(i))) ) *
(exp(- AlphaP));
      Ps(i+1)     =  Ps(i) * (exp (GammaS * (lambda(k,3)*N2(i) - lambda(k,2)*N1(i))) )
* (exp(- AlphaS)) ,
      PaF(i+1)    =  PaF(i)* (exp (GammaS*(lambda(k,3)*N2(i)-lambda(k,2)*N1(i))))*
(exp(- AlphaS)) + (2*lambda(k,3)*GammaS*N2(i)*h*Vs*dv) ;
      PaB(i+1)              =     PaB(i) * (exp (GammaS * (-lambda(k,3)*N2(i) +
lambda(k,2)*N1(i))) ) * (exp(+ AlphaS)) - 2*lambda(k,3)*GammaS*N2(i)*h*Vs*dv ;
      Ps_neg(i+1) =      Ps_neg(i) * (exp (GammaS * (-lambda(k,3)*N2(i) +
lambda(k,2)*N1(i))) ) * (exp(+ AlphaS));

      Rx       = ( Pp(i+1) * SigmaPA * GammaP) / (h * Vp * A) ;
      W12          = ( (PaB(i+1) + PaF(i+1) + Ps(i+1) + Ps_neg(i+1)) * lambda(k,2) *
GammaS) / (h * Vs * A) ;
      W21          = ( (PaB(i+1) + PaF(i+1) + Ps(i+1) + Ps_neg(i+1)) * lambda(k,3) *
GammaS) / (h * Vs * A) ;
      N1(i+1)   =  Ro * (   (1 + (W21*Tau))    /  (1 + ((W21+W12)*Tau) + (Rx*Tau)) );
      N2(i+1)   =  Ro * ( ((W12 + Rx)*Tau)   /  (1 + ((W21+W12)*Tau) + (Rx*Tau)) );

   end
   Pinput(k) = Ps(Length) ;
   Ps_neg(Length+1) = 0.9 * Ps(Length);
   Ps(Length);
   PaB(Length+1)    = 0;

   for i = Length: -1: 1

      Ps_neg(i)      =      Ps_neg(i+1) * (exp (GammaS * (lambda(k,3)*N2(i) -
lambda(k,2)*N1(i))) )* (exp(- AlphaS));
        PaB(i)       =      PaB(i+1) * (exp (GammaS * (lambda(k,3)*N2(i) -
lambda(k,2)*N1(i))) ) * (exp(- AlphaS)) + 2*lambda(k,3)*GammaS*N2(i)*h*Vs*dv ;
```

```
 end

disp([' PUMP POWER    SIGNAL POWER  Backward Signal       FORWARD SE'])
for i = 1: Length + 1

   disp([Pp(i), Ps(i), Ps_neg(i), PaF(i)])

end

end
EtaS = lambda(k,3)/lambda(k,2)  ;
   Nsp = (EtaS * N2) / ((EtaS * N2) - N1) ;
   NF(k) = 2 * Nsp;
   NF_dB(k) = 10 * log10 (NF(k));
  % Ps(Length) = 10 * log10 (Ps (Length)* (10^3));
  % Ps_neg(1) = 10 * log10 (Ps_neg (1)* (10^3));

% 1...To see Forward and Backward signal Vs EDF length

%my1-index  =1;

%plot(my1_index, Ps_(i+1))
%hold on
%plot(half_index, Ps_neg_(i+1), 'r')
%xlabel('EDF Length m');
%ylabel('Signal Power dBm');
%legend ('Forward Signal', 'Backward Signal');

Pinput(k) = Ps(1) ;
Poutput(k) = Ps_neg(1);
gain(k) = 10*log(Poutput/Pinput)
end
plot(lambda1,gain,'rx')
xlabel('Lambda');
ylabel('Gain');

plot(lambda1,NF,'g')
legend ('Gain dB', 'Noise Figure dB');
end
```

APPENDIX B

MATLAB PROGRAM

```
function L-band
global lambda2 ;
global gain2 ;

LambdaP   = 1480 * 10^(-9);
h         = 6.626 * 10^(-34);
C         = 3 * 10^8;
Tau       = 0.011;
AlphaP    = ( (0.24)/  (10 * log10 (exp(1))) ) * 10 ^ (-3);
AlphaS    = ( (0.20)/  (10 * log10 (exp(1))) ) * 10 ^ (-3);
dv        = 3100 * 10 ^ (9);
Length    = 20;
SigmaPA   = 2.787671233 * 10^(-25);
SigmaPE   = 0.810563905 * 10^(-25);
GammaP    = 0.18;
GammaS    = 0.15;
Ro        = 4.4 * 10^(24);
PPa = [ 22 ] ;

      lambda = [

         1565 * 10^(-9)     1.66922*10^(-25)   3.213979*10^(-25);
         1566 * 10^(-9)     1.54996*10^(-25)   3.061461*10^(-25);
         1567 * 10^(-9)     1.4722*10^(-25)    2.955901*10^(-25);
         1568 * 10^(-9)     1.37752*10^(-25)   2.824172*10^(-25);
         1569 * 10^(-9)     1.28928*10^(-25)   2.695054*10^(-25);
         1570 * 10^(-9)     1.20709*10^(-25)   2.568154*10^(-25);
         1571 * 10^(-9)     1.12812*10^(-25)   2.44346*10^(-25);
         1572 * 10^(-9)     1.05278*10^(-25)   2.328453*10^(-25);
         1573 * 10^(-9)     0.98469*10^(-25)   2.216455*10^(-25);
         1574 * 10^(-9)     0.92184*10^(-25)   2.112073*10^(-25);
         1575 * 10^(-9)     0.86221*10^(-25)   2.014082*10^(-25);
         1576 * 10^(-9)     0.80782*10^(-25)   1.925746*10^(-25);
         1577 * 10^(-9)     0.75947*10^(-25)   1.844767*10^(-25);
         1578 * 10^(-9)     0.71636*10^(-25)   1.768677*10^(-25);
         1579 * 10^(-9)     0.6805*10^(-25)    1.704039*10^(-25);
         1580 * 10^(-9)     0.64384*10^(-25)   1.646325*10^(-25);
         1581 * 10^(-9)     0.61039*10^(-25)   1.591886*10^(-25);
         1582 * 10^(-9)     0.58259*10^(-25)   1.547314*10^(-25);
         1583 * 10^(-9)     0.55479*10^(-25)   1.504657*10^(-25);
         1584 * 10^(-9)     0.52861*10^(-25)   1.464488*10^(-25);
         1585 * 10^(-9)     0.50806*10^(-25)   1.430074*10^(-25);
         1586 * 10^(-9)     0.487916*10^(-25)  1.403244*10^(-25);
```

```
1587 * 10^(-9)     0.47059*10^(-25)    1.37353*10^(-25);
1588 * 10^(-9)     0.45246*10^(-25)    1.349225*10^(-25);
1589 * 10^(-9)     0.43836*10^(-25)    1.324248*10^(-25);
1590 * 10^(-9)     0.42023*10^(-25)    1.297535*10^(-25);
1591 * 10^(-9)     0.40612*10^(-25)    1.27353*10^(-25);
1592 * 10^(-9)     0.39363*10^(-25)    1.251704*10^(-25);
1593 * 10^(-9)     0.37913*10^(-25)    1.23371*10^(-25);
1594 * 10^(-9)     0.36583*10^(-25)    1.207256*10^(-25);
1595 * 10^(-9)     0.35334*10^(-25)    1.187454*10^(-25);
1596 * 10^(-9)     0.34427*10^(-25)    1.164186*10^(-25);
1597 * 10^(-9)     0.33239*10^(-25)    1.14006*10^(-25);
1598 * 10^(-9)     0.3199*10^(-25)     1.124273*10^(-25);
1599 * 10^(-9)     0.30782*10^(-25)    1.104821*10^(-25);
1600 * 10^(-9)     0.29734*10^(-25)    1.08069*10^(-25);
1601 * 10^(-9)     0.28646*10^(-25)    1.05592*10^(-25);
1602 * 10^(-9)     0.2772*10^(-25)     1.035671*10^(-25);
1603 * 10^(-9)     0.26954*10^(-25)    1.016579*10^(-25);
1604 * 10^(-9)     0.26269*10^(-25)    1.995051*10^(-25);
1605 * 10^(-9)     0.25141*10^(-25)    1.968167*10^(-25);
1606 * 10^(-9)     0.24295*10^(-25)    1.945918*10^(-25);
1607 * 10^(-9)     0.23489*10^(-25)    1.918209*10^(-25);
1608 * 10^(-9)     0.22562*10^(-25)    1.89635*10^(-25);
1609 * 10^(-9)     0.22079*10^(-25)    1.87144*10^(-25);
1610 * 10^(-9)     0.20991*10^(-25)    1.841078*10^(-25);
1611 * 10^(-9)     0.20185*10^(-25)    1.812324*10^(-25);
1612 * 10^(-9)     0.19581*10^(-25)    1.782933*10^(-25);
1613 * 10^(-9)     0.18775*10^(-25)    1.752675*10^(-25);
1614 * 10^(-9)     0.18131*10^(-25)    1.713847*10^(-25);
1615 * 10^(-9)     0.17486*10^(-25)    1.682098*10^(-25);

 ]

lambda2 = lambda(:,1) ;

Vp      = (C) / LambdaP;
Vs      = (C) / lambda(1,1);
A       = 19.8 * 10^(-12);

len = length(lambda) ;
Pinput = zeros(1,len) ;
Poutput = zeros(1,len) ;
gain2 = zeros(1,len) ;
NF = zeros(1,len) ;
NF_dB = zeros(1,len) ;


for L = 1 : 1
for k = 1 : len
```

```
% _____________________________________________________________________
%                    4. Programm Variables.
% _____________________________________________________________________

Xi     = zeros(1,Length+1);
Pp     = zeros(1,Length+1);
PaF    = zeros(1,Length+1);
Ps     = zeros(1,Length+1);
Ps_neg = zeros(1,Length+1);
N1     = zeros(1,Length);
N2     = zeros(1,Length);



% _____________________________________________________________________
%  5. Calculation of Forward signal and Forward ASE from forward direction.
% _____________________________________________________________________

PaF(1)  = 0;
Xi(1)   = 1;
Ps(1)   = 10 ^ (-35/10)*(10 ^ -3) ;
Pp(1)   = PPa(L) * (10 ^ -3);
Rx      = ( Pp(1) * SigmaPA * GammaP) / (h * Vp * A);
W12     = ( (Ps(1) + PaF(1)) * lambda(k,2) * GammaS) / (h * Vs * A);
W21     = ( (Ps(1) + PaF(1)) * lambda(k,3) * GammaS) / (h * Vs * A);
N1(1)   = Ro * (   (1 + (W21*Tau) )   / (1 + ((W21+W12)*Tau) + (Rx*Tau)) );
N2(1)   = Ro * (   ((W12 + Rx)*Tau)   / (1 + ((W21+W12)*Tau) + (Rx*Tau)) );

for i = 1 : Length

  Xi(i+1)  =  i + 1;
  Pp(i+1)  =  Pp(i) * (exp (GammaP * (SigmaPE*N2(i) - SigmaPA*N1(i))) )* (exp(-
AlphaP)) ;
  Ps(i+1)  =  Ps(i) * (exp (GammaS * (lambda(k,3)*N2(i) - lambda(k,2)*N1(i))) )*
(exp(- AlphaS)) ;
  PaF(i+1) =  PaF(i)* (exp (GammaS * (lambda(k,3)*N2(i) - lambda(k,2)*N1(i))) )*
(exp(- AlphaS))+ 2*lambda(k,3)*GammaS*N2(i)*h*Vs*dv ;
  Rx       = ( Pp(i+1) * SigmaPA * GammaP) / (h * Vp * A) ;
  W12      = ( (PaF(i+1) + Ps(i+1)) * lambda(k,2) * GammaS) / (h * Vs * A);
  W21      = ( (PaF(i+1) + Ps(i+1)) * lambda(k,3) * GammaS) / (h * Vs * A);
  N1(i+1)  =  Ro * (   (1 + (W21*Tau))    /  (1 + ((W21+W12)*Tau) + (Rx*Tau)) );
  N2(i+1)  =  Ro * ( ((W12 + Rx)*Tau)     /  (1 + ((W21+W12)*Tau) + (Rx*Tau)) );

end

% _____________________________________________________________________
%6.Calculation of Backward signal and Backward ASE from backward direction.
% _____________________________________________________________________
```

```
Ps_neg(Length+1) = 0.9 * Ps(Length);
  PaB(Length+1) = 0;

for i = Length: -1: 1

  Ps_neg(i)    =    Ps_neg(i+1)  *  (exp  (GammaS  *  (lambda(k,3)*N2(i)  -
lambda(k,2)*N1(i))) )  * (exp(- AlphaS)) ;
    PaB(i)    =    PaB(i+1)  *  (exp  (GammaS  *  (lambda(k,3)*N2(i)  -
lambda(k,2)*N1(i))) ) * (exp(- AlphaS)) + 2*lambda(k,3)*GammaS*N2(i)*h*Vs*dv ;

end

% _____________________________________________________________
%       7. Stabilization of the system using relaxation method.
% _____________________________________________________________
for j = 1: 200

   Rx     =  ( Pp(1) * SigmaPA * GammaP)  / (h * Vp * A) ;
   W12     = (( Ps(1)+ PaF(1) + PaB(1) + Ps_neg(1)) * lambda(k,2) * GammaS) / (h *
Vs * A) ;
   W21     = (( Ps(1)+ PaF(1) + PaB(1) + Ps_neg(1)) * lambda(k,3) * GammaS) / (h *
Vs * A) ;
   N1(1)   =  Ro * (   (1 + (W21*Tau))     / (1 + ((W21+W12)*Tau) + (Rx*Tau)) );
   N2(1)   =  Ro * ( ((W12 + Rx)*Tau)      /  (1 + ((W21+W12)*Tau) + (Rx*Tau)) ) ;

   for i = 1 : Length

     Xi(i+1)    =  i + 1;
     Pp(i+1)     =  Pp(i) * (exp (GammaP * (SigmaPE*N2(i) - SigmaPA*N1(i))) ) *
(exp(- AlphaP));
     Ps(i+1)    =  Ps(i) * (exp (GammaS * (lambda(k,3)*N2(i) - lambda(k,2)*N1(i))) )
* (exp(- AlphaS)) ,
     PaF(i+1)    =  PaF(i)* (exp (GammaS*(lambda(k,3)*N2(i)-lambda(k,2)*N1(i))))*
(exp(- AlphaS)) + (2*lambda(k,3)*GammaS*N2(i)*h*Vs*dv) ;
     PaB(i+1)          =    PaB(i)  *  (exp  (GammaS  *  (-lambda(k,3)*N2(i)  +
lambda(k,2)*N1(i))) ) * (exp(+ AlphaS)) - 2*lambda(k,3)*GammaS*N2(i)*h*Vs*dv ;
     Ps_neg(i+1)  =    Ps_neg(i)  *  (exp  (GammaS  *  (-lambda(k,3)*N2(i)  +
lambda(k,2)*N1(i))) ) * (exp(+ AlphaS));

     Rx      = ( Pp(i+1) * SigmaPA * GammaP) / (h * Vp * A) ;
     W12       = ( (PaB(i+1) + PaF(i+1) + Ps(i+1) + Ps_neg(i+1)) * lambda(k,2) *
GammaS) / (h * Vs * A) ;
     W21       = ( (PaB(i+1) + PaF(i+1) + Ps(i+1) + Ps_neg(i+1)) * lambda(k,3) *
GammaS) / (h * Vs * A) ;
     N1(i+1)   =  Ro * (   (1 + (W21*Tau))    /  (1 + ((W21+W12)*Tau) + (Rx*Tau)) );
     N2(i+1)   =  Ro * ( ((W12 + Rx)*Tau)     /  (1 + ((W21+W12)*Tau) + (Rx*Tau))
);

   end
```

```
   Pinput(k) = Ps(Length) ;
   Ps_neg(Length+1) = 0.9 * Ps(Length);
   Ps(Length);
   PaB(Length+1)    = 0;

   for i = Length: -1: 1

     Ps_neg(i)     =     Ps_neg(i+1)  *  (exp  (GammaS  *  (lambda(k,3)*N2(i)  -
lambda(k,2)*N1(i))) )* (exp(- AlphaS));
       PaB(i)     =     PaB(i+1)  *  (exp  (GammaS  *  (lambda(k,3)*N2(i)  -
lambda(k,2)*N1(i))) ) * (exp(- AlphaS)) + 2*lambda(k,3)*GammaS*N2(i)*h*Vs*dv ;

   end

    disp([' PUMP POWER SIGNAL POWER Backward Signal
FORWARD ASE'])
for i = 1: Length + 1

  disp([Pp(i), Ps(i), Ps_neg(i), PaF(i)])

end

end
EtaS = lambda(k,3)/lambda(k,2)  ;
   Nsp = (EtaS * N2) / ((EtaS * N2) - N1) ;
   NF(k) = 2 * Nsp;
   NF_dB(k) = 10 * log10(NF(k));


  % Ps(Length) = 10 * log10 (Ps (Length)* (10^3));
  % Ps_neg(1) = 10 * log10 (Ps_neg (1)* (10^3));

% 1...To see Forward and Backward signal Vs EDF length

%my1-index  =1;

%plot(my1_index, Ps_(i+1))
%hold on
%plot(half_index, Ps_neg_(i+1), 'r')
%xlabel('EDF Length m');
%ylabel('Signal Power dBm');
%legend ('Forward Signal', 'Backward Signal');
   Pinput(k) = Ps(1) ;
Poutput(k) = Ps_neg(1);
gain2(k) = 10*log(Poutput/Pinput);

end
```

RELATED PUBLICATIONS

1. **B. A. Hamida**, X. S. Cheng, S. W. Harun, A. W. Naji, H. Arof, S. Khan and W. AL Khateeb and H. Ahmad ," Wideband **B. A. Hamida**, X. S. Cheng, S. W. Harun, A. W. Naji, H. Arof, S. Khan and W. ALKhateeb and H. Ahmad ," Wideband and Compact Erbium-doped Fiber Amplifier Using Parallel Double-pass Configuration", Microwave and Optical Technology Letters in vol. 54, No. 3, **USA** March 2012. (ISI cited publication).

2. **B. A. Hamida**, X. S.Cheng, A. W.Naji , H. Ahmad, W. AL-Khateeb, S.Khan and S. W. Harun," Optical Amplifier With Flat-gain And Wideband Operation Utilizing Highly Concentrated Erbium-doped Fibers ", Journal of Nonlinear Optical Physics and Materials vol. 21, No. 1, **23-April-2012**. (ISI cited publication).

3. **Belal A. G**. Allah, A. W. Naji, Sheroz Khan, Wajdi ALKhateeb, S. W. Harun and Harith Ahmad, "A novel wide-band dual function fiber amplifier", International Journal of the Physical Sciences. (ISSN 1992-1950), vol. 6, no.5, pp. 1118-1126, 4 **March 2011**. (ISI cited publication).

4. **B. A. Hamida**, X. S. Cheng, S. W. Harun, A. W. Naji, H. Arof, W. ALKhateeb, S. Khan , and H. Ahmad ," Wideband and flat-gain amplifier based on high concentration erbium-doped fibres in parallel double-pass configuration", IEEE Journal of quantum Electronics, vol. 42, no 3, pp. 241-243, **2012**. (ISI cited publication).

5. **B. A. Hamida**, A. A. Latiff , M. A. Ismail, X. S. Cheng," Flat-gain Single-Stage Amplifier Using High Concentration Erbium Doped Fibers in Single-Pass and Double-pass Configurations", Photonics and Optoelectronics (SOPO), pp. 1-5**,** Chine **2012** .(IEEE).

6. **B. A. Hamida**, A.A Latiff , A. W. Naji, X. S. Cheng, S. Khan , W. AL-Khateeb, H. Ahmad and S. W. Harun," Wideband and Flat-gain Amplifier Using High Concentration Erbium Doped Fibers in Series Double-pass Configuration", International Conference on Computer & Communication Engineering**,** 2012 , pp. 109 – 112, **July 2012 .**(IEEE)

7. **B. A. Hamida**, S. Khan, A.W. Naji, W. AL-Khateeb, H. Ahmad and S. W. Harun," Modeling and Experimental Analysis of Wide-Band Flat-Gain Amplifier Utilizing High Concentration of EDFA, Photonic global conference , Singapore , PGC **Dec 2012**. (IEEE)

8. **B. A. Hamida**, S. Khan, A.W. Naji, W. AL-Khateeb, H. Ahmad and S. W. Harun," Zirconium-based Erbium Doped Fiber Amplifier for Wideband Fiber Communications, **Feb 2013**. (ISI cited publication) (***Submitted***)

9. X. S. Chenga, **B. A. Hamid**, H. Arofa, H. Ahmadc, and S. W. Haruna," Highly Efficient Short Length Bismuth_based Erbium_doped Fiber Amplifier", Laser

Physics. (ISSN 1054_660X), vol. 21, no. 10, pp. 1793- 1769, 3 **August, 2011**. (ISI cited publication).

10. X.S. Cheng, **B.A. Hamida**, A.W. Naji, H. Ahmad, S.W. Harun ," 67 cm long bismuth-based erbium doped fiber amplifier with wideband operation", Laser Phys pp. 1-4, **1 September 2011**. (ISI cited publication).

11. X.S. Cheng, **B.A. Hamida**, A.W. Naji, H. Arof, H. Ahmad, S.W. Harun ," Compact and wide-band bismuth-based erbium-doped fibre amplifier based on two-stage and double-pass approaches, Institution of Engineering and Technology (IET) Optoelectron vol. 6, no. 3, pp. 127–130, **January 2012.** (ISI cited publication).

12. A. W. Naji, **B. A. Hamida**, X. S. Cheng , M. A. Mahdi, S. Harun, S. Khan, W. F. AL-Khateeb,A. A. Zaidan, B. B. Zaidan and H. Ahmad, " Review of Erbium-Doped Fiber Amplifier ", IJPS, (ISSN 1992-1950), vol. 6, no. 20, pp. 4674- 4689, 23 Sep 2011. (International Journal).

13. Naji, A.W. Mohammed, M.A. **Ahmed, B**. Harun, S.W. Mahdi, M.A.," Novel theoretical modeling of quadruple Pass Erbium Doped Fiber Amplifier", International Conference on Computer and Communication Engineering, pp. 1-4, 23 August, **2010** Malaysia. (IEEE).

14. A.W. Naji, H.F.H. Ibrahim**, Belal Ahmed**, S.W. Harun and M.A. Mahdi," Theoretical analysis of triple-pass Erbium-Doped Fiber Amplifier" International Conference on Computer and Communication Engineering, 23 August, **2010**. Malaysia. (IEEE).

15. Naji, A.W., Akhter, F., Ibrahimy, M.I., **Ahmed, B.,** Mahdi, M.A.; Siddiquei, H.R ,"A Computer based Simulator for Erbium-Doped Fiber Amplifier", International Conference on Computer and Communication Engineering, Vol. 9, pp. 1-5, 23 **August, 2010** Conference Malaysia (IEEE).

16. Tawfig Eltaif, Hesham A. Bakarman, Abdulrahman Khonji, and **B. A. Hamida**, "Fiber-to-the-home services based on OCDMA technique," the 2nd advanced electromagnetics symposium , University of Sharjah, March 19- 22, 2013. (IEEE).

17. Tawfig Eltaif,. Ahmed Ba Haretha1, Anitha Mohan1, Abdulrahman Khonji1, **B. A. Hamida**, Hesham A "Broadband services to the end users ," the 2nd advanced electromagnetics symposium , University of Sharjah, March 19- 22, 2013 (IEEE)